MELT INCLUSION GEOCHEMISTRY

Jay B. Thomas

Dissertation submitted to the Faculty of
the Virginia Polytechnic Institute and State University
in partial fulfillment of the requirements for the degree of

DOCTOR OF PHILOSOPHY
in
GEOLOGICAL SCIENCES

Robert J. Bodnar (Chair)
James S. Beard
Nobumichi Shimizu
A. Krishna Sinha
Robert J. Tracy

July 18, 2003
Blacksburg, Virginia

Keywords: Melt Inclusion, Melt, Magma, Geochemistry, Trace Element, Rare Earth Element, Partition Coefficient, Boundary Layer, Chemical Gradient, Crystal Growth

Melt Inclusion Geochemistry

Jay B. Thomas

(ABSTRACT)

Silicate melt inclusions (MI) are small samples of melt that are trapped during crystal growth at magmatic pressures and temperatures. The MI represent a sample of the melt that was isolated from the magma during host crystal growth. Thus, MI provide a valuable tool for constraining the magmatic history of igneous systems because they provide an unambiguous method to directly determine compositions of melts from which the host crystal grew. As such, coupled petrographic examination and geochemical analyses of MI and host crystals can reveal information about crystal/melt processes in igneous systems that are difficult (or impossible) to assess through conventional methods. Many studies have used MI to monitor large scale petrogenetic processes such as partial melting and fractional crystallization. The research presented below focuses on using MI to constrain processes that operate at the crystal/melt interface because MI are samples of melt that resided adjacent to the host crystal prior to entrapment as an inclusion. Chapter one addresses challenges associated with preparing small crystals containing MI for geochemical analysis. In chapter two trace element analyses of MI and the immediately adjacent host zircon crystals are used to determine zircon/melt partition coefficients. K_{REE} determined are lower than previously reported values. Calculated K_{REE} indicate that light REE with atomic numbers less than Sm are incompatible in zircon and become more incompatible with decreasing atomic number. This behavior is in contrast to most previously published results which indicate $K > 1$ and define a flat partitioning pattern for elements from La through Sm. The partition coefficients for the heavy REE determined are lower than previously published results by factors of ≈15-20 but follow a similar trend. In chapter 3 the significance of boundary layer development adjacent to growing crystals is evaluated by comparing the trace element compositions of MI host crystals that have significantly different trace element mineral/melt partitioning behavior. The results show trends opposite to what would be expected had boundary layers affected the MI. Melt inclusions contain the highest concentrations of elements that are most compatible in the host crystal structure. Furthermore, MI composition does not correlate with MI diameter.

Acknowledgements

I would first like to extend my greatest appreciation to my immediate family. My parent's names are Michael & Sandra Thomas and my siblings are named Kevin Thomas and Krista Beheler. They patiently and thoroughly supported me throughout all of my education. My girlfriend Lauren has been exceptionally understanding over the last three years during this endeavor, and she still puts up with me. Our animals Panda, Copper and AlleyCat helped keep us sane during the past several years and the dogs took us to the mountains to play! I have made many friends during my time here at Virginia Tech. There are two close friends who deserve to be specifically mentioned. Jay Wimmer has remained one of my closest friends since childhood. We had many great times during the last several years. I wish we had filmed all of our fishing trips to the New and Jackson Rivers. Maybe people would believe the numbers and sizes of the fish we truly did catch, especially that lunker he landed during the summer of 2000. The other friend I want to specifically thank is Jim Student. Jim and I have been roommates for several years now. We held many late night scientific debates (sometimes all night long!) that were heated, lively and intriguing. It is so funny how we ended up following such similar paths, only separated in time by ten years. Jim is a great geologist and teacher and I owe much of my knowledge to discussions with him.

My committee members helped me realize a successful completion to this project and discussions with them helped me peer into future prospects. My committee members are Bob Bodnar (Virginia Tech), Bob Tracy (Virginia Tech), Krishna Sinha (Virginia Tech), Jim Beard (Virgina Museum of Natural History, Martinsville, VA) and Nobu Shimizu (Woods Hole Oceanographic Institution, Woods Hole, MA) and they offered exceptional guidance during completion of this study. I should also mention that they placed great amounts of trust in me and always let me pursue interests that I believed were important. I should emphasize that the freedom they gave me was perhaps most importance for successful completion of this endeavor. They turned me loose in the wilds of Alaska, British Columbia and eastern California and also allowed me to explore new realms in mass spec, electron probe and ion probe labs. During these times of complete academic freedom I gained knowledge that I am sure will help me succeed throughout my career. I should also extend thanks to the front office staff within the Department of Geological Sciences at Virginia Tech because they were always friendly and helpful. The Department of Geological Sciences at Virginia Tech is a great place and someday I hope to obtain a permanent position in a similar environment. Craig Chesner from Eastern Illinois University graciously provided me with samples of the Toba Tuff. I am excited about my new post-doctoral fellowship that I will begin in October 2003 with Bruce Watson at Rensellaer Polytechnic Institute in Troy, New York.

Writing proposals was one of the most useful talents that I have learned during the completion of this degree. In the fall of 1999 I wrote a proposal that I wanted to submit to the National Science Foundation. I gave it to Bob Bodnar and Krishna Sinha and they made changes to it that helped shape it into a competitive manuscript. We submitted the proposal to the National Science Foundation in December 1999 and it was funded in full during May 2000 by grant EAR-0001168 to R. J. Bodnar and A. K. Sinha. All of the research presented below was funded by this grant.

Table of Contents

List of Tables

List of Figures

PROLOGUE

I am grateful to have had an advisor who urged me to pursue exciting research that would result in publications. As such, the research presented in this dissertation has either been published elsewhere, is in press, or is in preparation for immediate publication.

Much of chapter one was published in American Mineralogist during the fall of 2002. An excerpt from chapter two was published in Geochimica et Cosmochimica Acta in the spring of 2002. We recently finished final preparations of chapter 3 for submission to Earth and Planetary Science Letters and expect it to appear in press during the fall of 2003. Chapters two and three were summarized in a manuscript that will be published as a chapter in the prestigious book series Reviews in Mineralogy and Geochemistry, which will be available in the fall of 2003. I expect to produce two more manuscripts from research conducted during the past three years, although those results are not discussed in this dissertation. A listing of abstracts and ongoing research can be found in my vita at the end of the dissertation. Listed below are the full references to the completed manuscripts.

Thomas, J.B., and Bodnar, R.J. (2002) A technique for mounting and polishing melt inclusions in small (<1 mm) crystals. American Mineralogist, 87, 505-508.

Thomas J.B., Bodnar R.J. and Shimizu N. (2002) Determination of zircon/melt trace element partition coefficients from SIMS analysis of melt inclusions in zircon. Geochimica et Cosmochimica Acta 66, 2887-2901.

Thomas, J.B., Bodnar, R.J., Shimizu, N. and Chesner, C. (in press) Melt inclusions in zircon. Reviews in Mineralogy and Geochemistry, Mineralogical Society of America.

Thomas, J.B., Bodnar, R.J., Shimizu, N. and Chesner, C. (in preparation) The geochemistry of melt inclusions contained in allanite, plagioclase, quartz and zircon. Part 1: assessing the role of boundary layer processes on melt inclusion compositions. Intended for publication in Earth and Planetary Science Letters

CHAPTER 1: A TECHNIQUE FOR MOUNTING AND POLISHING MELT INCLUSIONS IN SMALL (<1 MM) CRYSTALS

Abstract

A method for mounting and polishing small crystals (<1 mm) was developed to expose melt inclusions for analysis. Individual crystals are mounted in epoxy on one end of a 3.2 mm x 1.3 cm polycarbonate rod. The rod is inserted into a two-piece polishing tool with an adjusting screw to control the amount of sample exposed for grinding and polishing. Thus, individual crystals can be ground and polished so that features of interest (e.g., melt inclusions) are exposed on the polished surface.

Introduction

The study of melt inclusions has become an important tool for investigating petrogenetic processes because inclusions provide information not easily obtainable from studies of whole rocks (Schiano and Bourdon 1999). Preparation of crystals for analyses of contained melt inclusions requires special care because melt inclusions, reentrants, and hourglass inclusions in individual crystals occur at different depths beneath the polishing surface. Therefore, grinding and polishing may expose a melt inclusion in one crystal while melt inclusions in other crystals either are destroyed by polishing or remain unexposed beneath the surface. Further polishing would destroy any exposed melt inclusions and it may not be possible to distinguish between true inclusions and reentrants, especially if the sample was not observed before grinding and polishing. Some workers have avoided this problem by removing crystals from the epoxy (or other glue) as melt inclusions become exposed. These crystals are then placed into a separate mount containing only crystals with exposed melt inclusions. However, if the individual crystals are less than ~1 mm, removing the crystals and remounting them is difficult. I desired a technique that allows individual crystals to be ground and polished to different depths, and which allows the grinding progress to be controlled and monitored carefully so that pre-selected inclusions can be exposed individually for analysis.

This technique was developed to study melt inclusions in <1 mm long zircon crystals (Thomas et al. 2002). The technique is applicable to other minerals in which melt inclusions are rare or in which selection of specific melt inclusions is necessary. The technique described here allows the maximum number of inclusions to be exposed for analysis. Similarly, the technique described here may be used to prepare small polished crystals for experiments in the hydrothermal diamond anvil cell (cf., Schmidt et al. 1998; Darling and Bassett 2001).

Materials

The polishing tool is a 2.5 cm diameter x 2.9 cm long piece of 316 stainless steel with a 3.3 mm diameter hole drilled through its center parallel to the long dimension (Fig. 1.1). The hole is threaded from one end to a depth of 0.7 cm and fitted with a threaded adjustment screw 2.9 cm long. This adjustment screw allows the amount of sample

exposed beyond the surface of the sample polisher to be controlled precisely during grinding-polishing.

Before grinding and polishing, individual crystals are mounted in epoxy on a clear polycarbonate rod 3.2 mm in diameter and ~1.3 cm long (McMaster-Carr Cat. No. 8571K11) (Figs. 1.1-1.3). After final grinding and polishing, the rods containing the polished crystals are inserted into a brass probe mount that holds 12 rods (Fig. 1.2). The probe mount is 2.54 cm in diameter and 1.3 cm thick with twelve 3.3 mm diameter holes drilled through the cylinder around the outer diameter (Fig. 1.2). The sample rods are held in place with small setscrews (2.3 mm) tightened with an Allen wrench (Fig. 1.2). The sample rods are placed into the probe mount by placing the probe mount face down on a flat surface, inserting the rods (sample-side down) and tightening the setscrews so that all the polished samples are secured at the same height.

Crystal Mounting and Polishing Procedure

Polycarbonate rods (~1.3 cm long) are inserted into the polishing tool and ground so that both ends are flat and perpendicular to the long axis of the rod, using 600 grit paper (Buehler Carbimet paper disks No. 30-5778-600) with water. Before inserting the rod into the polishing tool, a drop of water is placed in the hole. The surface tension of the water keeps the rod from falling out of the polishing tool. The polishing tool is placed on the 600 grit paper and the screw is continuously adjusted during grinding so that the end of the polycarbonate rod is in contact with the paper. The rods (including those containing attached crystals, as described below) are ground until the end is flush with the much larger metal surface of the polishing tool. This assures that the surface is flat and perpendicular to the long axis of the rod. After cleaning and drying the rods, ~200 μl of epoxy (Buehler Epoxide resin No. 20-8130-032 and hardener No. 20-8132-008) is applied to one end of each rod with a dissecting needle. Experience has shown that the best results are obtained if Buehler Epoxide resin and hardener are used because most other brands leave an excess of hardener after curing causing inadequate setting. The epoxy is mixed and allowed to cure for ~30 min prior to applying it to the rod tips to ensure that the resin and hardener have adequately mixed and reacted. Allowing the epoxy to cure for ~30 min before applying it to the polycarbonate rod increases its viscosity. This prevents the epoxy from flowing down the side of the rod when the droplet is applied. After the epoxy has hardened, epoxy-tipped rods are ground to produce a flat surface (Fig. 1.3b) following the same procedures described above to produce flat surfaces on the rods. After grinding, the epoxy on the rod tips is ~25-50% of its original thickness. The epoxy-tipped rods are cleaned, dried, and stored until needed to mount individual crystals. This first application of epoxy provides a base on which to mount the crystals and prevents them from becoming detached from the polycarbonate rod during polishing.

To identify crystals containing melt inclusions, the crystals are immersed in refractive index oils (e.g., Cargille Type A, Cat. No. 16482) and observed with a binocular microscope (Fig. 1.3a). Selected crystals are cleaned in an appropriate solvent (e.g., toluene) to remove the oil prior to mounting in epoxy. To mount the crystal to the

epoxy-tipped rods, a small droplet of epoxy (<10 μl) is placed on the pre-flattened surface and spread to the appropriate thickness (thinner than the crystal to be mounted) with a dissecting needle or cotton-tipped swab. This thin layer of epoxy fixes the crystal to the surface prior to the final application of epoxy. Using a binocular microscope, a single crystal is placed onto the end of the rod containing the thin layer of epoxy, and a final drop of epoxy is added to cover the crystal. As above, epoxy should be mixed and allowed to react for ~30 minutes prior to application. After curing, the rods are placed into the polishing tool (Fig. 1.1) and ground with 1200 grit polishing paper (Buehler Carbimet paper disks No. 30-5778-012) and water. Grinding progress is monitored through repeated grinding and observation under a binocular microscope using reflected light until the crystal is exposed on the surface (Fig. 1.3c). After exposing the crystal surface, the rod containing the crystal is removed from the polisher and placed "on end" on a microscope slide and observed under a petrographic microscope using both transmitted and reflected light. The rod acts as an optical fiber and transmits light to the crystal. If additional grinding is needed to expose the melt inclusion, the sample is further thinned with 1200 grit paper until the melt inclusion (or any other feature of interest) is exposed. Once the desired level within the crystal is reached, final polishing (Fig. 1.3d) is achieved using 0.3 μm aluminum oxide coated polyester film (Buehler Fibrmet sheets No. 69-3154) and water. It was found that crystals were less likely to break during this final polishing step if a paper towel was placed beneath the aluminum oxide coated polyester film, rather than placing the film directly on a hard surface. Each sample is archived until sets of samples are ready for microbeam analysis.

Depending on the types of analyses to be conducted, the steps described below may vary. I generally first perform electron microprobe analyses followed by secondary ion mass spectrometry (SIMS) analyses. Samples from archived sets were selected for electron microprobe analyses and placed into the probe mount (Fig. 1.2) as described above. Samples that gave desirable results and which contained sufficiently large melt inclusions (>30 μm) were selected for further analysis using SIMS.

The mount used for electron microprobe analyses is not normally used to hold the samples for SIMS analyses because the polished crystals are not all at exactly the same height. This occurs because tightening the setscrews causes slight random displacements in the Z-direction. Minor height variations are not generally a problem during electron microprobe analyses because the stage has an adequate range of Z-direction movement. However, slight vertical variations from one crystal to the next are problematic during SIMS analyses due to the primary ion beam angle of incidence and low range of Z-direction movement. Prior to SIMS analyses, the sample rods are permanently cast in epoxy (Fig. 1.4). A 2.54 cm (outside diameter) standard aluminum ring form is placed on double-sided tape. A 1.52 cm diameter thin-walled brass ring is placed in the center of the larger ring, and the sample rods are placed inside this ring in a close-packing configuration (~15 sample rods) with the crystal-side placed against the tape. Both rings are filled with epoxy and allowed to cure prior to removal from the double-sided tape. Minimal (if any) polishing may be necessary to reduce minor height variations from one crystal to the next prior to SIMS analyses. It should be noted that the ion probe mount described above may be inappropriate for hydrogen analyses of melt inclusions owing to

the large volume of epoxy used (Dunbar and Hervig 1992). Additionally, other resins may be preferable to Buehler for high vacuum applications.

The technique described above was developed through trial and error, and has been found to be an effective means of exposing individual melt inclusions contained within small (as small as 50 μm) crystals. An added benefit of this technique is that undesirable samples may be culled and those giving the best results may be included in a final epoxy mount for further analysis. This assures that all (or most) of the samples in the final mount will be suitable for SIMS analysis, minimizing the amount of time that has to be spent changing mounts. Finally, the technique described here may also be suitable for preparing individual, small crystals for many other applications.

References

Darling R.S. and Bassett W.A. (2001) Analysis of natural $H_2O + CO_2 + NaCl$ fluid inclusions in the hydrothermal diamond anvil cell. American Mineralogist, 87, 69-78.

Dunbar N.W. and Hervig, R.L. (1992) Petrogenesis and volatile stratigraphy of the Bishop Tuff; evidence from melt inclusion analysis. Journal of Geophysical Research, B, Solid Earth and Planets, 97, 15,129-15.

Schiano P. and Bourdon B. (1999) On the preservation of mantle information in ultramafic nodules; glass inclusions within minerals versus interstitial glasses. Earth and Planetary Science Letters, 169, 173-188.

Schmidt C., Chou I-M, Bodnar R.J. and Bassett, W.A. (1998) Microthermometric analysis of synthetic fluid inclusions in the hydrothermal diamond-anvil cell. American Mineralogist, 83, 995-1007.

Thomas J.B., Bodnar R.J. and Shimizu N. (2002) Determination of zircon/melt trace element partition coefficients from SIMS analysis of melt inclusions in zircon. Geochimica et Cosmochimica Acta 66, 2887-2901.

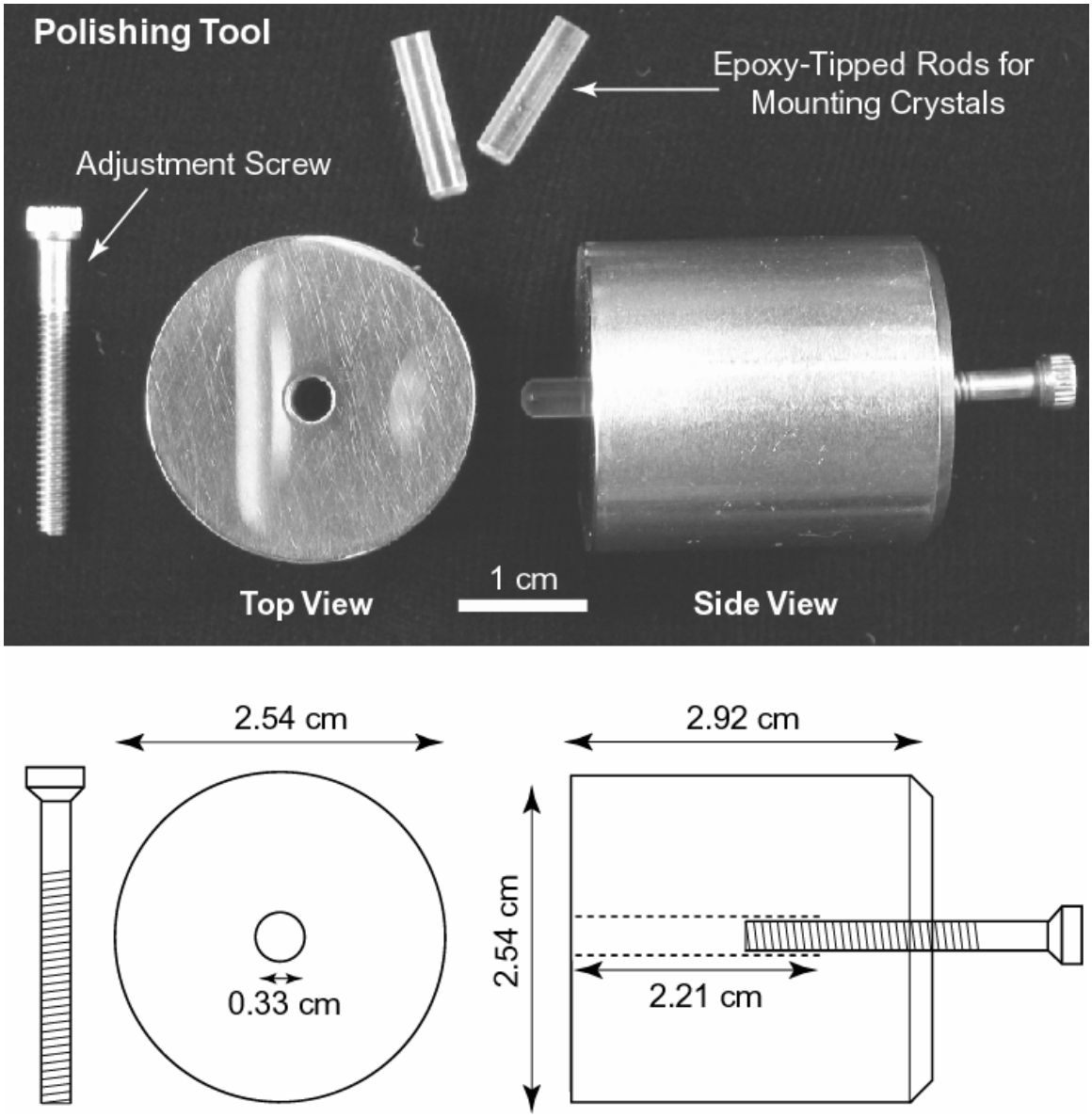

Figure 1.1. Photograph (top) and line drawing (bottom) of the polishing tool, adjusting screw and epoxy-tipped rods for mounting crystals. In the photograph, the body, adjustment screw and two sample rods are shown to the left, while the assembled polishing tool with a rod and the adjustment screw inserted is shown to the right.

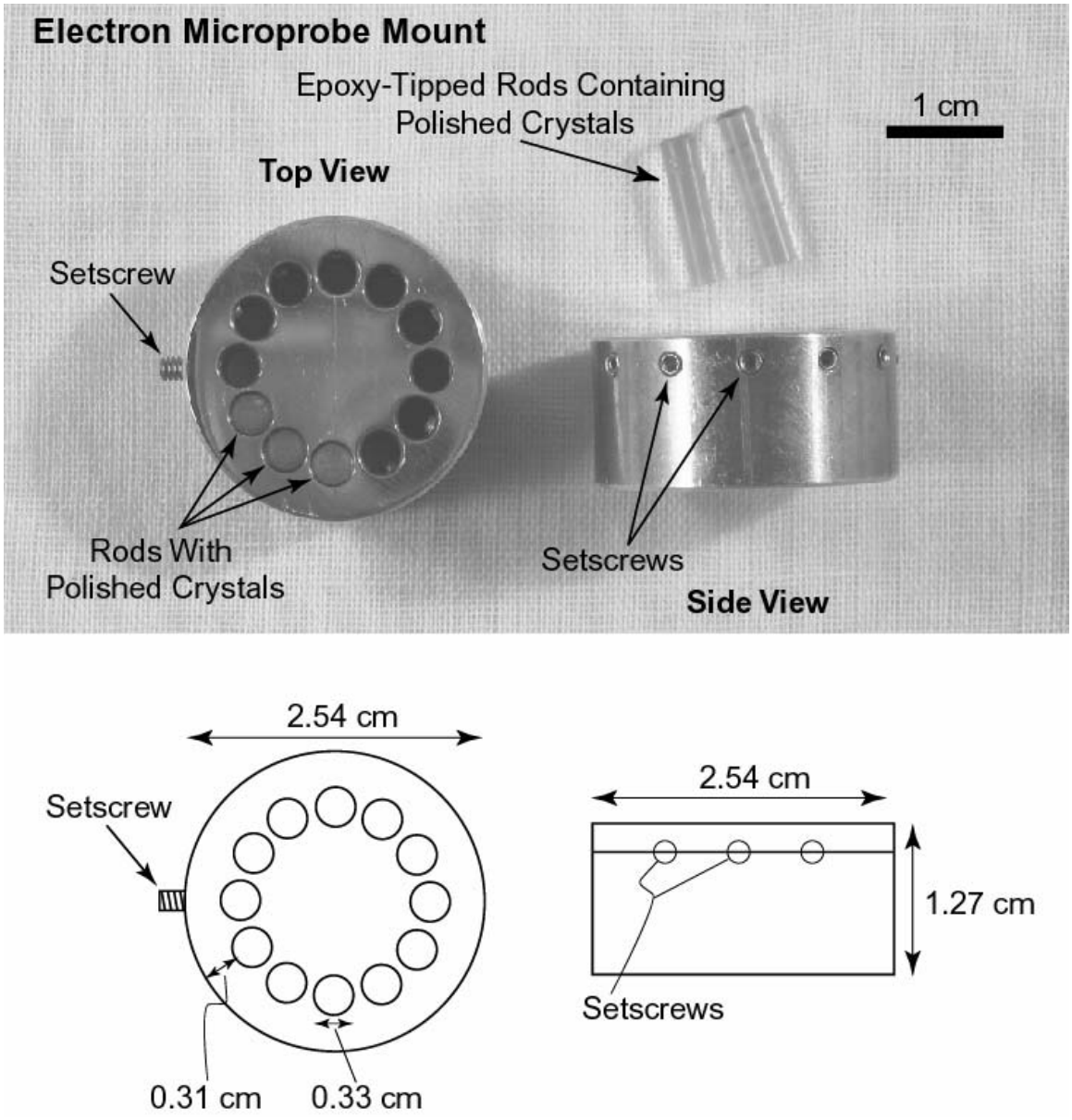

Figure 1.2. Photograph (top) and line drawing (bottom) of the electron microprobe mount and epoxy-tipped rods containing polished crystals.

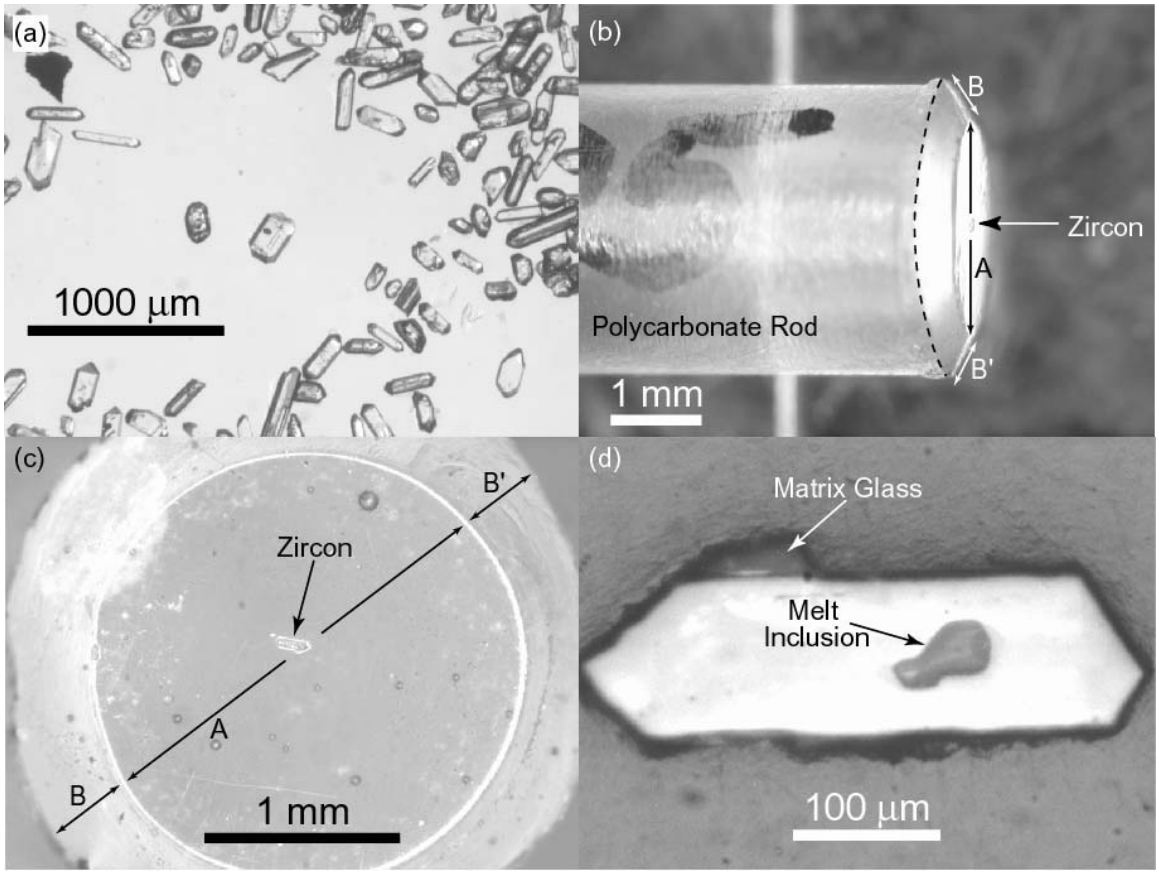

Figure 1.3. (a) Zircon crystals in refractive index oil (n=1.515). Two crystals in the center containing melt inclusions have been separated from the other crystals. (b) Side view of a polycarbonate rod containing a zircon crystal in epoxy. The dashed line shows the boundary between the polycarbonate rod and epoxy. Line A denotes the diameter of the polished surface of the epoxy, and lines B and B' denote the edges of the polished epoxy droplet. Lines A, B and B' are the same as those shown in (c). (c) Reflected light end view of a polycarbonate rod containing a zircon mounted in epoxy and exposed at the surface. The bright ~0.4 mm annulus surrounding the polished surface is the sloping edge of the original epoxy droplet (labeled B and B'). (d) Reflected light image of the same crystal as shown in (c) at higher magnification, showing the polished zircon crystal, melt inclusion and matrix glass.

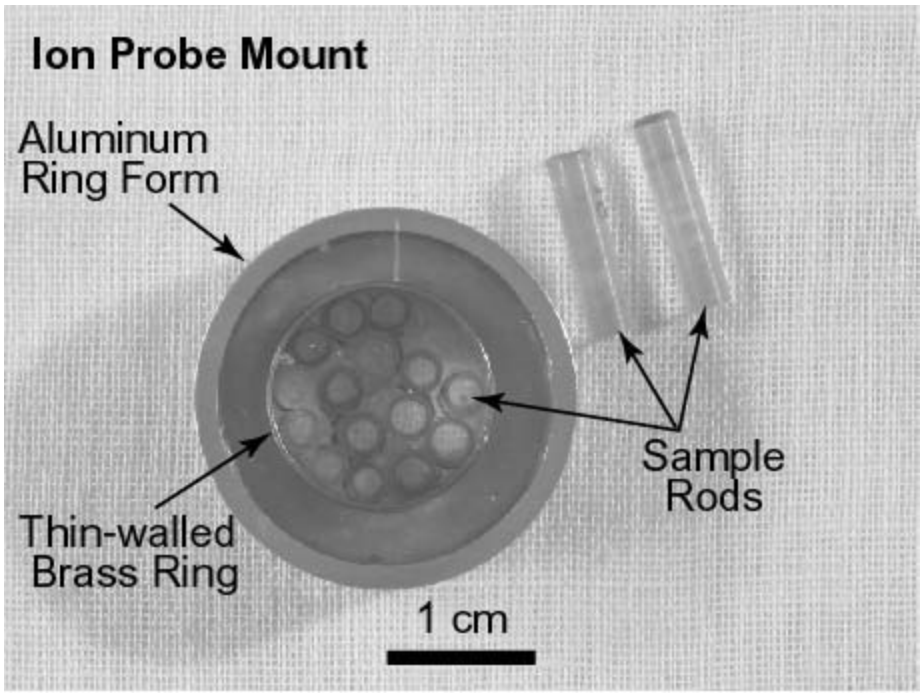

Figure 1.4. An ion probe mount with a 2.54 cm (outside diameter) standard aluminum ring and an internal 1.52 cm diameter thin-walled brass ring. The sample rods are contained within the internal ring in a close-packing configuration (~15 sample rods).

CHAPTER 2: ZIRCON/MELT TRACE ELEMENT PARTITION COEFFICIENTS DETERMINED FROM TRACE ELEMENT ANALYSIS OF MELT INCLUSIONS IN ZIRCON

Abstract

Partition coefficients ($^{zircon/melt}K_M$) for rare earth elements (REE) (La, Ce, Nd, Sm, Dy, Er and Yb) and other trace elements (Ba, Rb, B, Sr, Ti, Y and Nb) between zircon and melt have been calculated from secondary ion mass spectrometric (SIMS) analyses of zircon/melt inclusion pairs. The melt inclusion-mineral (MIM) technique shows that K_{REE} increase in compatibility with increasing atomic number, similar to results of previous studies. However, K_{REE} determined using the MIM technique are, in general, lower than previously reported values. Calculated K_{REE} indicate that light REE with atomic numbers less than Sm are incompatible in zircon and become more incompatible with decreasing atomic number. This behavior is in contrast to most previously published results which indicate $K > 1$ and define a flat partitioning pattern for elements from La through Sm. The partition coefficients for the heavy REE determined using the MIM technique are lower than previously published results by factors of ≈15-20 but follow a similar trend. These differences are thought to reflect the effects of mineral and/or glass contaminants in samples from earlier studies which employed bulk analysis techniques.

K_{REE} determined using the MIM technique agree well with values predicted using the equations of Brice (1975), which are based on the size and elasticity of crystallographic sites. The presence of Ce^{4+} in the melt results in elevated K_{Ce} compared to neighboring REE due to the similar valence and size of Ce^{4+} and Zr^{4+}. Predicted $^{zircon/melt}K$ values for Ce^{4+} and Ce^{3+} indicate that the Ce^{4+}/Ce^{3+} ratios of the melt ranged from about 10^{-3} to 10^{-2}. Partition coefficients for other trace elements determined in this study increase in compatibility in the order Ba <Rb <B <Sr <Ti <Y <Nb, with Ba, Rb, B and Sr showing incompatible behavior ($K_M < 1.0$), and Ti, Y and Nb showing compatible behavior ($K_M > 1.0$).

The effect of partition coefficients on melt evolution during petrogenetic modeling was examined using partition coefficients determined in this study and compared to trends obtained using published partition coefficients. The lower K_{REE} determined in this study result in smaller REE bulk distribution coefficients, for a given mineral assemblage, compared to those calculated using previously reported values. As an example, fractional crystallization of an assemblage composed of 35% hornblende, 64.5% plagioclase and 0.5% zircon produces a melt that becomes increasingly more enriched in Yb using the K_{Yb} from this study. Using K_{Yb} from Fujimaki (1986) results in a melt that becomes progressively depleted in Yb during crystallization.

Introduction

Accessory minerals in igneous rocks often contain high concentrations of REE and other trace elements (e.g. Arth, 1976; Pearce and Norry, 1979; Brooks et al., 1981;

Gromet and Silver, 1983; Mahood and Hildreth, 1983; Irving and Frey, 1984; Fujimaki, 1986; Reed, 1986; Green and Pearson, 1987; Heaman et al., 1990; Maas et al., 1992; Bea et al., 1994; Bea, 1996; Hoskin et al., 2000; O'Hara et al., 2001). Removal of even small quantities of accessory minerals in a fractionating assemblage, or retention of accessory minerals in restites, may strongly affect the trace element concentration of associated melts. For example, Bea (1996) notes that in peraluminous granites 90-95% of bulk rock LREE reside within accessories. Bea (1996) further notes that in metaluminous granites amphibole may contain as much as 30-35 wt.% of the total HREE, whereas the much less abundant zircon accounts for 30-50 wt.% of the HREE. Bea (1996) concludes that major minerals play a very subordinate role with respect to that of accessories in controlling REE abundances in melts, especially in peraluminous systems. Similarly, Chesner and Ettlinger (1989; see also Sawka et al., 1984) show that removal of as little as 0.052% modal allanite results in depletion of the LREE in the melt by about 50%.

The compositions of melts from which accessory minerals crystallize generally are not well constrained, especially in plutonic rocks. For this reason, inverse modeling using mineral chemistry and partition coefficients has been employed to back-calculate melt compositions (Hinton and Upton, 1991; Guo et al, 1996; Hoskin et al., 2000). Often, workers use the bulk rock as an approximation of the melt composition (e.g. Hoskin et al., 2000). Melt inclusions, such as those described here; provide an opportunity to directly determine the composition of the melt from which the zircon host crystallized. As such, analyses of melt inclusions and their hosts provide information about crystal/melt processes in plutonic (intrusive) magmatic systems that are difficult (or impossible) to assess through conventional methods.

Zircon is ubiquitous in crustal igneous rocks, is highly enriched in HREE, and may exert strong control on the REE evolution of melts from which it crystallizes (Nagasawa, 1970). In some cases, zircon ($\pm$ apatite) is the only HREE-enriched phase present in granitic rocks. Thus, the accurate determination of trace element partition coefficients for zircon ($^{\text{zircon/melt}}K_{\text{M}}$) is important for development and testing of models for melt generation and crystallization. (As this study only involves partitioning of trace elements between melt and host zircon, hereafter $^{\text{zircon/melt}}K_{\text{M}}$ is replaced with K_{M}, where the subscript M refers to the element or elements of interest.) Melt inclusions are common in zircon from a wide variety of rock-types (Fig. 2.1) including sandstones (detrital zircons), high grade gneisses, syenites, granitoids and basalts (Li, 1994; Chupin et al., 1998; Chesner, 1998).

This paper presents new partitioning data for the REE (La, Ce, Nd, Sm, Dy, Er and Yb) and Ba, Rb, B, Sr, Ti, Y and Nb, obtained from analyses of natural melt inclusions contained in zircon crystals. The melt inclusion-mineral (MIM) technique combines many of the advantages of conventional techniques used previously to determine K_{M}, while at the same time minimizing or eliminating many of the disadvantages of those techniques. Most previous studies of K_{M} used bulk analyses of zircon and either coexisting glass or whole rock separates to represent the melt composition (Nagasawa, 1970; Mahood and Hildreth, 1983; Murali et al., 1983; Fujimaki, 1986; Bea et al., 1994). Watson (1980) determined K_{REE} using synthetic

zircons grown from peralkaline melts. With the MIM technique, trace element concentrations in melt inclusions and in the immediately adjacent host mineral are measured and used to calculate mineral/melt partition coefficients. Lu et al. (1992) and Sobolev et al. (1996) pioneered this technique to determine partition coefficients in mineral/melt systems. Here, the technique is extended to determine zircon/melt partition coefficients for REE and other trace elements in granitic systems, using crystallized melt inclusions in zircon from the Quottoon Igneous Complex in British Columbia. It should be emphasized that the geological environment for the zircons studied here is of only secondary importance because the goal of this paper is to describe the feasibility of the MIM technique for determining trace element partitioning between melt and zircon.

Description of the field area

The Quottoon Igneous Complex (QIC) is an elongate, sheet-like body of calc-alkaline tonalite located in northwest British Columbia and southeast Alaska, and is part of the Coast Plutonic Complex (Hutchison, 1982). It is considered to be the southern terminus of the late Cretaceous to Eocene Great Tonalite Sill (Brew and Ford, 1981). Previous studies (Gehrels et al., 1991; Klepeis et al., 1998) have documented that zircon U-Pb ages in the QIC lack an inherited component and that zircons have remained a closed system (for U and Pb) since their formation (~65-55 Ma). The QIC stretches over a distance of ≈100 km from the Kowease River at 53º00'N to Pearse Canal near the Canada/United States international border, and is less than 15 km wide. The rocks are tonalitic to quartz dioritic in composition and were emplaced along the Coast shear zone at 4.6 ± 0.6 kb into upper amphibolite facies gneisses of the Central Gneiss Complex (Hutchison, 1982; Crawford et al., 1987). Details of the field relations, petrographic, and geochemical/isotopic data are given by Thomas and Sinha (1999; and references therein) and are briefly summarized below.

On the basis of field and bulk rock data, Thomas and Sinha (1999) divided the Quottoon rocks into two distinct suites. Suite I rocks contain abundant reacted mafic enclaves and are interpreted to have evolved dominantly by magma mixing and assimilation/fractional crystallization processes. The Suite II rocks are more homogeneous, contain fewer mafic enclaves, and evolved dominantly by assimilation and fractional crystallization processes. Mafic and felsic dikes occur in both suites and are interpreted as late stage features based on crosscutting relationships.

Methodology

Mineral and Melt Inclusion Petrography

The zircons studied here were extracted from sample 2093 (Thomas and Sinha, 1999), a coarse-grained hornblende-biotite quartz diorite from Suite I of the QIC. Accessory minerals include ilmenite, magnetite, apatite and zircon. Zircons have length:width ratios ranging from 2:1 to 10:1, are typically euhedral and clear, and contain both melt and solid inclusions. Zircon occurs as inclusions in early crystallizing plagioclase and hornblende, as well as in later crystallizing biotite and quartz, indicating

that zircon was forming early in the crystallization history, and may have continued to crystallize into the later stages of crystallization of the QIC.

Zircon crystals containing melt inclusions range from 500-1000 μm in maximum dimension. Melt inclusions in the zircons are primary and randomly distributed in the crystals (Roedder, 1984) with sizes ranging from <10 μm to >100 μm. The average size of studied inclusions is ≈25-50 μm because larger inclusions in the crystals tended to decrepitate during the homogenization process. Melt inclusion morphologies range from rounded to elongate to negative-crystal forms. Some melt inclusions are intersected by cracks but all of the inclusions studied occur in crack-free zones. Most melt inclusions do not contain recognizable bubbles and all melt inclusions are crystalline at room temperature (Fig. 2.2a). Before heating, all of the melt inclusions contained fine-grained aggregates of mostly quartz and feldspar (based on petrographic and electron microprobe analyses of unheated inclusions which were open to the surface) causing the inclusions to appear dark in color. Water that exsolved from the melt occurs as films and distorted bubbles within the crystallized inclusions (Yang and Bodnar, 1995; Lowenstern, 1995; Thomas and Webster, 2000).

Analytical Techniques

Zircons were separated by conventional techniques and examined under a petrographic microscope to identify crystals containing melt inclusions. Only inclusions near the cores of crystals (i.e., away from the crystal edges) and away from fractures were selected. All of the melt inclusions were partially to completely crystallized, due to slow cooling following entrapment in a plutonic environment. A zircon containing a crystallized (as found) melt inclusion is shown in Figure 2.2a; a back scattered electron image of the same inclusion after homogenization and exposure at the surface is shown in Figure 2.2b.

Selected zircons containing melt inclusions were heated under pressure (1200-1600 bars in argon) in a TZM vessel to homogenize the melt inclusions and produce a homogeneous glass. Previous workers (Thomas, 1994a,b; Schmidt et al., 1998; Student and Bodnar, 1996, 1999) have shown that heating inclusions under pressure minimizes decrepitation of the inclusions during homogenization, compared to heating at one atmosphere. Note that the internal pressure in the melt inclusions at homogenization is most likely higher than the confining pressure during the experiment (Student and Bodnar, 1996). Starting at 750°C, the inclusions were heated in approximately 20ºC increments to determine the homogenization temperature. After each increment of heating, the inclusions were quenched and examined to determine the degree of homogeneity. If an inclusion had not completely homogenized, the sample was placed back into the pressure vessel and heated to a temperature ≈20 degrees higher than the previous step. This process was repeated until complete homogenization was achieved. One inclusion (#B2, Table 2.1) was heated in a single step to 1000°C and quenched. Previous workers (Sobolev et al., 1990) noted that long duration heating experiments on melt inclusions in other minerals (olivine, plagioclase and clinopyroxene) can result in loss of hydrogen, effectively changing both the water content and oxidation state of the

melt. Results presented below suggest that melt inclusions in zircon studied here have not been similarly affected during the homogenization process.

Zircons containing homogenized melt inclusions were mounted in epoxy and polished to expose the glass inclusion at the surface (see Chapter 1) using the technique of Thomas and Bodnar (2002). Major and minor element compositions (Si, Ti, Al, Mg, Ca, Mn, Fe, Na, K, P, F, Cl, Table 2.1) of the melt inclusions were determined at Virginia Tech with a Cameca SX-50 electron microprobe equipped with four wavelength-dispersive spectrometers enabling four elements to be measured simultaneously. For glass (melt inclusion) analyses, an accelerating voltage of 15 kV was used with a beam current of 2 nA, and a beam diameter <5μm. Na and K were measured in the first 30 s to minimize the effect of volatization. For electron microprobe analyses of zircon (Table 2.2) the beam current was increased to 100 nA with a beam diameter of ~1μm. Analytical schemes for melt inclusions and zircons used 20-40 s counting times for major elements; for minor and trace elements the counting times were 60-600 s. Initial standardization was performed with a combination of minerals and glasses similar in composition to the melt inclusions and the host zircons. The accuracy of major element data is better than ±2% relative, and the accuracy of minor element analyses varies from 2-10% relative.

Trace element abundances were measured with a Cameca IMS 3f ion microprobe at Woods Hole Oceanographic Institute using previously described procedures (e.g. Shimizu and Hart, 1982; Shimizu et al., 1997; Shimizu, 1998). One analytical scheme was used for REE, and a different protocol was used for the other trace elements (Ba, Rb, B, Sr, Ti, Y, Nb). Gold-coated polished sections were analyzed using a primary O^- beam with a primary beam current of ~1 nA. A beam diameter of ~12-15 μm was used for REE analyses; for other trace elements an ~8-10 μm diameter beam was used. A larger beam diameter was required for REE analyses owing to the lower ion yield for these elements compared to the other trace elements analyzed. Molecular ion interferences were suppressed by offsetting the secondary-ion accelerating voltage by 60 V for REE (and 90 V for other trace elements) with an energy window of ±10 V using an energy-filtering technique (Shimizu and Hart, 1982). Element abundances were determined by converting secondary-ion intensity (ratioed against silicon), using empirical relationships between intensity and concentration based on analyses of rhyolite glass standards. Analytical uncertainties are mainly due to counting statistics; in the present study they are 5-15% for the REE and 3-8% for the other trace elements.

Fourteen zircons, each containing a single homogenized melt inclusion, were analyzed by electron microprobe (EPMA) and SIMS (Table 2.1). Zircon compositions obtained from EPMA and SIMS are listed in Table 2.2. EPMA totals for the homogenized melt inclusions range from 90.8 to 96.12. Differences from 100% are predominantly due to water (or other volatiles) in the glass (Devine et al., 1995). Water contents of melt inclusions were not determined by SIMS because such an analysis requires a different analytical scheme than that used for trace elements and multiple analyses of individual inclusions were not always possible, due to the small size of the melt inclusions. For those inclusions that were large enough for multiple analyses,

duplicate trace element analyses were conducted rather than water analyses. Zircon was analyzed immediately adjacent to the melt inclusions. Cathodoluminescence imaging of the zircons, back scattered electron imaging of melt inclusions and host zircons, and trace element EPMA traverses across melt inclusions and adjacent host zircon reveal no significant zoning of the host zircon in the immediate vicinity of the melt inclusion (Figs. 2.1-2.4).

As noted above, water contents of melt inclusions were estimated from EPMA data assuming that differences from 100% totals are due to water or other volatile elements. Anderson (1974) and Yang and Bodnar (1995) used this technique to determine water contnets of melt inclusions, and Devine et al. (1995) compared water contents of glasses determined by SIMS, FTIR and EPMA, and found that EPMA difference values provide acceptable estimates of H_2O contents as long as the water content is above 1 wt.%. Applying the difference technique to these melt inclusions suggests volatile contents from 4 to perhaps as high as 9 wt.% H_2O. As observed by numerous workers, the water in crystallized melt inclusions occurs as thin films and/or one or more distorted vapor bubbles within the crystalline mass (Skirius et al., 1990; Lowenstern 1995; Yang and Bodnar, 1995; Thomas and Webster, 2000). High water contents are not unusual or unexpected in melt inclusions from deep intrusive systems such as the QIC. Thus, Yang and Bodnar (1995) found water contents up to 4.2 wt.% in melt inclusions in granodiorites, Lowenstern (1994) found water contents up to 8 wt.% in melt inclusions from the Pine Grove system, and Thomas and Webster (2000) report water contents as high as 11 wt. % in crystallized melt inclusions from pegmatites. That the inclusions in this study maintain these high water contents during homogenization and quenching is also consistent with results of previous studies. Thus, Skirius et al. (1990) note that "*few or no volatiles leak from inclusions during heating*", and Lowenstern and Mahood (1991) showed that crystallized melt inclusions were *more* likely to retain the original water content compared to glassy inclusions.

Results

Results of heating experiments to homogenize melt inclusions are listed in Table 2.1. Twelve of the fourteen melt inclusions homogenized between 925º and 1000°C, with one at 875°C and one at 785°C. One melt inclusion (#B2) was homogenized by heating to 1000°C in a single step. Therefore, the actual homogenization temperature (TH) of this one inclusion is somewhat less than 1000°C. However, as the majority of the inclusions have homogenization temperatures in the range 950-1000°C (Table 2.1), the reported TH of inclusion #B2 (1000°C) is probably only a few tens of degrees higher than the actual temperature.

The goal of the heating experiments was to produce a homogeneous glass for subsequent electron and ion probe analyses, and not to determine the TH. However, if these analytical data are to be used to calculate partition coefficients, it is imperative that the melt and the host be in chemical equilibrium. If the melt and the host are in equilibrium, then the calculated zircon saturation temperature (ZST; Watson and Harrison, 1983) and the temperature to which the inclusion was heated should be in

agreement. The reasonably good agreement between TH and ZST (Table 2.1), suggests that the zircon and coexisting melt were in equilibrium at TH.

Petrographic observation (Fig. 2.1), back-scattered electron images (Fig. 2.2b), electron microprobe major element traverses (Fig. 2.3) and electron microprobe trace element traverses (Fig. 2.4) confirm the chemical homogeneity of individual inclusions and the host zircons. Additionally, three of the melt inclusions were large enough for duplicate SIMS analyses and show reasonably good reproducibility (Fig. 2.5). On the basis of major element compositions, all homogenized melt inclusions from this study are calc-alkaline and chemically classified as granite (Barker, 1979), with SiO_2 ranging between 75.88 and 79.40 wt.% (Fig. 2.6; Table 2.1) calculated on an anhydrous basis. The Na_2O and K_2O contents of the melt inclusions show little correlation with SiO_2 content (Fig. 2.6). Most of the melt inclusions are peraluminous with the exception of inclusions #1-11 and #16, which have aluminum saturation indices of 0.86 and 0.95, respectively.

Chondrite-normalized (Nakamura, 1974) REE abundances in melt inclusions and immediately adjacent zircon host are shown in Figs. 2.7a and b, respectively. The melt inclusions display smooth U-shaped chondrite-normalized REE patterns (Fig. 2.7a) that differ significantly from the host zircons. Moreover, zircon is enriched in HREE (Dy, Er, Yb), but depleted in the LREE La, relative to melt (Fig. 2.7b). While REE abundances show significant variation from one zircon to the next, the patterns are similar to one another and are simply displaced to higher or lower values. With the exception of Ce, concentrations of REE in zircons increase smoothly from La to Yb. The zircons display large positive Ce anomalies ($Ce/Ce^* = Ce_N/\sqrt{[La_N \times Nd_N]}$) ranging from 3.16 to 15.8 (average = 9.4) and La_N/Yb_N ranging from 0.00093 to 0.00927 (Table 2.2). Total REE of the zircons (for the seven REE analyzed in this study) ranges from 263 to 2411 ppm (average = 910 ppm). This range is consistent with abundances for these same REE measured in zircons from other granitic rocks (Hoskin et al., 2000).

Melt inclusion La_N/Yb_N ratios range from 0.63 to 7.51 (average = 2.61; Table 2.1) indicating that LREE are not strongly fractionated from HREE, as evidenced by the chondrite-normalized REE patterns on Fig. 2.7a. The highest La_N/Yb_N ratios correspond to inclusions with the lowest Yb abundances. While the LREE are not strongly fractionated from the HREE in melt inclusions, LREE are somewhat fractionated from the middle REE (Fig. 2.7a) as indicated by La_N/Sm_N ratios that range from 4.3 to 9.8, with one value at 28.9 (average = 8.7).

Assumptions Involved With the MIM Technique

The determination of REE zircon/melt partition coefficients with the MIM technique involves several assumptions. First, it is assumed that the REE concentration of the trapped melt is not affected by boundary layer processes. Secondly, it is assumed that once the melt is trapped the inclusion represents a closed system and that the REE budget of the melt inclusion does not change, either through crystallization onto the walls of the inclusion or through diffusive loss (or gain) of components (or that these changes

can be accounted for or reversed in the laboratory). Thirdly, it is assumed that the analytical techniques (homogenization of the crystallized melt inclusions, and electron and ion beam analyses) do not introduce errors. Below each of these assumptions is tested to assess the validity of the MIM technique.

When a crystal grows from a melt, the concentration of compatible elements is depleted at the crystal/melt interface as these elements are incorporated into the growing crystal. Similarly, the incompatible elements accumulate in this narrow zone as they are excluded from the growing crystal. The rate at which compatible elements can be replaced in this boundary layer, and the rate at which incompatible elements can be removed, depends upon the diffusion rates for these elements in the melt phase and crystal growth rates (Watson et al., 1982; Bacon, 1989). Based on studies of melt inclusions, the effect of chemical gradients within the boundary layer on melt inclusion compositions is thought to be small for most inclusions greater than ≈25 μm (Anderson, 1974; Lowenstern, 1995) and can be ignored for inclusions >50 μm in diameter (Lu et al., 1995). Webster and Rebbert (2001) found no boundary layer effects in melt inclusions smaller than 70 μm in maximum dimension in quartz from Ascension Island.

In the present study, most of the inclusions analyzed were between 25-50 μm. While it is not possible to prove that these inclusions were not affected by boundary layer processes during trapping, systematic variations in REE concentrations with size over the limited range of sizes examined were not observed. Further evidence that boundary layer processes have not significantly affected the trace element chemistry of the inclusions is that the least compatible REE (La) does not appear to be enriched (relative to typical granitic compositions) in the melt inclusions, and the most compatible REE (Yb) does not appear to be depleted (Fig. 2.7a), as would be expected if boundary layer processes were operating. Thus, it is concluded that the composition of the melt trapped in the inclusions was not significantly affected by boundary layer processes.

The second assumption involved in the use of melt inclusions to determine mineral/melt partitioning behavior is that the melt inclusions remain closed systems after trapping. However, under some conditions, melt trapped in an inclusion may continue to equilibrate with the bulk melt surrounding the host mineral as a result of diffusive exchange of components. For example, it is well known that the water content (Sobolev et al., 1990; Lowenstern and Mahood, 1991; Lu, 1991; Vityk et al., 2000) and the major element content (Gaetani and Watson, 2000; Danyushevsky et al., 2000, 2002) of melt and fluid inclusions can change, either during slow cooling in nature or during prolonged heating experiments in the laboratory. Qin et al. (1992) determined that for a species with a partition coefficient, k, ≥1, contained in an inclusion of diameter a in a host mineral of diameter b, with a size ratio (a/b) of 0.01, the dimensionless time τ (= Dt/b^2; where D is the diffusion coefficient, t is time, and b is the host crystal diameter) required to reach 10% reequilibration is approximately 0.1. Thus, for a crystal 1 mm in diameter containing a melt inclusion 10 μm in diameter, and a diffusion coefficient of 10^{-29} m^2 sec^{-1} (diffusion coefficient for Lu in zircon at 800°C; Cherniak et al., 1997), approximately 10^{22} seconds, or 3 x 10^{14} years is required for the Lu concentration in the melt inclusion to reach 10% reequilibration with the external melt.

The amount of time required to reach a given degree of reequilibration increases as the diffusion coefficient decreases. According to Cherniak et al. (1997), the diffusion coefficients decrease with decreasing atomic number for the REE; thus, the time required for all other REE lighter than Lu will be longer than that calculated above for Lu. Moreover, as trace element compatibility increases, the time to reach a given degree of reequilibration decreases. Using the data of Qin et al. (1992), the time required to reach a given degree of reequilibration for the inclusions in this study will be *greater* than that calculated for the 10 μm inclusion above, or *greater* than about 300 trillion years! In summary, the theoretical model of Qin et al. (1992) indicates that the possible change in the REE concentration of melt inclusions in zircon as a result of diffusion is essentially nil, even if the melt inclusions had been maintained at the formation temperature from their time of formation until the present.

As discussed above, compositions of melt inclusions in this study were unlikely to have been affected by boundary layer processes or diffusion-related reequilibration of the melts following entrapment as inclusions. This allows us to focus on errors resulting from homogenizing the inclusions, and analytical errors. All of the melt inclusions in this study crystallized as a result of the slow cooling following entrapment in the plutonic environment. During the course of heating the inclusions to produce a homogeneous glass for microbeam analysis, it was assumed that any zircon that precipitated on the walls following entrapment would have been incorporated back into the melt during the homogenization process. Furthermore, the amount of zircon precipitated during cooling (or dissolved during later reheating) is controlled by zircon solubility in the melt as a function of temperature (and melt composition). The relatively good agreement between measured THs and temperatures predicted from the zircon saturation equation of Watson and Harrison (1983) (using the measured Zr concentrations in the melt inclusions; Table 2.1), suggests that the melt inclusions equilibrated with the zircon host during the homogenization process.

Potential errors associated with dissolving too much or too little zircon host during homogenization may be estimated by considering the effect on the ZST (Watson and Harrison, 1983). For example, application of the zircon saturation equation to melt inclusion #G, which contains 649 ppm Zr (Table 2.1), yields a temperature (937°C) that is in excellent agreement with the measured homogenization temperature (950°C). If it is assumed that during cooling and crystallization of the melt that all of the Zr in the original melt was incorporated into zircon crystallizing on the walls, and if only 10% (65 ppm) of the Zr that precipitated was re-incorporated into the melt during homogenization, then the calculated ZST would be 721°C. Similarly, overheating the inclusion and adding 1% excess zircon (containing ~500,000 ppm Zr) to melt inclusion #G (Table 2.1) would change the Zr concentration in the melt from 649 to 5573 ppm. The ZST predicted from this Zr concentration is 1242°C. Note that dissolving excess zircon during homogenization is analogous to placing the ion beam partially on the melt inclusion and partially on the host zircon during SIMS analysis. Incorporation of excess zircon in the inclusion, either from overheating or incorrect beam placement, would result in ZST significantly different from those calculated for the melt inclusions (and

significantly different from the measured homogenization temperatures), and is not supported by the measured Zr concentrations of the melt inclusions (Table 2.1).

Trace Element Partitioning

Rare Earth Elements

Zircon/melt partition coefficients for each inclusion/host pair were calculated from SIMS data and are listed in Table 2.3 and shown on Figure 2.8a. Zircon/melt partition coefficients determined in this study increase with increasing atomic number — the trend is similar to that determined by other workers (Nagasawa, 1970; Hinton and Upton, 1991; Watson, 1980; Fujimaki, 1986; Guo et al., 1996; Hoskin et al., 2000; and others; see also the compilation at the GERM website at: http://earthref.org/GERM/). While the concentrations of individual trace elements vary by more than one order of magnitude from one melt inclusion to the next (Fig. 2.7a; Table 2.1), and from one zircon crystal to the next (Fig. 2.7b; Table 2.2), the calculated partition coefficients for individual REE generally vary by less than one order of magnitude (Table 2.3), reflecting the fact that melt inclusions with the highest REE abundances are generally associated with zircons with the highest REE abundances. For example, the La concentration in melt inclusions varies from about 14 to 97 ppm (Table 2.1), and the La concentration in host zircon ranges from 0.4 to 7.89 ppm. Assuming that the La concentrations in melt inclusions and zircon host vary randomly, one would expect a range in calculated K_{La} of greater than two orders of magnitude (from 0.0041 to 0.563). However, partition coefficients calculated for the two end-member melt concentrations reported above are identical at 0.03 (Table 2.4), and the total range in K_{La} is only about one order of magnitude (from 0.02 to 0.26; Table 2.3). The variations in partition coefficients determined here are consistent with those determined in both experimental studies (Watson, 1980) and from analyses of natural samples Mahood and Hildreth (1983). Thus, Watson (1980) reports a range in K_{Lu} from less than 20 to greater than 100 based on experimental results, and Mahood and Hildreth (1983) report a range in K_{La} from 7.2 to 26.6 based on analyses of zircon and rhyolitic glass from the Bishop Tuff.

The range in REE contents of melt inclusions and zircon shown in Figures 2.7a and 2.7b, respectively, reflect the natural variation in REE in the QIC igneous system with time. As noted above, zircon is believed to have formed over a significant portion of the crystallization history of the QIC. As such, the REE budgets of the melt and the zircons precipitating from that melt would be expected to vary with time as the melts are depleted in REE by zircon and other crystallizing phases. The variation observed at the individual melt inclusion/single zircon host scale in this study is analogous to the variation observed at the bulk rock (or glass)/zircon separate scale in some other studies (c.f., Mahood and Hildreth, 1983).

The zircon lattice contains two sites for cation substitution, a tetragonal Si site and a larger triangular dodecahedral Zr^{4+} site (Speer, 1982). HREE enrichment is due to substitution into the site containing Zr^{4+} (0.84 Å) (Speer, 1982; ionic radii in VIII coordination are from Shannon, 1976). Xenotime-type substitution (whereby an REE^{3+}

ion and a P^{5+} ion substitute for Zr^{4+} and Si $^{4+}$) has been reported in zircon (e.g. Speer, 1982; Hoskin et al., 2000; Hanchar et al., 2001; Finch et al., 2001). The P content of the zircons from this study is below detection limits (Table 2.2).

The compatibility of REE^{3+} in zircon is controlled mostly by REE^{3+} radii and to a lesser extent the charge of the ion (Hinton and Upton, 1991; Guo et al., 1996). As such, K_{REE} increase from La through Yb as the ionic radii decrease from 1.16 Å to 0.985 Å, and approach the ionic radius of Zr^{4+} (0.84 Å). However, due to differences in the ionic radius of Zr^{4+} compared to the REE^{3+}, substitution of REE^{3+} for Zr^{4+} in the zircon lattice results in lattice strain compensated by the excess free energy required to replace Zr^{4+} with substantially larger REE^{3+} (Blundy and Wood, 1994).

Blundy and Wood (1994) and Wood and Blundy (1997) describe a method based on equations developed by Brice (1975) to predict the partitioning behavior in mineral/melt systems. The predicted partition coefficients should display a parabolic form when log $^{mineral/melt}K_M$ is plotted versus ionic radii for a group of isovalent cations. The maximum on the parabola defines the optimum cation size that fits into the site involved in the partitioning (Onuma et al., 1968), and is generally close to the size of the major cation that is being replaced. For zircon, the maximum on the parabola should be at approximately 0.84 Å, which corresponds to the ionic radius of Zr^{4+} in the zircon structure (Speer, 1982; Shannon, 1976).

The K_{REE} values predicted from the Brice (1975) equation are compared to K_{REE} values calculated from melt inclusion and zircon analyses on Figure 2.8. The predicted K_{REE} were obtained using 0.84 Å as the optimum cation radius (r_o) of the Zr site onto which partitioning occurs, a Young's modulus for the Zr site (E) of 2003 kb, and temperature = TH. The Young's modulus was derived by fitting the MIM partitioning data to Eqn. 10 of Wood and Blundy (1997), and then using the relationship between Young's modulus and bulk modulus described by Hazen and Finger (1979) and shown in Blundy and Wood (1994; their Fig. 3). The Brice (1975) model requires that the partition coefficient for one cation of the isovalent group be known in order to calculate partition coefficients for other elements of the isovalent group. In the model calculations here the value for K_{Sm} from each inclusion was used to represent the "known" (K_a) value for that inclusion (Table 2.3). The predicted values shown on Figure 2.8b define only one limb of the parabola because the Zr site (0.84 Å) is smaller than the size of the smallest REE (Yb) measured; i.e., the maximum on the parabola is at a radius of 0.84 Å and lies off of the diagram to the left. The value predicted by the Brice (1975) equation lies within the range of measured K_{REE} for all of the REE measured in this study, and the predicted values vary by less than one order of magnitude from the median K_{REE} values reported in Table 2.3 (except for Ce, which is discussed in more detail below).

Partition coefficients predicted by the Brice equation from the melt inclusion data are compared to published values on Figure 2.8c. As expected, all previous studies show an increase in compatibility with decreasing ionic radius. However, in contrast to most previously published results (with the exception of the data of Murali et al., 1983), the MIM data indicate that La and Nd behave incompatibly in felsic melts (i.e., $K_M<1$).

Petrogenetic implications of this difference are considered later. Most previous studies show flat partitioning patterns for the light through middle REE (i.e., no change in the partition coefficient with ionic radius), whereas the MIM results indicate continuously decreasing compatibility from Yb through La as predicted by the Brice equation. Watson (1980) shows the same general pattern as in the present study (Fig. 2.8c), although the absolute values for K_M differ by more than one order of magnitude for La (and less for the other REE) between the two studies. These differences are currently unresolved but are possibly related to the differing melt compositions in these two studies. Note that the K_{LREE} trends from previously published studies are the opposite of that predicted by the Brice (1975) model. Related to this, Hinton and Upton (1991) noted that many published K_{LREE} are higher than would be expected if REE substitution is a function exclusively of ionic radius and attributed this difference to impurities contained in mineral separates in those studies.

Differences described above reflect the different experimental and analytical techniques employed in these various studies. Hinton and Upton (1991), Maas et al. (1992) and Guo et al. (1996) suggested that many of the reported K_M values are incorrect owing to bulk analysis of zircons containing solid inclusions or areas of alteration, and other workers have documented the significant effects of small amounts of contaminants during analysis (Michael, 1988; Beattie, 1994). My calculations indicate that including less than 1% of an accessory mineral that strongly partitions the LREE (e.g. allanite or monazite) within the bulk sample could produce the observed flat K_{LREE} pattern reported by other workers (Fig. 2.8c). It is suggested that the good agreement between MIM values and model results predicted by the Brice equation indicate that K_{REE} obtained using the MIM technique may be more reliable than those obtained from bulk analyses of mineral separates.

It is important to emphasize that partition coefficients in natural systems vary as a function of many parameters, including ionic potential, temperature, pressure, oxygen fugacity, crystal chemistry, and melt composition, including water content (Onuma et al., 1968; Drake and Weill, 1975; Watson, 1977; Matsui et al., 1977; Philpotts, 1978; Hart and Davis, 1978; Lindstrom and Weill, 1978; Ryerson and Hess, 1978; Green and Pearson, 1983, 1986; Dunn, 1987; Blundy and Wood, 1991; Hill et al., 2000). A significant difference between melt inclusions studied here and melts (volcanic glass) studied by most other workers is the water content. As noted previously, melt inclusions studied here may contain up to 8 or 9 wt.% water, compared to concentrations generally less than 2 or 3 wt.% water in volcanic glass. Blundy (private communication, 2002) notes that water has the effect of lowering ${}^{cpx/melt}K_{REE}$ but that water has no effect on ${}^{garnet/melt}K_{REE}$. Blundy (private communication, 2002) further notes that zircon may behave more like garnet. Finally, it should be noted that Watson and Harrison (1983) saw no effect of water content on zircon solubility.

Other Trace Elements

Fewer analyses were conducted for the trace elements Ba, Rb, B, Sr, Ti, Y and Nb (Tables 2.1 and 2.2). Zircon/melt partition coefficients for these elements were

calculated as described above for the REE, and are plotted on Fig. 2.9 in terms of increasing compatibility. K_M values are listed in Table 2.5. As expected based on charge/size ratios, Ba, Rb, B and Sr behave incompatibly, whereas Y and Nb are highly compatible, with Ti showing moderate compatibility. These values are consistent with elevated Nb and Y concentrations often reported for zircon (cf., Hoskin et al., 2000), and with the single value for K_Y from Bea et al. (1994).

Positive Ce Anomalies in Zircon

Zircon commonly shows a positive Ce anomaly (e.g. Hinton and Upton, 1991), which has been interpreted to indicate the incorporation of Ce into zircon as Ce^{4+}. Because Ce^{4+} has the same charge as the Zr^{4+} it replaces, and a similar ionic radius (Ce^{4+} = 0.97; Zr^{4+} = 0.84 Å), it is incorporated into the zircon structure much more readily than the larger Ce^{3+} (Ce^{3+} = 1.143 Å). Thus, the calculated partition coefficient for Ce (Fig. 2.8a) represents an apparent partition coefficient that includes both Ce^{3+} and Ce^{4+} (Hinton and Upton, 1991). The strong positive Ce anomalies in zircon (e.g. Murali et al., 1983; Hinton and Upton, 1991; Maas et al., 1992; Guo et al., 1996; Hoskin et al., 2000) indicate that Ce occurs in melts as both Ce^{4+} and Ce^{3+}, although Ce^{3+} dominates in terrestrial melts (Schreibber et al., 1980). Ce anomalies are absent in lunar zircons (Hinton and Myer, 1991) that formed under reducing conditions.

The expected partition coefficient assuming 100% Ce^{3+} was calculated using the Brice (1975) equation described earlier. Using the same values for the input parameters as described above for the other REE^{3+} gives K_{Ce3+} = 0.14 (Fig. 2.8b). The median value for the apparent partition coefficient for Ce determined from the MIM technique is 0.99 (Table 2.3). The partition coefficient for Ce^{4+} in zircon was predicted using the ionic radius for Ce^{4+} (0.97 Å), a Young's modulus (E) for the site of 4226 kb (based on the relationship between cation charge/site volume ratio (Z/d^3) and bulk modulus, after Hazen and Finger, 1979) and using K_{Zr4+} = 1700 (based on the average Zr concentration in the melt inclusions (Table 2.1) and host zircon (Table 2.2)). Using these values, the Brice (1975) equation predicts K_{Ce4+} = 102.6.

The Ce^{4+}/Ce^{3+} ratio in the melt inclusions was estimated using the calculated K_{Ce4+} and K_{Ce3+} values, the apparent K_{Ce} values from Table 2.3, and equation 2 from Hinton and Upton (1991). The calculated Ce^{4+}/Ce^{3+} ratios range from 0.0029 to 0.0188, and (except for one value) show a systematic increase in Ce concentration in zircon with increasing Ce^{4+}/Ce^{3+} ratio in the melt. This is interpreted to indicate that zircons with the highest Ce content in the QIC crystallized from melts with the highest Ce^{4+}/Ce^{3+} ratios. The wide range in Ce concentration in zircon is likely the result of both variable total Ce and evolving Ce^{4+}/Ce^{3+} ratio in the melt during crystallization. It should be noted, however, that zircons with positive Ce anomalies (reflecting an elevated concentration of Ce^{4+} in the zircon) can be produced from melts with relatively low Ce^{4+}/Ce^{3+} ratios if other phases which preferentially remove Ce^{3+} from the melt are crystallizing at the same time as zircon (Hinton and Upton, 1991).

Petrogenetic Implications

One important application of partition coefficients is for quantitative modeling of petrogenetic processes. In such calculations, relatively small errors in partition coefficients can have relatively large effects on model predictions. To illustrate this, batch partial melting and fractional crystallization was modeled using the K_{La} and K_{Yb} determined in this study and compared these results to those predicted using the partition coefficients of Fujimaki (1986). La and Yb were selected for these calculations because published partition coefficients for these elements show the largest departure from results of the present study. The results are compared to those of Fujimaki (1986) because those values are widely used in published petrogenetic models.

The evolution of La and Yb during batch partial melting (Eqn. 11 of Shaw, 1970) of a mafic (amphibolite) protolith containing 16.1 ppm La and 4.2 ppm Yb is shown in Figure 2.10a. The La and Yb concentrations are taken from Thomas and Sinha (1999; their Table 2.5), and were obtained from analysis of an amphibolite thought to represent the source for the melts that formed the QIC. The model assumes a residual assemblage containing 75% clinopyroxene, 24.5 % plagioclase and 0.5 % zircon. For comparison, batch partial melting of a zircon-free residual assemblage containing 75% clinopyroxene, 25% plagioclase was modeled (Fig. 2.10a). The residual assemblages were selected in accordance with observed experimental partial melting residues (e.g. Beard and Lofgren, 1991; Rushmer, 1991; Wolf and Wyllie, 1994; Patiño-Douce and Beard, 1995), and use partition coefficients for clinopyroxene and plagioclase from Klein et al. (2000), Schnetzler and Philpotts (1970) and Fujimaki et al. (1984).

The melt generated by 10% partial melting of the zircon-free assemblage contains 6.1 ppm Yb and 83 ppm La (Fig. 2.10a). For the zircon-bearing assemblage, the melt generated by 10% partial melting contains 4.8 ppm Yb using the partition coefficient from this study, but only 2.7 ppm Yb using the partition coefficient of Fujimaki (1986). The La concentrations are not significantly different between the zircon-free or zircon-bearing models, or using the Fujimaki data or MIM data. As shown on Figure 2.10a, Yb is most incompatible in the residue for the model with 0% zircon in the residual assemblage, as well as in the model including 0.5% zircon and using the K_{REE} from this study. However, using K_{REE} of Fujimaki (1986) results in Yb depletion in the melt for the zircon-bearing case.

Fractional crystallization (Greenland, 1970) was modeled using melt inclusion #4 (Table 2.1) as the parental melt, and published partition coefficients for hornblende and plagioclase (Fujimaki et al., 1984; Green and Pearson, 1985). Melt inclusion #4 was selected because it has relatively high REE concentrations compared to the other melt inclusions studied. As shown on Figure 2.10b, Yb is conserved in the melt for the model with 0% zircon in the fractionated assemblage, as well as in the model including 0.5% zircon and using the K_{REE} from this study. However, using K_{REE} of Fujimaki (1986) results in a strongly Yb-depleted melt for the zircon-bearing case. These calculations illustrate the significant differences that might result using different values for REE

partition coefficients in petrogenetic models and highlight the need for accurate partitioning data for use in these models.

Limitations of the Melt Inclusion-Mineral (MIM) Technique

The MIM technique described above to determine trace element partition coefficients is valid for the mineral zircon. The validity of the technique is based on the fact that diffusion rates for REE in zircon are extremely slow (Cherniak et al., 1997). Thus, the REE concentrations of melt inclusions and host zircon are unlikely to change as a result of diffusion following trapping. However, similar behavior is not expected for all minerals from all environments. While Sobolev et al. (1996) were able to determine trace element partitioning behavior between basaltic melt and clinopyroxene based on melt inclusions in clinopyroxene from the Upper lavas of the Troodos Massif, Cyprus, it is not clear that the approach would have worked for clinopyroxene (or other minerals) that cooled more slowly in a deep-seated environment. It is important to note that the diffusion coefficients for other trace elements (Ba, Rb, B, Sr, Ti Y and Nb) examined in this study are not as well constrained as those for REE in zircon, and could have been modified by later processes. Finally, we note that zircon immediately surrounding the melt inclusions in this study appears to be relatively homogeneous in trace element concentration over a distance of at least several tens of microns (Fig. 2.4). However, many zircons described in the literature are zoned on a fine scale (e.g. Heaman et al., 1990). If zircon exhibits zoning on a scale that is smaller than the size of the ion beam (approximately 10-20 μm), use of the technique described here might not provide reliable partitioning information.

Cherniak et al. (1997) note that the closure temperature for REE diffusion in zircon is higher than that for other minerals (such as diopside, titanite, garnet and apatite), suggesting that these other minerals would continue to exchange REE with the surrounding bulk melt to a lower temperature compared to zircon (Qin et al., 1992). Based on low ionic porosity, Dahl (1997; see also Lee et al., 1997) estimates closure temperatures for Pb in zircon that are higher than those for Pb in Ca-clinopyroxene, epidote, monazite and xenotime, but lower than for staurolite and garnet. The MIM technique should only be used to determine partitioning behavior of minerals with low ionic diffusivities, low ionic porosity and high closure temperatures, and/or from environments in which post-entrapment cooling was rapid.

Conclusions

Melt inclusions in zircon have been used to determine the partitioning behavior of REE in the zircon/granitic melt system. Due to the refractory nature of zircon and the slow diffusivities of trace elements through the crystal lattice, REE abundances measured in zircons today represent those present during crystal growth from the melt. Trace element partitioning is unaffected by postentrapment modifications and laboratory procedures. Partition coefficients for HREE determined using the MIM technique are in general agreement with published values, whereas, partition coefficients for LREE obtained in this study are significantly lower than most published values. K_{REE}

determined from the MIM technique are consistent with the Brice model that relates the partition coefficient to the size and elasticity of crystallographic sites. Positive Ce anomalies in zircons are related to the presence of both Ce^{3+} and Ce^{4+} in the melts from which the zircons crystallized. The Ce^{4+}/Ce^{3+} ratio of the melt has been predicted from the measured apparent partition coefficient and partition coefficients for Ce^{3+} and Ce^{4+} calculated using the Brice equation.

During fractional crystallization, removal of an assemblage containing 35% hornblende, 64.5% plagioclase and 0.5% zircon yields a bulk distribution coefficient of 1.6 for Yb, using K_{REE} reported by Fujimaki (1986). However, using the K_M values from this study predicts that Yb will be conserved in the melt (i.e. bulk distribution coefficient <1). The net result is that the predicted melt compositions will follow significantly different evolutionary paths during crystallization. It is recognized that no single mineral controls the trace element evolution during separation of crystals from melt, and I do not propose that zircon alone determines the REE budget of the system. Rather, the purpose of this study is to further document the application of the MIM technique to determine trace element partitioning behavior in mineral-melt systems. With the noted precautions taken, the MIM technique provides a robust and simple technique for determination of partitioning behavior in other mineral/melt systems.

References

Anderson A.T. (1974) Evidence for a picritic, volatile-rich magma beneath Mt. Shasta, California. Journal of Petrology 15, 243-267.

Arth J.G. (1976) Behavior of trace elements during magmatic processes-a summary of theoretical models and their applications. Journal of Research U. S. Geological Survey 4, 41-47.

Bacon C.R. (1989) Crystallization of accessory phases in magmas by local saturation adjacent to phenocrysts. Geochimica et Cosmochimica Acta 53, 1055-1066.

Barker F. (1979) Trondhjemites: definition, environment and hypothesis of origin. In Trondhjemites, dacites and related rocks. (ed. F. Barker), pp. 1-12. Elsevier.

Bea F. (1996) Residence of REE, Y, Th and U in granites and crustal protoliths; implications for the chemistry of crustal melts. Journal of Petrology 37, 521-552.

Bea F., Pereira M.D. and Stroh A. (1994) Mineral/leucosome trace-element partitioning in a peraluminous migmatite (a laser ablation-ICP-MS study). Chemical Geology 117, 291-312.

Beard J.S. and Lofgren G.E. (1991) Dehydration-melting and water-saturated melting of basaltic and andesitic greenstones and amphibolites at 1, 3, and 6.9 kb. Journal of Petrology 32, 365-401.

Beattie P. (1994) Systematics and energetics of trace-element partitioning between olivine and silicate melts: Implications for the nature of mineral/melt partitioning. Chemical Geology 117, 57-71.

Blundy, J. D. and Wood, B. J. (1991) Crystal-chemical controls on the partitioning of Sr and Ba between plagioclase feldspars, silicate melts and hydrothermal solutions. Geochimica et Cosmochimica Acta 55, 193-209.

Blundy J. and Wood B. (1994) Prediction of crystal-melt partition coefficients from elastic moduli. Nature 372, 452-454.

Brew D.A. and Ford A.B. (1981) The Coast plutonic sill, southeastern Alaska. In The U.S. Geologic Survey in Alaska-accomplishments during 1980. (Ed. N. R. D. Albert and T. L. Hudson), pp. B99-B102, 823-B. U.S. Geological Survey, Circular.

Brice J.C. (1975) Some thermodynamic aspects of the growth of strained crystals. Journal of Crystal Growth 28, 249-253.

Brooks C.K., Henderson P. and Ronsbo J.G. (1981) Rare earth element partitioning between allanite and glass in the obsidian of Sandy Braes, northern Ireland. Mineralogical Magazine 44, 157-160.

Cherniak D.J., Hanchar J.M. and Watson E.B. (1997) Rare-earth diffusion in zircon. Chemical Geology 134, 289-301.

Chesner C.A. (1998) Petrogenesis of the Toba Tuffs, Sumatra, Indonesia. Journal of Petrology 39, 397-438.

Chesner C.A. and Ettlinger A.D. (1989) Composition of allanite from the Toba tuffs, Sumatra, Indonesia. American Mineralogist 74, 750-758.

Chupin S.V., Chupin V.P., Barton J.M. and Barton E.S. (1998) Archean melt inclusions in zircon from quartzite and granitic orthogneiss from South Africa: magma compositions and probable sources of protoliths. European Journal of Mineralogy 10, 1241-1251.

Crawford M.L., Hollister L.S. and Woodsworth G.J. (1987) Crustal deformation and regional metamorphism across a terrane boundary, Coast Plutonic Complex, British Columbia. Tectonics 6, 343-361.

Dahl P.S. (1997) A crystal-chemical basis for Pb retention and fission-track annealing systematics in U-bearing minerals, with implications for geochronology. Earth and Planetary Science Letters 150, 277-290.

Danyushevsky L.V., Della-Pasqua F.N. and Sokolov S. (2000) Re-equilibration of melt inclusions trapped by magnesian olivine phenocrysts from subduction-related magmas: petrological implications. Contributions to Mineralogy and Petrology 138, 68-83.

Danyushevsky L.V., McNeill A.W. and Sobolev A.V. (2002) Experimental and petrological studies of melt inclusions in phenocrysts from mantle-derived magmas: an overview of techniques, advantages and complications. Chemical Geology 183, 5-24.

Devine J.D., Gardener J.E., Brack H.P., Layne G.D. and Rutherford M.J. (1995) Comparison of microanalytical methods for estimating H_2O contents of silicic volcanic glasses. American Mineralogist 80, 319-328.

Drake M.J. and Weill D.F. (1975) Partition of Sr, Ba, Ca, Y, Eu^{2+} , Eu^{3+}, and other REE between plagioclase feldspar and magmatic liquid; an experimental study. Geochimica et Cosmochimica Acta 39, 689-712.

Dunn T. (1987) Partitioning of Hf, Lu, Ti, and Mn between olivine, clinopyroxene and basaltic liquid. Contributions to Mineralogy and Petrology 96, 476-484.

Finch R.J., Hanchar J.M., Hoskin P.W.O. and Burns P.C. (2001) Rare earth elements in synthetic zircon: Part 2. A single-crystal X-ray study of xenotime substitution. American Mineralogist 86, 681-689.

Fujimaki H. (1986) Partition coefficients of Hf, Zr, and REE between zircon, apatite, and liquid. Contributiona to Mineralogy and Petrology 94, 42-45.

Fujimaki H., Tatsumoto M. and Aoki K. (1984) Partition coefficients of Hf, Zr and REE between phenocrysts and groundmass. Journal of Geophysical Research 89, Suppl. B662-B672.

Gaetani G.A. and Watson E.B. (2000) Open system behavior of olivine-hosted melt inclusions. Earth and Planetary Science Letters 183, 27-41.

Gehrels G.E., McClelland W.C., Samson S.D., Patchett P.J. and Brew D.A. (1991) U-Pb geochronology and tectonic significance of late Cretaceous Early Tertiary plutons in the northern Coast Mountains batholith. Canadian Journal of Earth Science 28, 899-911.

Green T.H. and Pearson N.J. (1983) Effect of pressure on rare earth element partition coefficients in common magmas. Nature 305, 414-416.

Green T.H. and Pearson N.J. (1985) Experimental determination of REE partition coefficients between amphibole and basaltic liquids at high pressure. Geochimica et Cosmochimica Acta 49, 1465-1468.

Green T.H. and Pearson N.J. (1986) Rare-earth element partitioning between sphene and coexisting silicate liquid at high pressure and temperature. Chemical Geology 55, 105-119.

Green T.H. and Pearson N.J. (1987) An experimental study of Nb and Ta partitioning between Ti-rich minerals and silicate liquid at high pressure and temperature. Geochimica et Cosmochimica Acta 51, 55-62.

Greenland L.P. (1970) An equation for trace element distribution during magmatic crystallization. American Mineralogist 55, 455-465.

Gromet L.P. and Silver L.T. (1983) Rare earth element distributions among minerals in a granodiorite and their petrogenetic implications. Geochimica et Cosmochimica Acta 47, 925-939.

Guo J., O'Reilly S.Y. and Griffin W.L. (1996) Zircon inclusions in corundum megacrysts: I. Trace element geochemistry and clues to the origin of corundum megacrysts in alkali basalts. Geochimica et Cosmochimica Acta 60, 2347-2363.

Hanchar J.M., Finch R.J., Hoskin P.W.O., Watson E.B., Cherniak D.J. and Mariano A.N. (2001) Rare earth elements in synthetic zircon: Part 1. Synthesis, and rare earth element and phosphorous doping. American Mineralogist 86, 667-680.

Hart S.R. and Davis K.E. (1978) Nickel partitioning between olivine and silicate melt. Earth and Planetary Science Letters 40, 203-219.

Hazen R.M. and Finger L.W. (1979) Bulk modulus-volume relationship for cation-anion polyhedra. Journal of Geophysical Research 84, 6723-6728.

Heaman L.M., Bowins R. and Crocket J. (1990) The chemical composition of igneous zircon suites: Implications for geochemical tracer studies. Geochimica et Cosmochimica Acta 54, 1597-1607.

Hill E., Wood B.J. and Blundy J.D. (2000) The effect of Ca-Tschermaks component on trace element partitioning between clinopyroxene and silicate melt. Lithos 53, 203-215.

Hinton R.W. and Myer C. (1991) Ion probe analysis of zircon and yttrobetafite in a lunar granite. Lunar and Planetary Science Conference XXII, 575-576.

Hinton R.W. and Upton B.G.J. (1991) The chemistry of zircon: Variations within and between large crystals from syenite and alkali basalt xenoliths. Geochimica et Cosmochimica Acta 55, 3287-3302.

Hoskin P.W.O., Kinny P.D., Wyborn D. and Chappell B.W. (2000) Identifying accessory mineral saturation during differentiation in granitoid magmas: an integrated approach. Journal of Petrology 41, 1365-1396.

Hutchison W.W. (1982) Geology of the Prince Rupert-Skeena map area, British Columbia. Geological Survey of Canada, Memoir 394.

Irving A.J. and Frey F.A. (1984) Trace element abundances in megacrysts and their host basalts: Constraints on partition coefficients and megacryst genesis. Geochimica et Cosmochimica Acta 48, 1201-1221.

Klein M., Stosch H.-G., Seck H.A. and Shimizu N. (2000) Experimental partitioning of high field strength and rare earth elements between clinopyroxene and garnet in andesitic and tonalitic systems. Geochimica et Cosmochimica Acta 64, 99-115.

Klepeis K.A., Crawford M.L. and Gehrels G. (1998) Structural history of the crustal-scale Coast shear zone north of Portland Canal, Southeast Alaska and British Columbia. Journal of Structural Geology 20, 883-904.

Lee J.K.W., Williams I.S. and Ellis D.J. (1997) Pb, U and Th diffusion in natural zircon. Nature 390, 159-162.

Li Z. (1994) The silicate melt inclusions in igneous rocks. In Fluid Inclusions in Minerals, Methods and Applications (ed. B. De Vivo and M. L. Frezzotti), pp. 73-94.

Lindstrom D.J. and Weill D.F. (1978) Partitioning of transition metals between diopside and coexisting silicate liquids; I, Nickel, cobalt, and manganese. Geochimica et Cosmochimica Acta 42, 817-832.

Lowenstern J.B. (1994) Dissolved volatile concentrations in an ore-forming magma. Geology 22, 893-869.

Lowenstern J.B. (1995) Applications of silicate-melt inclusions to the study of magmatic volatiles. In Magma, Fluids, and Ore Deposits (ed. Thompson, F. H.), pp. 71-99. Mineral. Assoc. of Canada, Short Course Series 23.

Lowenstern J.B. and Mahood G. (1991) New data on magmatic H_2O contents of pantellerites, with implications for petrogenesis and eruptive dynamics at Pantelleria. Bulletin of Volcanology 54, 78-83.

Lu F. (1991) The Bishop Tuff: Origin of the high-silica rhyolite and its thermal and compositional zonations. Unpub. Ph. D. Dissertation, University of Chicago, Chicago, Illinois.

Lu F., Anderson A.T., and Davis A.M. (1992) New and larger sanidine/melt partition coefficients for Ba and Sr as determined by ion microprobe analyses of melt inclusions and their sanidine host crystals. Geological Society of America Abstracts with Programs 24, A44.

Lu F., Anderson A.T. and Davis A.M. (1995) Diffusional gradients at the crystal/melt interface and their effect on the compositions of melt inclusions. Journal of Geology 103, 591-597.

Maas R., Kinny P.D., Williams I.S., Froude D.O. and Compston W. (1992) The earth'soldest known crust: A geochronological and geochemical study of 3900 Ma detrital zircons from Mt. Narryer and Jack Hills, western Australia. Geochimica et Cosmochimica Acta 56, 1281-1300.

Mahood G. and Hildreth W. (1983) Large partition coefficients for trace elements in high-silica rhyolites. Geochimica et Cosmochimica Acta 47, 11-30.

Matsui Y., Onuma N., Nagasawa H., Higuchi H. and Banno S. (1977) Crystal structure control in trace element partition between crystal and magma. Bulletin de la Societe Francaise de Mineralogie et de Cristallographie 100, 315-324.

Michael P.J. (1988) Partition coefficients for rare earth elements in mafic minerals of high silica rhyolites: The importance of accessory mineral inclusions. Geochimica et Cosmochimica Acta 52, 275-282.

Murali A.V., Parthasarathy R., Mahadevan T.M. and Sankar D. (1983) Trace element characteristics, REE patterns and partition coefficients of zircons from different geological environments-A case study on Indian zircons. Geochimica et Cosmochimica Acta 47, 2047-2052.

Nagasawa, H. (1970) Rare earth concentrations in zircon and their host dacites and granites. Earth Planet. Sci. Lett. 9, 359-364.

Nakamura N. (1974) Determination of REE, Ba, Fe, Mg, Na, and K in carbonaceous and ordinary chondrites. Geochim. Cosmochim. Acta 38, 757-775.

O'Hara M.J., Fry N. and Prichard H.M. (2001) Minor phases as carriers of trace elements in non-modal crystal-liquid separation processes II: illustrations and bearing on behaviour of REE, U, Th and the PGE in igneous processes. Journal of Petrology 42, 1887-1910.

Onuma N., Higuchi H., Wakita H. and Nagasawa H. (1968) Trace element partitioning between two pyroxenes and the host lava. Earth and Planetary Science Letters 5, 47-51.

Patiño Douce A.E. and Beard J.S. (1995) Dehydration-melting of biotite gneiss and quartz amphibolite from 3 to 15 kb. Journal of Petrology 36, 707-738.

Pearce J.A. and Norry M.J. (1979) Petrogenetic implications of Ti, Zr, Y, and Nb variations in volcanic rocks. Contributions to Mineralogy and Petrology 69, 33-47.

Philpotts J.A. (1978) The law of constant rejection. Geochimica et Cosmochimica Acta 42, 909-920.

Qin Z., Fangqiong F. and Anderson A.T. (1992) Diffusive reequilibration of melt and fluid inclusions. American Mineralogist 77, 565-576.

Reed S.J.B. (1986) Ion microprobe determination of rare earth elements in accessory minerals. Mineralogical Magazine 50, 3-15.

Roedder E. (1984) Fluid Inclusions (ed. P. H. Ribbe), Mineralogical Society of America, Reviews in Mineralogy, 12, 644pp.

Rushmer T. (1991) Partial melting of two amphibolites: contrasting experimental results under fluid absent conditions. Contributions to Mineralogy and Petrology 107, 41-59.

Ryerson F.J. and Hess P.C. (1978) Implications of liquid-liquid distribution coefficients to mineral-liquid partitioning. Geochimica et Cosmochimica Acta 42, 921-932.

Sawka W.N., Chappell B.W. and Norrish K. (1984) Light-rare-earth-element zoning in sphene and allanite during granitoid fractionation. Geology 12,131-134.

Schmidt C., Chou, I-M. Bodnar, R.J. and Basset W.A. (1998) Microthermal analysis of synthetic fluid inclusions in the hydrothermal diamond anvil cell. American Mineralogist 83, 995-1007.

Schnetzler C.C. and Philpotts J.A. (1970) Partition coefficients of rare earth elements between igneous matrix material and rock-forming mineral phenocrysts-II. Geochimica et Cosmochimica Acta 34, 331-340.

Schreibber H.D., Lauer H.V. and Thanyasir T. (1980) The redox state of cerium in basaltic magmas: An experimental study of iron-cerium interactions in melts. Geochimica et Cosmochimica Acta 44, 1599-1612.

Shannon R.D. (1976) Revised effective ionic radii and systematic studies of interatomic distances in halides and chalcedonides. Acta Crystallography A32, 751-767.

Shaw D.M. (1970) Trace element fractionation during anatexis. Geochimica et Cosmochimica Acta 34, 237-243.

Shimizu N. (1998) The geochemistry of olivine-hosted melt inclusions in a FAMOUS basalt ALV519-4-1 Physics of Earth and Planetary Interiors 107, 183-201.

Shimizu N. and Hart S. (1982) Applications of the ion microprobe to geochemistry and cosmochemistry. Annual Review of Earth and Planetary Science 10, 483-526.

Shimizu N., Sobolev N.V., Yefimova E.S. (1997) Chemical heterogeneities of inclusions in garnet and juvenile character of peridotitic diamonds from Siberia. Russian Geology and Geophysics 38, 356-372.

Skirius C.M., Peterson J.W. and Anderson A.T., Jr. (1990) Homogenizing rhyolitic glass inclusions from the Bishop Tuff. American Mineralogist 75, 1381-1398.

Sobolev A.V., Kamenetskiy V.S., Metrich N., Clochiatti R., Konokova N.N., Devirts A.L., Ustinov V.I. (1990) Volatile regime and crystallization conditions in Etna Hawaiite lavas. Geochemistry International 1990, pp. 53-65.

Sobolev A.V., Migdisov A.A. and Portnyagin M.V. (1996) Incompatible element partitioning between clinopyroxene and basaltic liquid revealed by study of melt inclusions in minerals from Troodos Lavas, Cyprus. Petrology 4, 307-317.

Speer J. A. (1982) Zircon. In Orthosilicates (ed. P. H. Ribbe), pp. 67-112. Mineralogical Society of America.

Student J.J. and Bodnar R.J. (1996) Melt inclusion microthermometry: petrologic constraints from the H_2O-saturated haplogranite system. Petrology 4, 310-325.

Student J.J. and Bodnar R.J. (1999) Synthetic Fluid Inclusions XIV: Coexisting silicate melt and aqueous fluid inclusions in the haplogranite-H_2O-NaCl-KCl system. Journal of Petrology 40, 1509-1525.

Thomas J.B. and Sinha A.K. (1999) Field, geochemical, and isotopic evidence for magma mixing and AFC processes in the Quottoon Igneous Complex, northwestern British Columbia and southeastern Alaska. Canadian Journal of Earth Sciences 36, 819-831.

Thomas R. (1994a) Estimation of viscosity and water content of silicate melts from melt inclusion data. European Journal of Mineralogy 6, 511-535.

Thomas R. (1994b) Fluid evolution in relation to the emplacement of the Variscan granites in the Erzgebirge region: A review of the melt and fluid inclusion evidence. In Metallogeny of collisional orogens focussed on the Erzgebirge and comparable metallogenetic settings (ed. Seltmann, R., Kampf, H. & Moller, P.), pp. 70-81. Czech Geological Survey.

Thomas R. and Webster J.D. (2000) Strong tin enrichment in a pegmatite-forming melt. Mineralium Deposita, 35, 570-582.

Vityk M.O., Bodnar R.J. and Doukhan J.C. (2000) Synthetic fluid inclusions XV. TEM investigation of plastic flow associated with reequilibration of fluid inclusions in natural quartz. Contributions to Mineralogy and Petrology 56: 119-134.

Watson E. B. (1977) Partitioning of Mn between forsterite and silicate liquid. Geochimica et Cosmochimica Acta 41, 1363-1374.

Watson E.B. (1980) Some experimentally determined zircon/liquid partition coefficients for the rare earth elements. Geochimica et Cosmochimica Acta 44, 895-897.

Watson E.B. (1996) Dissolution, growth and survival of zircons during crustal fusion: kinetic principles, geological models and implications for isotopic inheritance. Transactions of the Royal Society of Edinburgh Earth Sciences 87, 43-56.

Watson E.B. and Harrison T.M. (1983) Zircon saturation revisited: temperature and composition effects in a variety of crustal magma types. Earth and Planetary Science Letters 64, 295-304.

Watson E.B., Sneeringer M.A. and Ross A. (1982) Diffusion of dissolved carbonate in magmas: experimental results and applications. Earth and Planetary Science Letters 61, 346-358.

Webster J.D. and Rebbert C.R. (2001) The geochemical signature of fluid-saturated magma determined from silicate melt inclusions in Ascension Island granite xenoliths. Geochimica et Cosmochimica Acta 65, 123-136.

Wolf M.B. and Wyllie P.J. (1994) Dehydration melting of amphibolite at 10 kb: the effects of temperature and time. Contributions to Mineralogy and Petrology 115, 369-383.

Wood B.J. and Blundy J.D. (1997) A predictive model for rare earth element partitioning between clinopyroxene and anhydrous silicate melt. Contributions to Mineralogy and Petrology 129, 166-181.

Yang K. and Bodnar R.J. (1994) Magmatic-hydrothermal evolution in the "Bottoms" of porphyry copper systems: evidence from silicate melt and aqueous fluid inclusions in granitoid intrusions in the Gyeongsang Basin, South Korea. International Geologic Review 36, 608-628.

Table 2.1. Major oxides and trace element concentrations from melt inclusions.

	#1	#1-1	#B1	#B2	#4	#7	#1-11	#35	#46	#I	#G	#8	#9	#16
SiO_2 (wt. %)	78.55	78.88	76.67	77.91	77.8	76.99	75.88	76.20	75.96	78.12	77.47	79.4	79.25	76.63
TiO_2	0.04	n.d.	0.18	0.24	0.08	0.18	0.06	0.31	0.38	0.25	0.10	0.45	n.d.	0.48
Al_2O_3	12.47	12.93	13.94	12.21	13.63	12.91	12.87	13.20	13.67	12.4	13.03	11.95	12.88	12.38
MgO	0.06	0.03	0.07	0.02	0.01	0.02	n.d.	0.08	0.08	0.05	0.02	0.03	0.02	0.13
CaO	0.59	0.66	1.07	0.50	1.00	0.97	0.66	0.68	0.80	0.83	0.97	0.97	0.75	1.19
MnO	n.d.	0.03	0.04	n.d.	0.01	0.01	0.03	0.17	0.03	0.01	0.06	n.d.	0.04	0.02
FeO_t	0.49	0.48	0.87	0.64	0.32	0.59	0.46	0.43	0.81	0.21	0.29	0.54	0.45	0.97
Na_2O	2.26	1.29	2.11	2.6	2.32	3.02	5.23	2.84	2.86	2.53	2.78	2.55	1.36	3.62
K_2O	5.47	5.58	4.98	5.83	4.8	5.31	4.71	6.05	5.38	5.56	5.21	4.11	5.23	4.53
P_2O_5	0.06	0.06	0.06	0.05	0.03	n.d.	n.d.	0.04	0.03	0.03	0.06	n.d.	0.02	0.04
F	0.44	-	-	0.17	0.30	-	-	-	0.19	-	-	-	-	0.84
Cl	0.05	0.04	0.17	0.14	0.06	0.13	0.05	0.00	0.15	0.18	0.16	0.20	0.11	0.11
Total (norm. to 100%)	100	100	100	100	100	100	100	100	100	100	100	100	100	100
Total (measured)	94.92	92.56	94.28	96.12	94.13	95.14	90.80	93.46	91.42	90.85	92.50	91.96	91.68	94.21
Ba (ppm)	-	-	-	-	-	-	-	-	-	-	-	1646	640	1879
Rb	-	-	-	-	-	-	-	-	-	-	-	150	138	166
B	-	-	-	-	-	-	-	-	-	-	-	83.8	137	71.2
Sr	-	-	-	-	-	-	-	-	-	-	-	191	81.3	193
Ti	-	-	-	-	-	-	-	-	-	-	-	1966	350	1748
Y	-	-	-	-	-	-	-	-	-	-	-	17.1	5.94	345
Nb	-	-	-	-	-	-	-	-	-	-	-	11.1	6.03	16.8
La	20.9	22.8	38.5	19.4	96.6	20.1	31.9	30.4	31	13.6	16.9	-	-	-
Ce	34.4	41.4	76.8	39.2	133	36.3	56.7	53.8	55.5	25.3	32	-	-	-
Nd	9.96	12.6	28.1	11	37	13	16.3	20	22.6	6.79	8.37	-	-	-
Sm	1.55	2.04	5.58	1.91	6.06	1.67	3.19	3.23	3.47	0.29	1.62	-	-	-
Dy	3.35	3.30	8.98	6.35	18.8	1.98	13.6	3.06	3.35	1.58	1.29	-	-	-
Er	5.36	3.88	9.91	9.21	34.9	2.33	21.8	4.04	2.17	2.15	0.79	-	-	-
Yb	13	6.13	13.8	15.9	83.4	4.38	33.7	7.46	3.15	7.64	1.50	-	-	-
Ce/Ce*	1.26	1.28	1.23	1.41	1.13	1.18	1.31	1.15	1.1	1.39	1.42			
La_N/Yb_N	1.07	2.49	1.87	0.82	0.78	3.07	0.63	2.72	6.59	1.19	7.51			
Zr	881	207	327	348	939	728	713	70.2	390	508	649	167[d]	553[e]	1063[f]
ZST (°C)[a]	984	844	881	869	999	943	912	725	885	908	937	809	949	974
TH(°C)[b]	960	925	875	1000[c]	960	960	960	785	992	950	950	960	960	960

Dashes = not analyzed; n.d. = not detected.

$FeO_t = FeO+Fe_2O_3$.

$Ce/Ce^* = Ce_N/\sqrt{(La_N \times Nd_N)}$; Chondrite normalization values of Nakamura, 1974.

(a) ZST = zircon saturation temperature (Watson and Harrison, 1983).

(b) TH = total homogenization temperature.

Zr = Zr measured by electron microprobe.

Zr from SIMS: (d) = 234 ppm; (e) = 431 ppm; (f) = 1001 ppm.

Table 2.2. Major oxides and trace element concentrations of zircon hosts. Major oxides were not determined for #G and #I.

	#1	#1-1	#B1	#B2	#4	#7	#1-11	#35	#46	#I	#G	#8	#9	#16
SiO_2 (wt. %)	31.26	31.46	31.31	31.22	31.50	31.36	31.52	30.89	31.15	-	-	31.54	31.98	31.37
TiO_2	n.d.	n.d.	0.01	0.01	n.d.	n.d.	0.01	0.01	n.d.	-	-	n.d.	n.d.	0.01
Al_2O_3	0.01	0.03	0.01	n.d.	n.d.	n.d.	0.01	0.01	0.02	-	-	0.01	0.01	n.d.
FeO_t	n.d.	n.d.	n.d.	n.d.	0.01	n.d.	n.d.	n.d.	n.d.	-	-	n.d.	n.d.	n.d.
MnO	n.d.	n.d.	n.d.	n.d.	0.01	n.d.	n.d.	n.d.	n.d.	-	-	0.01	n.d.	n.d.
MgO	n.d.	n.d.	n.d.	n.d.	0.01	n.d.	n.d.	n.d.	n.d.	-	-	n.d.	n.d.	n.d.
CaO	n.d.	0.01	0.01	0.01	0.01	n.d.	n.d.	n.d.	0.02	-	-	n.d.	n.d.	0.01
K_2O	n.d.	n.d.	n.d.	n.d.	n.d.	n.d.	0.01	0.01	0.01	-	-	0.01	0.01	0.03
P_2O_5	n.d.	n.d.	n.d.	n.d.	n.d.	n.d.	n.d.	n.d.	n.d.	-	-	n.d.	n.d.	n.d.
Y_2O_3	0.04	0.05	0.04	0.16	0.04	0.05	0.05	0.12	0.02	-	-	0.03	0.01	0.06
ZrO_2	66.59	66.59	66.49	66.71	67.27	66.85	65.99	66.61	66.80	-	-	66.68	66.68	67.14
HfO_2	0.68	0.74	0.58	0.58	0.78	0.77	0.69	0.81	0.71	-	-	1.05	1.18	0.97
Total	98.59	98.88	98.45	98.70	99.62	99.04	98.28	98.45	98.72	-	-	99.32	99.89	99.59
Ba (ppm)	-	-	-	-	-	-	-	-	-	-	-	4.94	3.20	7.52
Rb	-	-	-	-	-	-	-	-	-	-	-	1.20	0.83	0.66
B	-	-	-	-	-	-	-	-	-	-	-	1.59	1.92	1.21
Sr	-	-	-	-	-	-	-	-	-	-	-	6.49	3.5	2.7
Ti	-	-	-	-	-	-	-	-	-	-	-	6496	5891	5508
Y	-	-	-	-	-	-	-	-	-	-	-	860	1135	825
Nb	-	-	-	-	-	-	-	-	-	-	-	3454	1424	3442
La	1.04	0.91	2.69	4.27	2.9	0.4	1.92	7.89	0.62	0.41	0.84	-	-	-
Ce	70.8	34.4	112	38.8	186	22.1	52.7	67.8	23.9	27.9	24	-	-	-
Nd	15.7	2.53	14	5.84	30.8	1.43	9.14	16.2	7.91	2.1	1.34	-	-	-
Sm	18	5.51	19.9	7.91	30.4	4.16	14.6	10.5	2.6	3.26	2.06	-	-	-
Dy	245	66.3	202	107	365	72.4	168	159	64.7	82.7	34.1	-	-	-
Er	388	113	291	194	625	137	284	303	114	131	55.3	-	-	-
Yb	670	249	494	348	1170	290	439	569	259	268	145	-	-	-
Ce/Ce*	9.2	11.9	9.61	4.09	10.4	15.4	6.63	3.16	5.67	15.8	11.9	-	-	-
La_N/Yb_N	0.00104	0.00245	0.00365	0.00820	0.00166	0.00093	0.00292	0.00927	0.00160	0.00101	0.00388	-	-	-

Abbreviations and symbols are the same as in Table 2.1.

Table 2.3. Partition coefficients (K_{REE}) calculated from REE abundances of melt inclusions and coexisting zircon hosts. Data listed in Tables 2.1 and 2.2.

	K_{La}	K_{Ce}	K_{Nd}	K_{Sm}	K_{Dy}	K_{Er}	K_{Yb}
#1	0.05	2.06	1.58	11.61	72.98	72.39	51.52
#1-1	0.04	0.83	0.2	2.7	20.09	29	40.63
#B1	0.07	1.46	0.5	3.56	22.45	29.35	35.88
#B2	0.22	0.99	0.53	4.14	16.79	21.09	21.9
#4	0.03	1.4	0.77	5.02	19.41	17.89	14.04
#7	0.02	0.61	0.11	2.49	36.56	58.88	66.1
#1-11	0.06	0.93	0.56	4.58	12.37	13.07	13.04
#35	0.26	1.26	0.81	3.24	51.95	74.99	76.32
#46	0.02	0.43	0.35	0.75	19.31	52.72	82.29
#I	0.03	1.1	0.31	11.24	52.31	60.74	35.11
#G	0.05	0.75	0.16	1.27	26.42	70	96.72
Median	0.05	0.99	0.5	3.56	22.45	52.72	40.63

Table 2.4. K_{REE} calculated for lowest (top) and highest (bottom) La, Sm and Yb abundances in the melt inclusions. Data for the coexisting zircon are also shown.

$^{a}La_{MI}$	$^{b}La_{zircon}$	K_{La}	$^{a}Sm_{MI}$	$^{b}Sm_{zircon}$	K_{Sm}	$^{a}Yb_{MI}$	$^{b}Yb_{zircon}$	K_{Yb}
13.6	0.41	0.03	0.29	3.26	11.24	1.495	144.6	96.72
96.6	2.9	0.03	6.06	30.4	5.02	83.35	1170	14.04

(a) REE abundance in melt inclusion.
(b) REE abundance in zircon.

Table 2.5. K_M calculated from the 3 melt inclusions in Table 2.1 and REE abundances of coexisting zircon hosts.

	K_{Ba}	K_{Rb}	K_B	K_{Sr}	K_{Ti}	K_Y	K_{Nb}
#8	0.003	0.008	0.019	0.034	3.30	50.2	312
#9	0.005	0.006	0.014	0.043	16.8	191	236
#16	0.004	0.004	0.017	0.014	3.15	2.39	204
Median	0.004	0.006	0.017	0.034	3.15	50.2	236

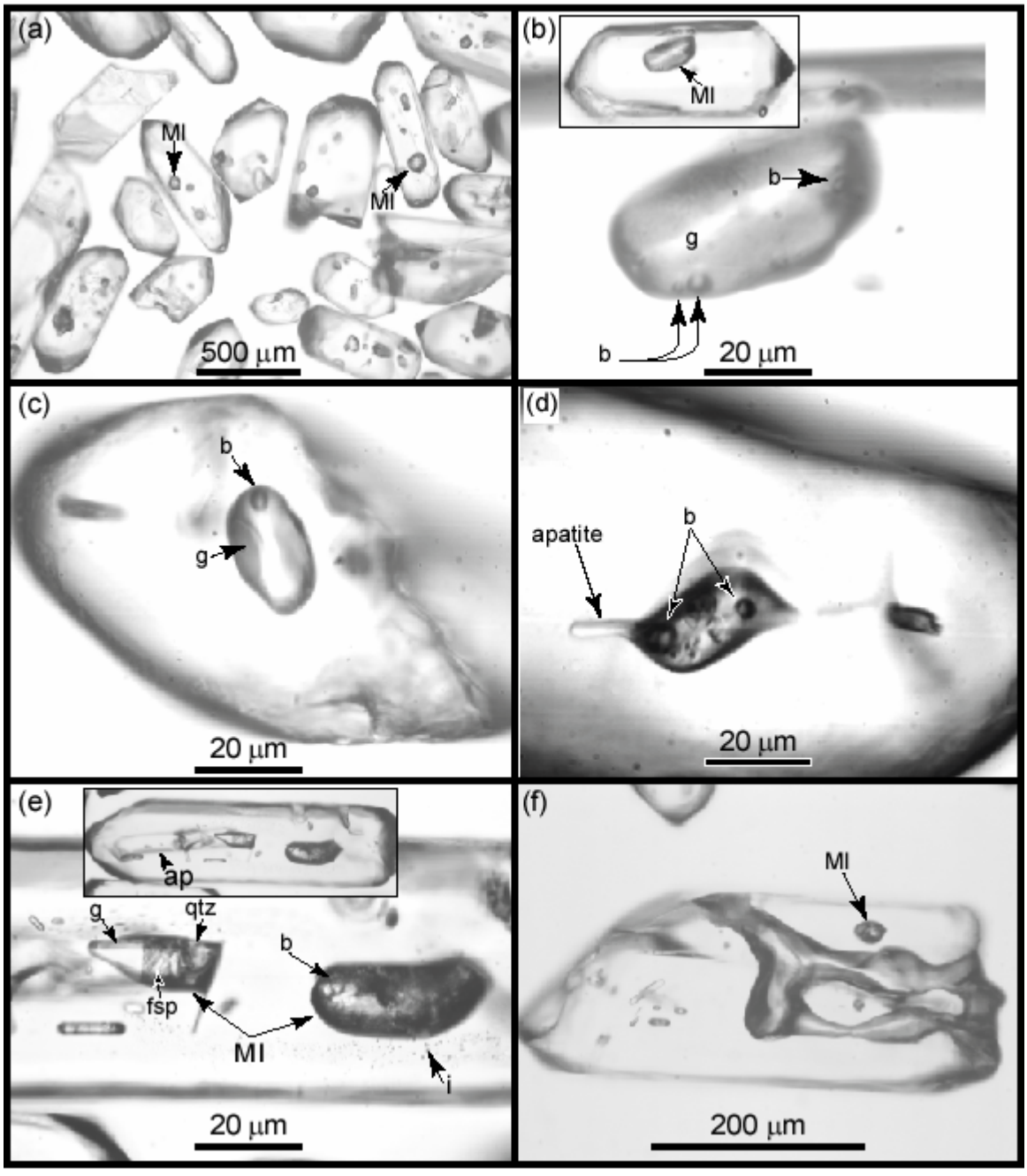
(a)
MI
MI
500 μm
(b)
MI
b
g
b
20 μm
(c)
b
g
20 μm
(d)
apatite
b
20 μm
(e)
ap
g
qtz
b
fsp
MI
i
20 μm
(f)
MI
200 μm

Figure 2.1 Transmitted light photographs of crystalline and glass melt inclusions (MI) in zircons. The zircons commonly contain solid inclusions of apatite (labeled "ap"), feldspar (labeled "fsp") and less commonly, oxide minerals. The zircons in the photographs are from: the 56 Ma quartz dioritic Quottoon Igneous Complex in British Columbia, Canada (shown in a, e and f), a rhyolitic member of the 74 ka youngest Toba Tuff of Sumatra, Indonesia (shown in b), and a heavy mineral sand deposit from north Stradbroke Island, Queensland, Australia (shown in c and d). (a) Crystalline melt inclusions in zircons extracted from the Quottoon quartz diorite. Most zircons contain dark-colored, ovoid inclusions that are crystalline melt inclusions. (b) The inset shows a low magnification photograph of a zircon from the Toba rhyolite containing an ovoid-shaped glass inclusion that is shown below the inset at higher magnification. The melt inclusion is comprised of crystal-free glass (labeled "g") and three bubbles (labeled "b"). (c) A glass melt inclusion is preserved in a rounded and broken fragment of a detrital zircon. The melt inclusion is comprised of glass and a bubble. (d) A partially crystalline melt inclusion hosted by a detrital zircon contains a crystal of apatite that was trapped along with the inclusion-forming melt. The partially crystalline melt inclusion also contains two bubbles, several transparent daughter crystals and feathery masses of dark-colored daughter crystals. (e) The inset shows a zircon from the Quottoon quartz diorite that contains a solid inclusion of apatite (labeled "ap") and two large crystalline melt inclusions that are shown below the inset at higher magnification. The large melt inclusion on the left contains a large transparent phase (glass? or quartz?), many transparent lath-shaped daughter crystals (feldspar?), a large anhedral daughter crystal (quartz? labeled "qtz"), and interstitial dark-colored daughter crystals. The large melt inclusion on the right contains a bubble that is partially obscured by daughter crystals. A decrepitation halo of small inclusions (labeled "i") occurs around the large melt inclusion on the right. (f) Zircon from the Quottoon quartz diorite containing a crystalline melt inclusion and an elongated tube-shaped inclusion that parallels the c-axis of the zircon host. The tube-shaped inclusions are commonly composed mostly of glass, however, some tube-shaped inclusions were found to be empty after the tubes were exposed at the surface.

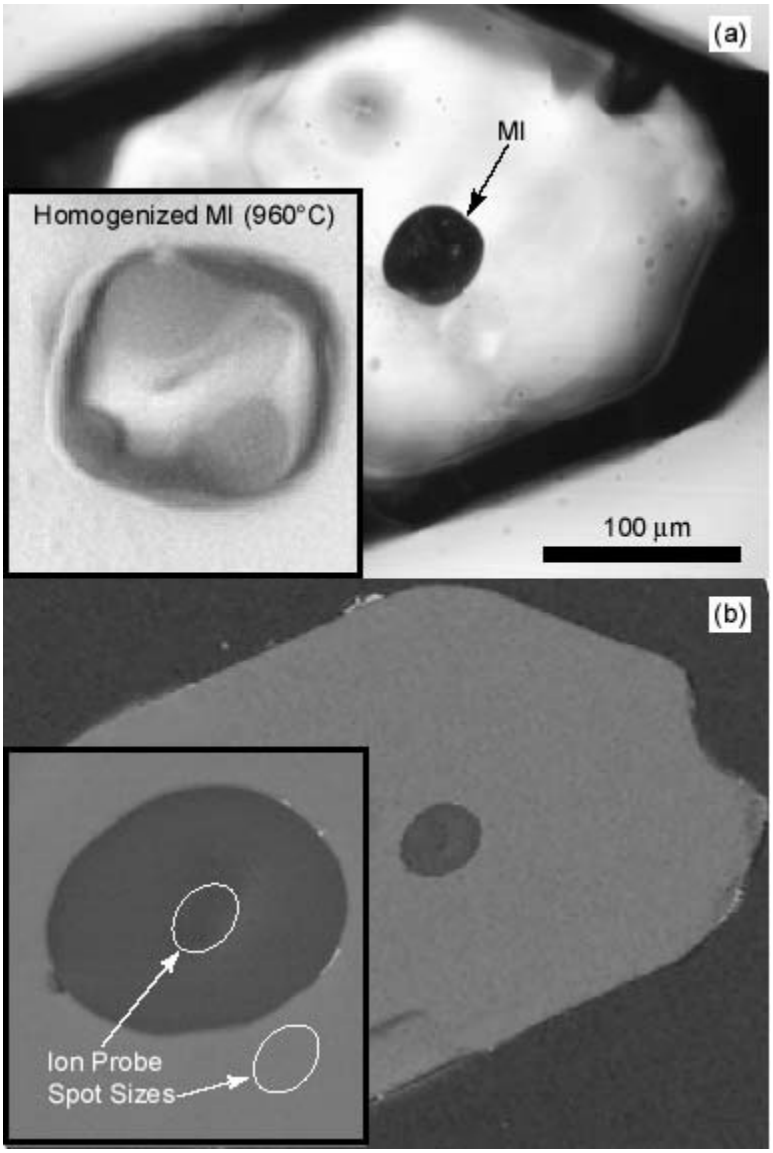

Figure 2.2. Melt inclusion in zircon crystal #8 (Table 2.1). (a) Transmitted light photograph of a zircon containing an unhomogenized (as found) melt inclusion (MI). Inset shows an enlargement of the same inclusion after homogenization. (b) Back-scattered electron image of the same zircon containing the homogenized melt inclusion exposed at the surface by polishing. Inset shows enlargement of the same inclusion along with representative ion probe spot sizes.

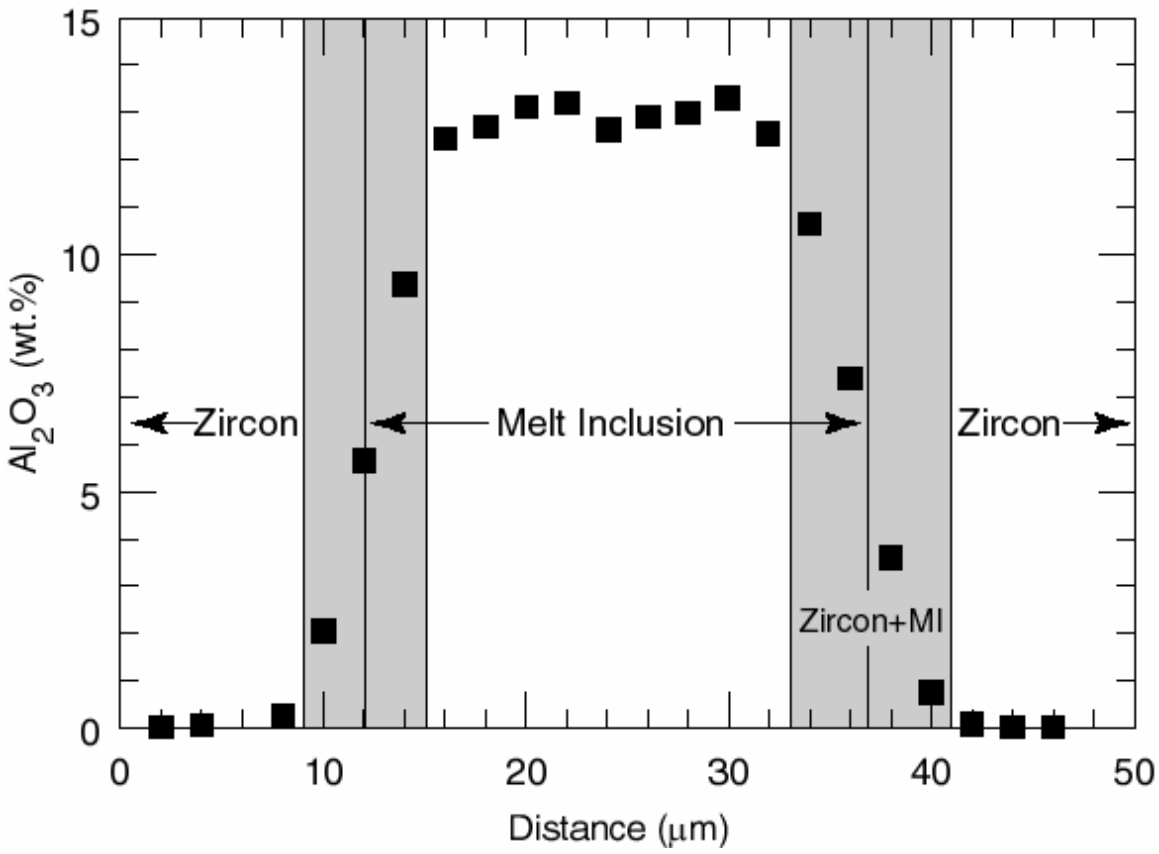

Figure 2.3. Electron microprobe traverse showing Al_2O_3 concentration (wt.%) in melt inclusion #1-1 and host zircon. Shaded portions denote analyses that include both zircon and the melt inclusion (MI). The beam diameter during analysis was approximately 2 μm.

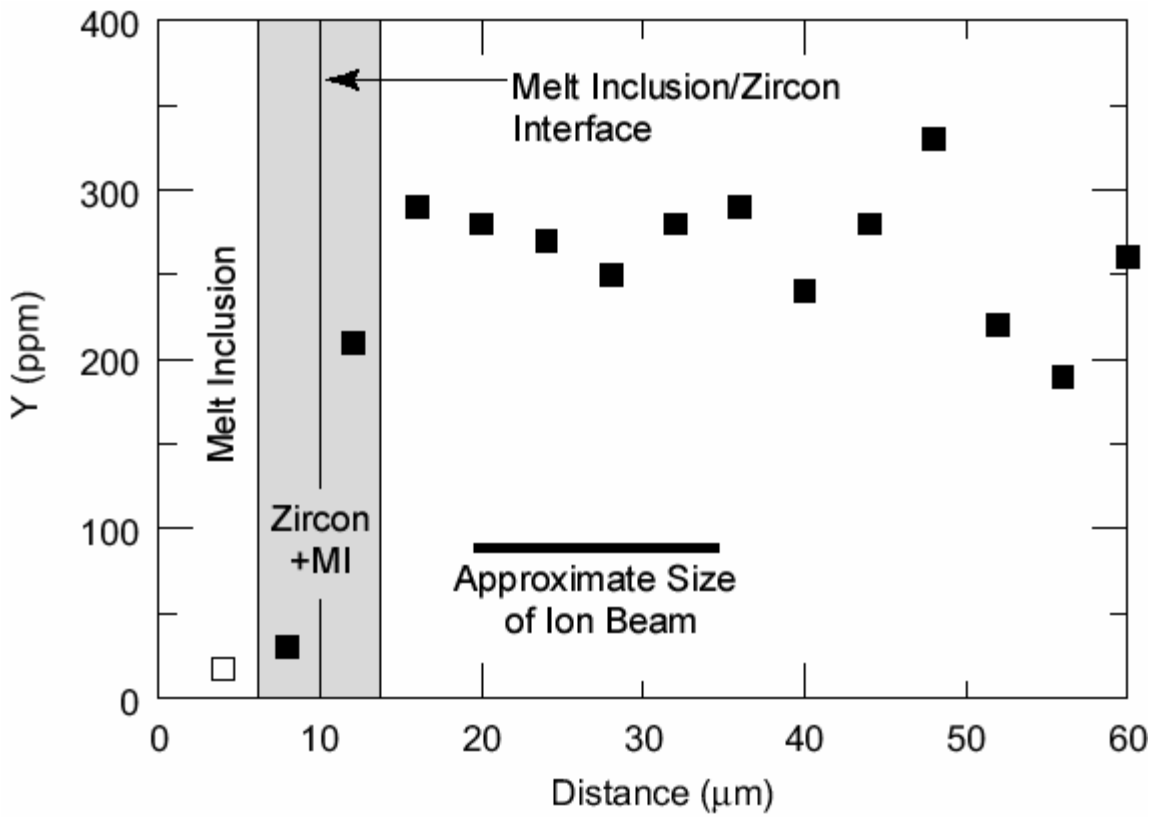

Figure 2.4. Electron microprobe traverse showing Y concentration (ppm) in zircon adjacent to melt inclusion #8 shown in Figure 2.2. Also shown is the size of the ion beam used during SIMS analysis. The zircon appears to be relatively homogeneous in Y at the scale of the ion beam.

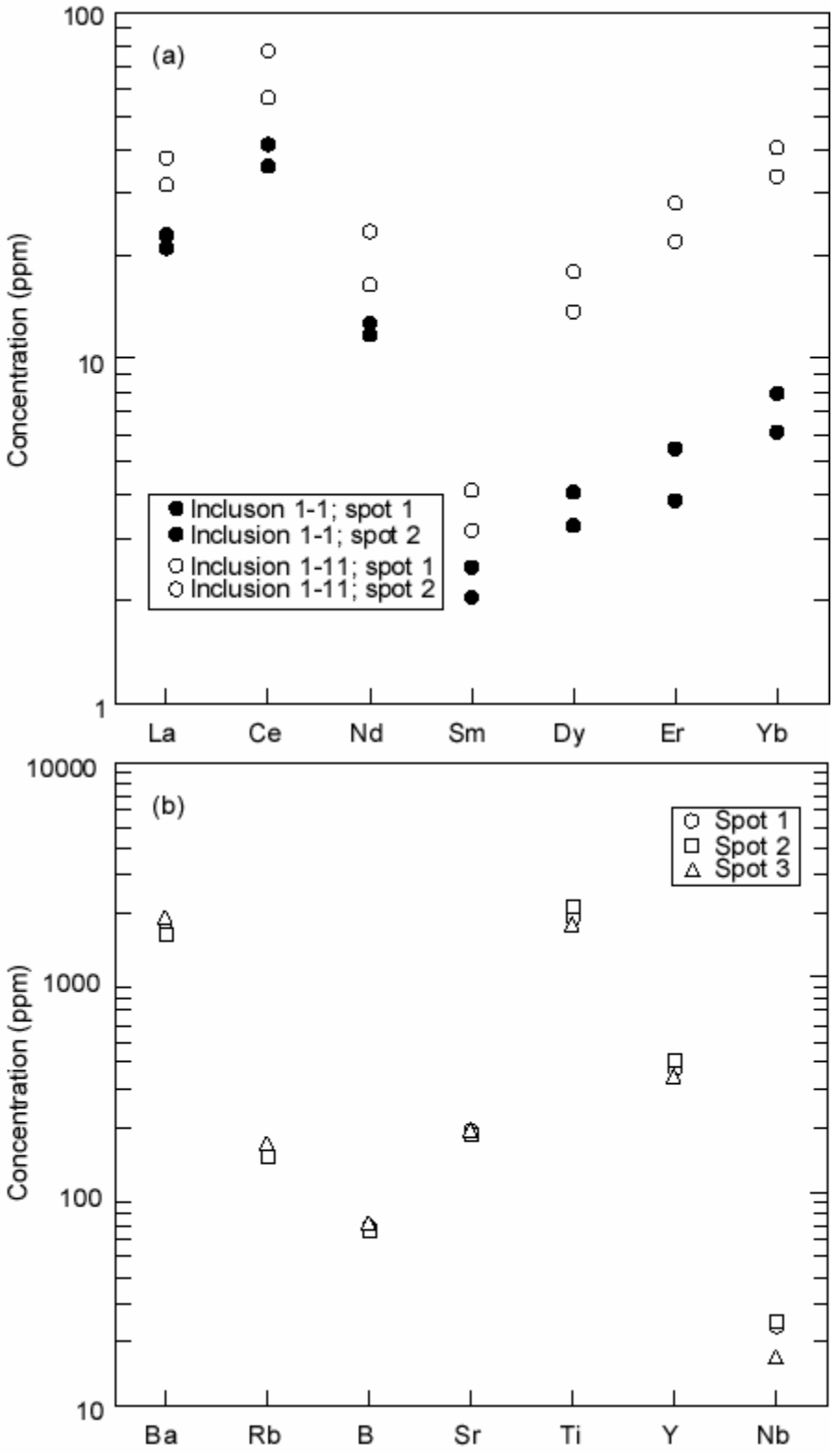

Figure 2.5. Results of duplicate analyses of larger melt inclusions for (a) REE and (b) other trace elements documenting the homogeneity of individual melt inclusions.

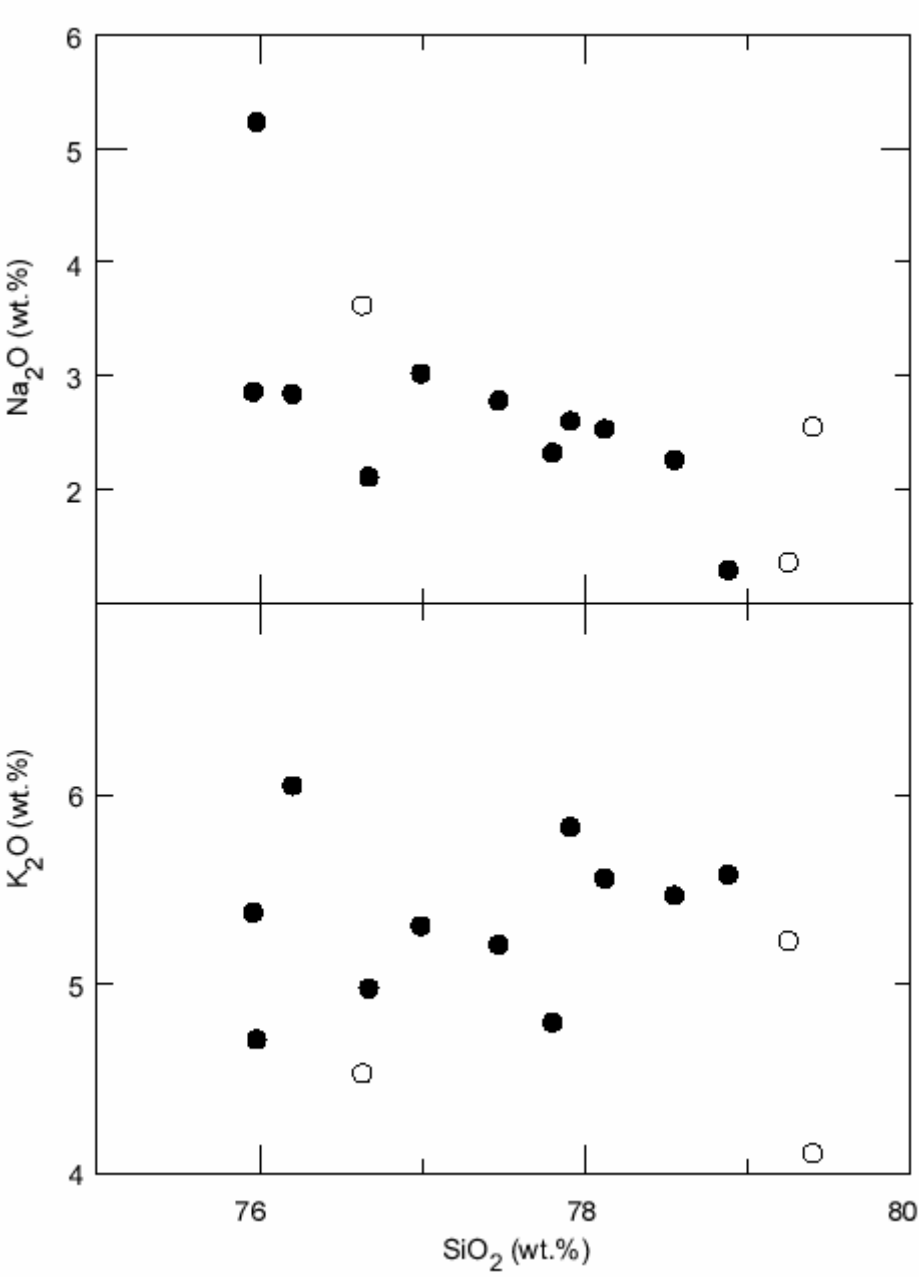

Figure 2.6. Na_2O and K_2O concentration versus SiO_2 (wt.%) for melt inclusions reported in Table 2.1. The filled symbols represent inclusions analyzed for REE and the open symbols represent samples analyzed for other trace elements.

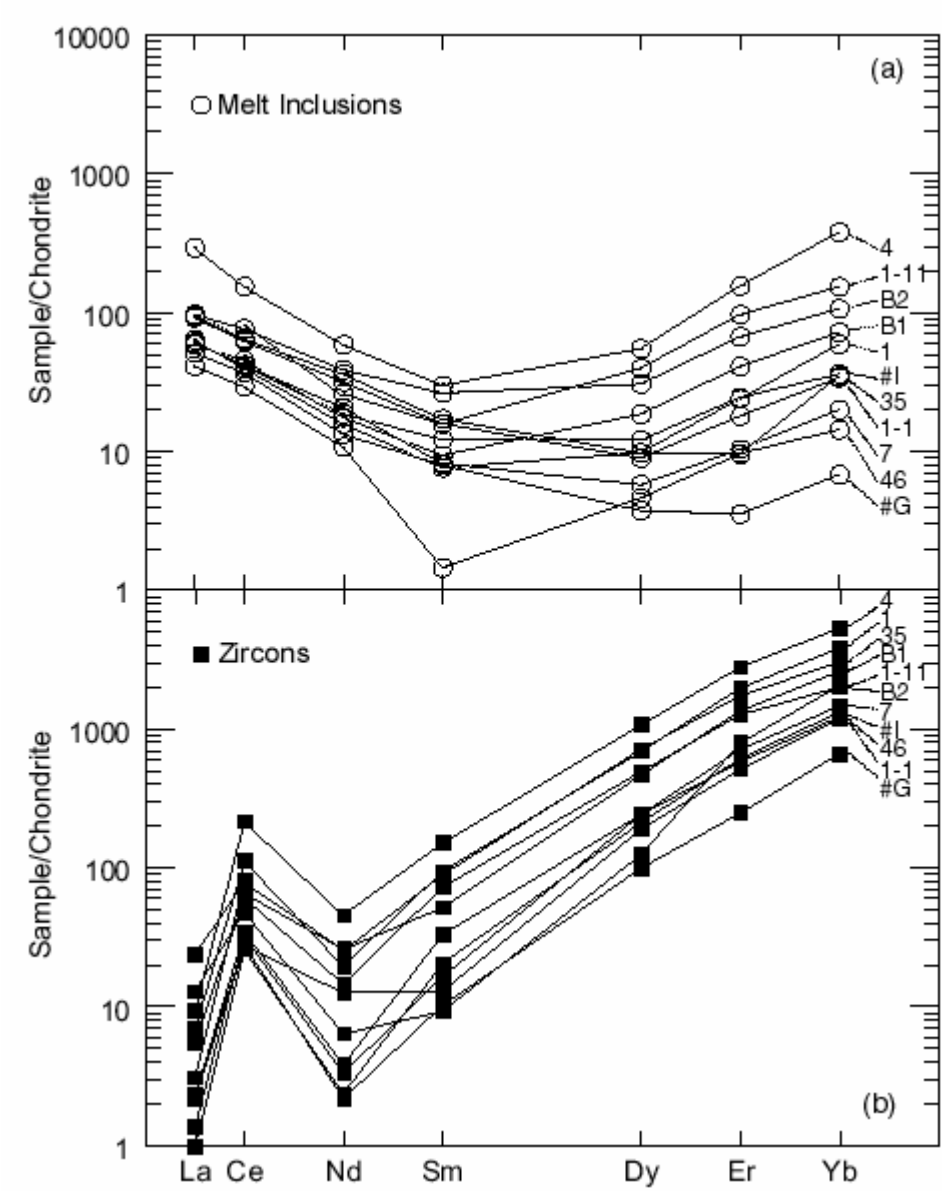

Figure 2.7. Chondrite-normalized concentrations of REE in melt inclusions (a) and host zircons (b). Lines connect data from the same inclusion or zircon. The sample numbers for both melt inclusions and zircon are shown on the right. Data are listed in Tables 2.1 and 2.2.

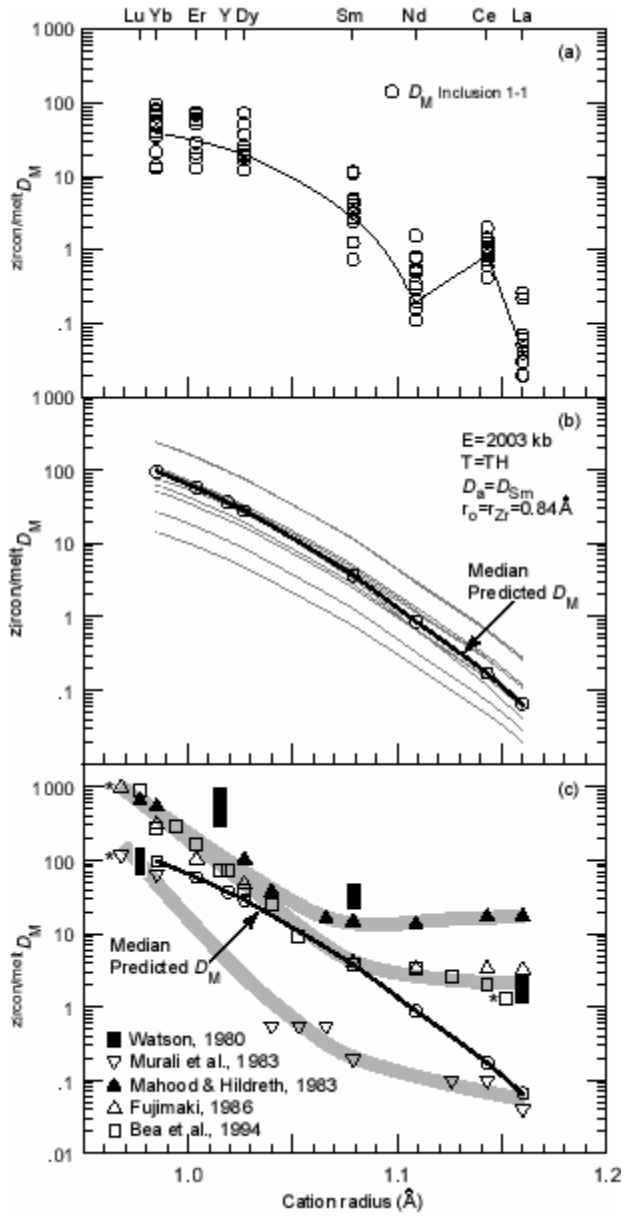

Figure 2.8. (a) Zircon/melt partition coefficients (K_{REE}) calculated from data listed in Tables 2.1 and 2. The calculated values are also listed in Table 2.3. The line connects values for melt inclusion #1-1, showing the expected parabolic trend (see Fig. 2.8b) as well as the significant Ce anomaly. Similar trends are exhibited by the other ten inclusions, but are not shown because the overlap in data makes it difficult to identify lines connecting individual inclusions. (b) K_{REE} predicted by the Brice (1975) equation for rare earth elements and Y calculated from melt inclusion/zircon pairs of this study at a temperature corresponding to the homogenization temperature listed in Table 2.1. The heavy solid line shows the median predicted K_M. (c) Comparison of median predicted K_M vs. cation radius from this study with previously published results. The upper shaded line shows the trend for the data of Mahood and Hildreth (1983), the middle shaded line approximates the trends for the data of Fujimaki (1986) and Bea et al. (1994), and the lower shaded line shows the trend for the data of Murali et al. (1983). Three of the data points (denoted by asterisks) have been offset to the left along the cation radius axis to avoid overlapping of the symbols. Cation radii are from Shannon (1976).

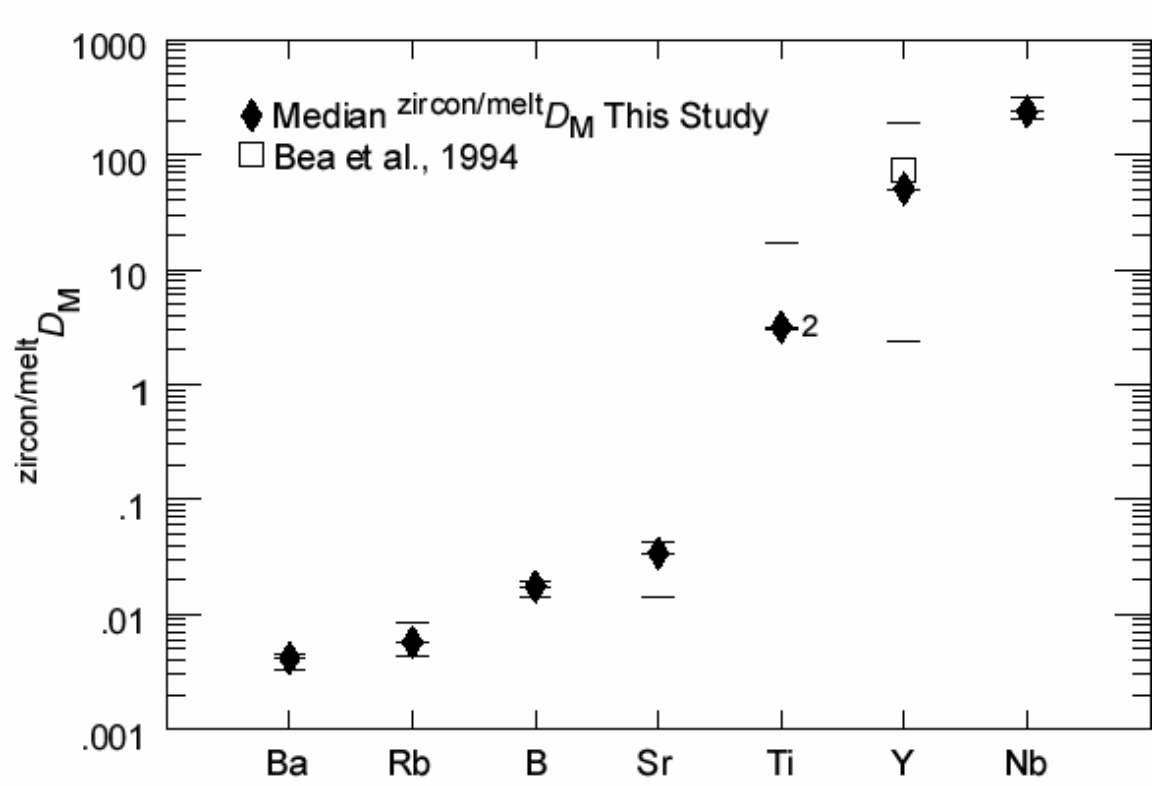

Figure 2.9. K_M for trace elements calculated from zircon/melt inclusion pairs. The elements are plotted in terms of increasing compatibility in zircon. Tic marks indicate individual values, and the "2" adjacent to the tic mark for Ti indicates two data points with overlapping values. Also shown is a single value for K_Y from the literature (Bea et al., 1994).

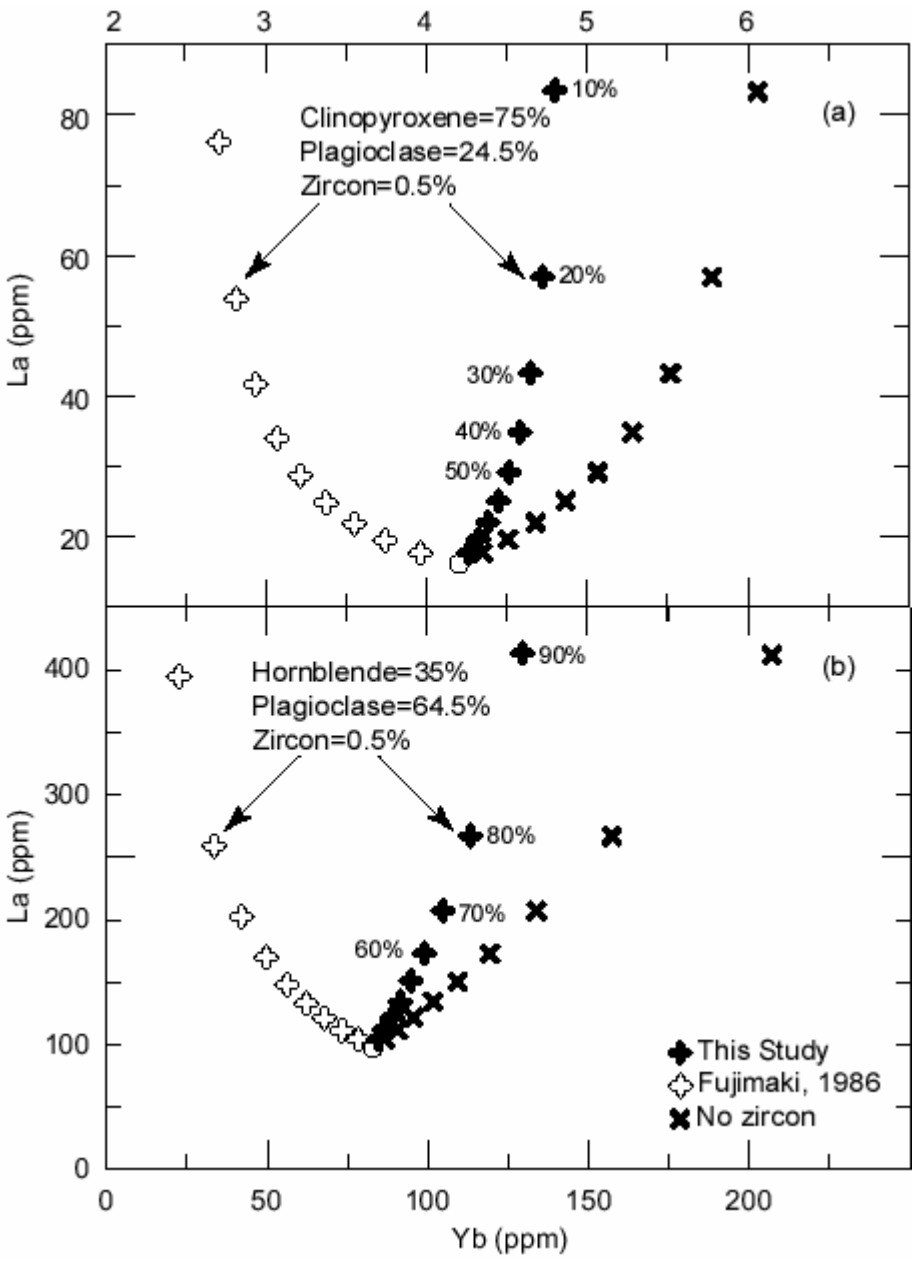

Figure 2.10. Petrogenetic models for (a) batch partial melting (Shaw, 1970) and (b) fractional crystallization showing the effect of variation in K_{La} and K_{Yb} on melt evolution, using values from this study and from Fujimaki (1986). Also shown for comparison are model results without zircon in the residual assemblage for batch partial melting (a) and in the fractionation assemblage for fractional crystallization (b). The numbers next to the model values indicate the mass percent melt generated for partial melting and the mass percent crystallization for fractional crystallization.

CHAPTER 3: THE GEOCHEMISTRY OF MELT INCLUSIONS CONTAINED IN ALLANITE, PLAGIOCLASE, QUARTZ AND ZIRCON: EVALUATING THE ROLE OF BOUNDARY LAYERS ON MELT INCLUSION COMPOSITIONS

Abstract

Melt inclusions (MI) are commonly used to gain insights into magmatic processes because ideally they provide a sample of the melt from which the host crystal grew. However, their use has remained controversial in part due to speculation that MI compositions have been affected by chemical gradients (boundary layers) in the melt caused by growth of the host crystal, and therefore, their compositions might not be representative of the far-field melt. It has been proposed that boundary layers most strongly affect MI when crystal/melt partition coefficients of the host crystal deviate far from unity and that smaller inclusions are more adversely affected than larger inclusions. The potential effects of boundary layer processes on MI compositions was investigated by comparing the compositions of MI ranging from 20 to 120 μm in diameter that were trapped in co-crystallizing host crystals with significantly different trace element partitioning behavior. The major and trace element (Sr and REE) compositions of MI in allanite, plagioclase, quartz and zircon from the 74 ka Youngest Toba Tuff of Sumatra, Indonesia were investigated. If boundary layer processes had affected the MI investigated, then it was expected that the elements most compatible in the host crystals should be depleted in the MI (compared to far-field melt) and that elements incompatible in the hosts should be enriched in the MI. The results show trends opposite to what would be expected had boundary layers affected the MI. Regardless of MI diameter, the MI contain the highest concentrations of elements that are most compatible in the host crystal structure and elements that are incompatible in the host crystal structure are not enriched in the MI. These results indicate that boundary layer processes have not affected MI.

Introduction

One of the main goals of igneous petrology is to gain insights into the processes responsible for geochemical variations observed in magmatic systems. In many cases it is difficult or impossible to obtain pristine samples of melt that represent discrete time intervals removed from a dynamic system because rock samples may be significantly altered during outgassing, eruption and subsequent exposure at the earth's surface. Melt inclusions (MI) provide us with a sample of melt from which the host crystal grew, and most inclusions likely formed over a relatively small interval of time compared even to the duration of host crystal growth. Ideally, MI have remained chemically isolated inside of host crystals. For these reasons, MI are of tremendous petrologic value and have been used extensively to monitor processes that occurred in magma chambers (Anderson, 1972; Anderson, 1974; Hervig, 1992; Sobolev, 1993; Anderson, 1991; Anderson, 2000; Roggensack, 2001; Fedele, 2003). However, it has been shown that MI compositions can be modified by a variety of processes that can be generally described as either pre-entrapment or post-entrapment modification. In such cases, the measured MI

compositions may not be the same as the composition of the melts that existed in the pre-eruptive magma far from the host crystal.

A variety of post-entrapment processes have been investigated. Crystallization of the host crystal onto the MI walls and crystallization of daughter crystals can change the composition of the MI by removing host and daughter crystal components from the inclusion forming melt (e.g., Sobolev, 1975; Kamenetsky, 1997; Nielsen, 1997; Webster, 1991; Manley, 1996). Other studies have shown that diffusive re-equilibration of MI with its host container and/or the external magma (Qin, 1992; Danushevsky, 2000; Gaetani, 2000: Gaetani, 2001) can significantly modify the composition of the original inclusion-forming melt. Cottrell et al. (Cottrell, 2002) recently developed a model that describes diffusive re-equilibration between MI and host crystal, which crystallized during non-equilibrium entrapment conditions. They presumed that compositional heterogeneity observed in some suites of MI may reflect non-equilibrium trapping conditions in which the MI were initially out of equilibrium with the host crystal. That study was concerned with post-entrapment modifications of the inclusion-forming melt, which resulted from pre-entrapment modifications to the melt at the crystal/melt interface. Below I address non-equilibrium pre-entrapment conditions and the potential that MI may be affected by chemical gradients (boundary layers) that develop in the melt during host crystal growth and MI trapping.

The region adjacent to a growing crystal, in which some elements might be enriched or depleted relative to the far-field melt, is referred to as the boundary layer. Chemical differentiation occurs within the boundary layer as compatible elements are depleted in the melt at the crystal/melt interface because they are preferentially incorporated into the crystal, whereas incompatible elements are enriched in the melt because they are excluded from the growing crystal. The size and shape of boundary layers are also dependent upon crystal/melt partition coefficients, chemical mobility in the melt, crystal growth rate and the extent of crystal growth. Crystal growth rates, in turn, might be expected to govern the sizes of MI that form (Roedder, 1984). The scale of boundary layers and their role in affecting MI trace element chemistry is poorly understood.

Boundary layers have been reported in glass surrounding crystals in both natural (Bottinga, 1972; Donaldson, 1975) and synthetic systems (Peterson, 1986; Muncill, 1987; Aoki, 1993). Boundary layer widths in these cases are generally less than ~25 μm. A boundary layer model was invoked (Bacon, 1989) to explain accessory mineral inclusions in major rock-forming minerals. The model suggests that boundary layers may develop in felsic to intermediate composition melts adjacent to growing major rock-forming minerals causing local saturation-nucleation of accessory minerals from a chemically differentiated boundary layer. Such a scenario does provide a plausible explanation for the common occurrence of accessory minerals as solid-phase inclusions in major rock-forming minerals; however, it is unclear whether such a boundary layer process could also have modified the compositions of melts that are eventually enclosed as MI. Other workers have also considered that since MI represent samples of melt that was adjacent to a growing crystal before it was enclosed by the advancing crystal face that they may not

be representative of the far-field melt due to boundary layers in the melt caused by growth of the host crystal (Watson, 1982; Roedder, 1984; Anderson, 2003; Lowenstern, 2003). Lu et al. (Lu, 1995) conducted a detailed study that addressed the significance of boundary layer development on rhyolitic MI compositions and concluded that the effect is negligible for inclusions greater than ~25 μm. They showed that compatible and incompatible trace element variations in rhyolitic Bishop Tuff MI in quartz and sanidine do not vary as would be expected if they had been affected by boundary layer processes. Rather, the geochemical variations observed in the Bishop Tuff MI reflect magma-wide evolution. Even though this study found that the rhyolitic MI studied were not affected by boundary layer processes, the use of MI has remained somewhat controversial because of speculation that their compositions are not representative of the far-field melt. Anderson (Anderson, 2003) suggested that future studies "*should deliberately continue to test for boundary layer effects in various magmatic settings*."

The question addressed in this study is not whether boundary layer processes can affect the composition of a melt adjacent to a growing crystal. But rather, whether boundary layers occur on spatial and temporal scales such that compositions of MI trapped in growing crystals might not represent the composition of the far-field melt. A critical test to determine if boundary layer processes have affected MI would be to investigate the major and trace element compositions of MI that trapped the same melt in several different host crystals with significantly different partitioning behavior for various trace elements. The theoretical development of boundary layers is discussed first to show that they could potentially affect the compositions of MI under certain conditions. Then I consider if measured compositional differences in a suite of MI might be attributable to boundary layer processes by comparing relationships between the compositions of MI with diameters ranging from 20 to 120 μm contained in host crystals with significantly different trace element partitioning behavior. The major, minor and trace element chemistry (rare earth elements (REE) and Sr) of glassy MI in allanite (n=9), plagioclase (n=15), quartz (n=16) and zircon (n=13) from two samples of the rhyolitic 74 ka Youngest Toba Tuff of Sumatra, Indonesia were examined. Matrix glass adhering to zircon crystals was also analyzed. Due to differing partitioning behavior of the four host crystals, this suite of MI is particularly well suited for examination of both pre- and post-entrapment modifications that may cause the MI to deviate significantly from the far-field melt that initially existed. The main goal of this study is to determine the significance of boundary layer processes on measured MI compositions. A separate study will use thi same suite of MI to address post-entrapment processes.

A Theoretical Review of Boundary Layer Development

When a crystal grows from a melt some elements may become enriched or depleted near the growing crystal surface to produce a boundary layer if the dominant mechanism of mass transfer of components towards and away from the crystal surface is diffusion (Albarede, 1972). Convection may disturb the boundary layer allowing unmodified melt from outside the near-crystal environment to replace the boundary layer melt; however, diffusion is probably the dominant mechanism of mass transfer near the crystal/melt interface (Albarede, 1972). As shown schematically in Fig. 3.1a, during

crystal growth compatible elements will diffuse along chemical gradients towards the crystal/melt interface and eventually may be incorporated into the growing crystal. Incompatible elements will diffuse away from the crystal/melt interface as these elements accumulate within the boundary layer (Fig. 3.1a). Smith et al. (Smith, 1955) developed a one dimensional numerical model that describes the development of boundary layers in the melt adjacent to growing crystals as:

$$c_x = c_i \bullet \{1+(q/2K)\exp[-Rx/K] \bullet \mathrm{erfc}[0.5(1/Dt)^{0.5} \bullet (x-Rt)] - 0.5\mathrm{erfc}[0.5(1/Dt)^{0.5}(x+Rt)] + 0.5q/(1/q-1/K) \bullet \exp[-q(R/D)(x+Rt)] \bullet \mathrm{erfc}\{0.5(1/Dt)^{0.5}[x+(2K-1)Rt]\}\} \quad (1)$$

Equation 1 predicts the concentration, c_x, of an element at distance, x, from the crystal/melt interface as a function of its concentration in the melt at infinite distance from the interface, c_i, its diffusivity in the melt, D, the crystal/melt partition coefficient, K, the crystal growth rate, R, and time, t. The size and shape of a boundary layer depends on the interplay between D, K, R and t.

Crystal growth rate can be governed by either supply of essential structural constituents to the crystal surface by diffusion in the melt or by interface kinetics during attainment of rational crystal faces. In natural systems, crystal growth rate is one of the most poorly constrained variables. Reported crystal growth rates range over several orders of magnitude. For example, reported quartz and plagioclase growth rates in silicic melts range from 10^{-6} to 10^{-11} cm/s (Swanson, 1977; Brandeis, 1987; Cashman, 1988) and zircon growth rates range from 10^{-15} to 10^{-19} cm/s (Watson, 1996; Charlier, 2000). Based on the slowest reported zircon growth rates it would take an unrealistically long interval of time to trap a 50 μm inclusion (1.6 Ga). It is likely that MI entrapment occurs during episodes of relatively rapid crystal growth (Roedder, 1984). The following calculations show how boundary layers develop adjacent to a crystal grown at various crystal growth rates.

As an example of the application of Eq. 1 to understanding potential effects of boundary layers on MI compositions, consider the case of La in a system that is precipitating zircon. La is incompatible in the zircon structure (Nagasawa, 1970) and should accumulate to form a boundary layer as it is excluded from a growing zircon crystal. Figure 3.2a shows model results assuming a partition coefficient of 0.1 (Thomas, 2002) and R/D values ranging from 0.0001 to 1000. The model assumes that a crystal must grow at least 50 μm in order to trap an inclusion 50 μm in diameter. The amount of time used in the calculation is that required to precipitate 50 μm of zircon, at the assumed growth rate and ranges from 5×10^{4} to 5×10^{11} s (corresponding to growth rates ranging from 10^{-7} to 10^{-14} cm/s). Due to the wide range in reported crystal growth rates, model calculations were conducted by varying the crystal growth rate with a fixed La diffusivity. The La diffusion rate in the melt (10^{-10} cm^2/s) was calculated from the data of Koepke and Behrens (Koepke, 2001) for melts that contained ~5 wt.% H_2O, assuming a temperature of 780ºC. The temperature is based on the inferred temperature of the Toba Tuff rhyolitic melt (Beddoe-Stephens, 1983; Newman, 1989; Chesner, 1998) and the water content is similar to values determined from melt inclusions in crystals of the

Youngest Toba Tuff (Newman, 1989). In order to obtain an R/D value of 1000 based on a La diffusivity of ~10^{-10} cm^2/s, a zircon would had to have grown 500 μm in 0.01 y, which corresponds to a growth rate of ~10^{-7} cm/s. This value is eight orders of magnitude faster than the fastest zircon growth rate reported (Watson, 1996) and serves to provide a 'worst case' scenario for the development of boundary layers in melts adjacent to growing zircon crystals. Calculations using smaller R/D values (i.e., slower growth rates or faster diffusivities) yield shallower gradients (Fig. 3.2a) that are less enriched above c_i at the crystal/melt interface and no boundary layer is predicted by Eq. 1 when reported zircon growth rates are used.

Equation 1 was also used to model depletion of compatible elements adjacent to a growing crystal as shown schematically in Fig. 3.1b. As previously recognized (Bacon, 1989), profiles for compatible elements as predicted by Eq. 1 extend to unrealistically large distances away from the crystal/melt interface, especially when R/D values are small. For example, the predicted La concentration gradient adjacent to an allanite crystal for an R/D of 0.0001 (La diffusivity of 10^{-10} cm^2/s), an ${}^{\text{allanite/melt}}K_{\text{La}}$ of 3650, a c_i=30 ppm La and the amount of time required to grow 50 μm of crystal, yielded a boundary layer that extended ~12 cm from the allanite/melt interface!

To examine the relationship of inclusion size and boundary layers, profiles corresponding to different amounts of crystal growth were calculated. It was assumed that correspondingly less crystal growth would be required to trap a smaller inclusion and more crystal growth would be required to trap a larger inclusion. If crystal growth proceeds at a constant rate, more time would be required to enclose large inclusions compared to smaller ones. Concentration gradients for the incompatible element La after 50 μm of zircon growth, corresponding to the minimum amount of growth necessary to trap a 50 μm melt inclusion, are shown on Fig. 3.2a. Figure 3.2b shows concentration gradients that would develop after 10, 50 and 100 μm of crystal growth calculated using an R/D value of 100. For comparison, the gradient for the 50 μm inclusion shown on Fig. 3.2a is included. The model calculations indicate that the boundary layer becomes more enriched in incompatible elements with increasing crystal growth. Therefore, larger inclusions should have higher concentrations of incompatible elements than smaller inclusions because more crystal growth is required to trap larger inclusions (Fig. 3.2b). Likewise, for compatible elements larger inclusions should contain melt that is more depleted than the melt contained in smaller inclusions. It should be noted that the observation that compositions of larger inclusions are enriched or depleted to a greater extent by boundary layer processes than smaller inclusions trapped from melt with the same c_i disagrees with some previous work (Anderson, 1974; Anderson, 2003).

Based on the boundary layer model outlined above, boundary layers have the greatest potential to affect the compositions of melt inclusions when:

(1) a large amount of crystal growth accompanies inclusion formation (larger inclusions affected more than smaller inclusions)
(2) the crystal growth rate is high (e.g., rapid cooling) relative to the diffusive transport of components in the melt (i.e., large R/D)

(3) the crystal melt partition coefficients for elements of interest deviate far from unity

Sample Description and Methods

Samples

Chesner (Chesner, 1998) divided the Youngest Toba Tuff into two groups based on whole rock geochemistry. Sample T87 is from a "high-SiO_2" group containing >73 wt% SiO_2 and sample T89A2 is from a "low-SiO_2" group containing <73 wt% SiO_2. Further descriptions of the Toba Tuff samples and petrogenetic interpretations are given in Chesner (Chesner, 1988) and Chesner (Chesner, 1998). Solid inclusions of each host crystal occur in one another. For example, zircon crystals can be found in allanite and inclusions of allanite can be found in zircon (Fig. 3.3). Similar petrographic relations are found in all the host crystals studied here and petrographic observations suggest that all four host crystals were co-crystallizing from the melt. Quartz occurs in both T87 and T89A2 but only quartz-hosted MI from T87 were analyzed.

The MI range from 20-120 μm and are randomly distributed throughout host crystals, which range from ~50-1000 μm. A variety of MI morphologies occur and range from rounded to elongate to negative-crystal forms, but most inclusions are round to slightly ovoid. Two inclusions in zircon have hourglass shapes (Anderson, 1991) that are connected to the crystal exterior by a small capillary; therefore, they may have gained or lost components prior to quenching. Melt inclusions in allanite, quartz and zircon usually contain only one shrinkage bubble, whereas some MI in plagioclase contain several bubbles. The analyzed inclusions in all host crystals, except those in quartz, are composed entirely of glass. All MI in quartz contain small acicular to dendritic daughter crystals of augite (identified by electron microprobe in unheated MI exposed at the surface) in addition to glass (Fig 3.4), and therefore required heating to produce a homogeneous glass prior to analysis. After determining the homogenization temperature (950°C) by step heating in a one atmosphere vertical furnace, all quartz-hosted MI were heated to 950ºC in a single step and held at temperature for five minutes prior to quenching. The daughter crystals in a quartz-hosted MI also melted at 950ºC when heated using a microscope mounted heating stage and a slower heating rate (10°C/min). Additional details regarding techniques for homogenizing MI are given in Thomas et al. (Thomas, 2002).

Analytical methods

Crystals containing homogeneous glass MI were mounted in epoxy and ground/polished to expose the glass inclusion at the surface using the method of Thomas and Bodnar (Thomas, 2002 #29). Major and minor element compositions (P, Si, Zr, Ti, Al, Mg, Ca, Mn, Fe, Na, K, F, Cl) of MI and host minerals were determined at Virginia Tech by electron probe microanalysis using a Cameca SX-50 microprobe. Trace element abundances (La, Ce, Nd, Sm, Dy, Er, Yb and Sr) were measured by secondary ion mass spectrometry using a Cameca IMS 3f ion microprobe at Woods Hole Oceanographic

Institution. Details of analytical protocols are listed in Thomas et al. (Thomas, 2002) (and references therein). Following ion probe analysis, the gold coat was removed and the analytical spots were examined with a petrographic microscope to confirm that the ion beam was entirely within the MI.

Results

During homogenization of the quartz-hosted MI, the shrinkage bubble disappeared before the daughter crystals of augite completely melted at 950ºC (Fig. 3.4). Beddoe-Stephens et al. (Beddoe-Stephens, 1983) found similar homogenization temperatures for quartz-hosted MI from the Youngest Toba Tuff, but believed that this temperature was higher than the actual formation temperature by ~150ºC (also see (Chesner, 1998)).

The MI and matrix glass are rhyolitic with SiO_2 contents ranging from 70.5 to 78.8 wt.% (Fig. 3.5; Tables 3.1 and 3.2). Melt inclusions hosted in allanite, plagioclase (An_{36-56}) and zircon have overlapping major element compositions and there are no discernable differences between the MI compositions from T87 and T89A2 even though they have different whole rock compositions (Table 3.1). Electron probe totals for the MI range from 93.4 to 100 wt.% (except one value at 91.8 wt.% and another at 91.9 wt.%), and differences from 100% are predominantly due to water (and other volatiles) in the glass. This interpretation is consistent with results of Newman and Chesner (Newman, 1989), who found 4.9-5.7 wt.% H_2O in MI from similar samples of the Youngest Toba Tuff. MI in quartz have lower SiO_2 and higher contents of all other major and minor elements compared to MI contained in the other host crystals (Fig. 3.5).

Partition coefficients ($^{crystal/melt}K_M$, where the subscript M refers to the element of interest) for Sr and REE were calculated using the melt inclusion-mineral technique (Thomas, 2002; Lu, 1992; Sobolev, 1996) which is based on analysis of the MI (Tables 3.1 and 3.2) and the immediately adjacent host mineral (Appendix A). Results are shown on Fig. 3.6 and listed in Tables 3.3 and 3.4. Partition coefficients determined using the melt inclusion-mineral technique are similar to previously published values (Thomas, 2002; Lu, 1992; Chesner, 1989; Sawka, 1984; Nash, 1985). Two hourglass inclusions in zircon (T87-Z-88 h.g. and T89A2-Z-39 h.g.; Table 3.3) yielded higher partition coefficients for Er and Yb that are more similar to values obtained from matrix glass adhering to the zircon crystals (T89A2-Z-36 m.g., T89A2-Z-38 m.g. and T89A2-Z-42 m.g.; Table 3.4) than those determined for other MI.

The salient features of the results are summarized as follows:

(1) Sr concentrations of MI hosted by plagioclase are not depleted relative to Sr contents of MI hosted in allanite, quartz and zircon (Fig. 3.7a).
(2) La abundances of MI in allanite are not depleted compared to La concentrations of MI in plagioclase, quartz and zircon (Fig. 3.7b).
(3) Except for hourglass inclusions, Yb is higher in the zircon-hosted MI compared to MI in allanite, plagioclase and quartz (Fig. 3.7c).

(4) The MI in quartz have lower SiO_2, Sr and most REE than MI in the other host crystals (Figs. 3.5, 3.7, 3.8).
(5) MI compositions do not vary as a function of MI diameter (Fig. 3.8).

The results summarized above indicate that incompatible trace elements are not enriched in the MI, and compatible trace elements are not depleted in MI. Rather, for a given trace element, concentrations appear to be highest in MI hosted in crystals in which that element is most compatible. These results are opposite of trends predicted by the boundary layer model as described by Eq. 1 (Figs. 3.1 and 3.2).

Discussion

Model results as described by Eq. 1 and shown in Fig. 3.2 indicate that boundary layers that may result from growth of host crystals could cause MI compositions to deviate significantly from the far-field melt composition. Below, the results of MI analyses are discussed with the conception that if boundary layer processes were significant, then evidence of them should be evident in the analyses of MI contained in this suite of host crystals that have significantly different partition coefficients. First, I consider the possibility that the lower SiO_2 contents of the MI in quartz may result from the existence of a boundary layer depleted in SiO_2 surrounding quartz crystals. Next I consider how MI contained in the different host crystals may be affected by boundary layer processes as a function of their trace element partitioning behavior. I then assess MI compositions as a function of inclusion size because larger MI should be more strongly affected by boundary layer processes than smaller inclusions. Finally, other processes that may have affected the compositions of MI are briefly discussed.

Major element evidence that boundary layer processes affected quartz-hosted MI?

Solid-phase petrographic relationships of all host crystals suggests co-crystallization, however, only MI contained in allanite, plagioclase and zircon have overlapping major element compositions. The lower SiO_2 contents in the quartz-hosted MI could be interpreted as evidence that a boundary layer depleted in SiO_2 developed adjacent to the growing quartz crystals. However, if SiO_2 was depleted near the crystal/melt interface by boundary layer formation during growth of host quartz crystals, then we would also expect to see enrichment of the trace elements analyzed in those same inclusions because all trace elements analyzed are incompatible in quartz (Fig. 3.6). Similarly, crystallization of quartz host crystal onto inclusion walls would also cause the trace element concentrations to increase in the MI. However, the MI contained in quartz actually contain lower concentrations of the trace elements analyzed, compared to the inclusions in the other host crystals. Our favored interpretation is that the melt originally trapped in the quartz-hosted MI initially contained lower trace element concentrations (see below), compared to the melt trapped in the other inclusions. And, the low SiO_2 contents are due to post-entrapment crystallization of quartz onto the inclusion walls that was not re-melted during homogenization. Next we briefly address the post-entrapment process of host crystallization and a mass-balance correction that was applied to only the

MI in quartz. A detailed investigation is beyond the scope of the present manuscript and will be presented elsewhere.

Melt inclusion compositions may be changed by crystallization of the host crystal onto the walls of the MI and by crystallization of daughter crystals from the inclusion-forming melt. Both of these compositional modifications may occur during cooling/quenching of the MI (Skirius,1990; Manley, 1996) and can modify the composition of the melt within the inclusion by removing host and daughter crystal components from the melt within the inclusion. Manley (Manley, 1996) homogenized rhyolitic MI in quartz crystals from the Badlands lava flow of southwestern, Idaho that had textures ranging from coarse-grained to glassy as found. He suggested the coarse-grained inclusions resulted from slow cooling and that finer-grained and glassy inclusions resulted from relatively faster cooling. Both fine- and coarse-grained inclusions homogenized to clear glass during laboratory heating. However, electron microprobe analyses revealed that coarse-grained MI did not regain all the SiO_2 that precipitated onto the inclusion walls during post-entrapment crystallization, even after prolonged runs above the homogenization temperature (see also(Skirius, 1990).

We suggest that a similar mechanism of SiO_2 depletion affected the quartz-hosted MI from the Toba Tuff. The analyzed inclusions contained in allanite, plagioclase and zircon do not show any petrographic or geochemical evidence of post-entrapment crystallization, possibly because the amount of host that can crystallize is limited due to the low concentrations of essential structural constituents in the melt that are necessary for host crystallization. The trends displayed by MI contained in allanite, plagioclase and zircon are opposite to trends that would result from host crystal crystallization onto the inclusion walls. However, we suggest that the lower SiO_2 contents and higher contents of all other major and minor elements (compared to the MI in other host crystals) in the quartz-hosted MI (Fig. 3.5) are due to post-entrapment crystallization of the host. Further evidence of host crystallization is that the quartz-hosted MI contain small daughter crystals of augite that we interpret to have grown from the melt within the inclusion, possibly due to depletion of SiO_2 as quartz crystallized onto the inclusion walls.

Based on the arguments stated above for crystallization of quartz onto the inclusion walls, we adjusted the major, minor and trace element compositions of the MI in quartz for post-entrapment crystallization using the calculations of Webster and Duffield (Webster, 1991). The average SiO_2 contents of the MI contained in the other host crystals is 75.85 wt.% and the average SiO_2 of the quartz-hosted MI is 72.71 wt.%. This difference in SiO_2 indicates that the difference between the quartz-hosted MI and those contained in the other host crystals can be accounted for by failure to re-melt 13% quartz from the inclusion walls during the five minute homogenization runs. Complete homogenization and restoration of the original inclusion-forming melt composition was assumed when daughter crystals and shrinkage bubbles dissolved to yield a single phase homogeneous glass. The small amount of host quartz crystallized onto the inclusion walls would not be easily recognized, even before homogenization. For example, in a 50 μm diameter MI 11.5% of the volume is contained in the outer one micron of the

inclusion radius. The adjusted quartz-hosted MI major element compositions overlap the major element compositions of the MI contained in the other host crystals (Fig. 3.5). The correction of the quartz-hosted MI compositions for quartz crystallized onto the inclusion walls decreases the trace elements by a maximum of 14 ppm (usually <10 ppm) for trace elements with the highest concentrations, in inclusions with the lowest SiO_2 by 'dilution' of the melt with essentially pure SiO_2.

Based on overlapping major element compositions and the occurrence of inclusions of the host minerals in one another (Figs. 3.3 and 3.5), we suggest that allanite, plagioclase, quartz and zircon co-crystallized from a melt of similar major element composition, but not necessarily contemporaneously. The similarity of the major element compositions of the MI contained in this suite of crystals indicates that boundary layer processes did not affect the major element compositions. Next we examine the potential effects of boundary layer processes on the trace element contents of MI.

Trace element evidence against boundary layer effects

According to the model presented above in Section 2 and assuming that boundary layer processes have affected MI compositions, they should be manifested as a function of: (1) host crystal partition coefficient, and (2) MI size. Below we first consider the results of MI trace element compositions as a function of host crystal partition coefficient followed by consideration of trace element compositions as a function of MI size.

There are relatively minor but distinct differences in MI compositions, which vary as a function of host crystal. However, the observed variations are opposite of what would be expected if boundary layers had affected the compositions of the MI. Specifically, the MI are enriched in trace elements that are most compatible (Fig. 3.6) in the host crystal structure. Melt inclusions in plagioclase have the highest concentrations of Sr (Fig. 3.7a), MI in allanite have the highest La concentrations (Fig. 3.7b), and MI in zircon have the highest concentrations of Yb (Fig. 3.7c). Quartz does not partition any of the trace elements measured, but the MI in quartz contain lower abundances of all the trace elements analyzed (Figs. 3.7 and 3.8; Table 3.1). However, if boundary layer processes had affected the MI, then the MI in plagioclase would have the lowest Sr and the highest concentrations of the REE analyzed. Similarly, boundary layer processes should cause strong depletion of La in allanite-hosted MI and La enrichment in MI in zircon, plagioclase and quartz. We do not observe depletion of La in the allanite-hosted MI, and we do not observe La enrichment in MI hosted by the other crystals (Figs. 3.7 and 3.8). Ranges of Sr and La concentrations are similar and overlapping in all the MI regardless of their host partition coefficients. Zircon partitions the middle through heavy REE and excludes all other trace elements analyzed. However, the Yb contents in the zircon-hosted MI are higher than those found in the other host crystals (Fig. 3.7c) and the other incompatible trace elements are not enriched in the zircon-hosted MI. If a boundary layer process had affected the MI contained in these four host crystals, then a negative correlation should exist between a trace element and its partition coefficient (see inset on Fig. 3.7b), and this is not observed. Thus, the MI in the four host crystals do not

show the variation expected based on the known partitioning behavior, if boundary layer processes were operating at the scale of MI.

Now that we have shown that the MI do not display compositional characteristics expected to occur based on trace element partitioning behavior, we will next explore MI size versus compositional variations. As described above in the section outlining the boundary layer model and shown on Fig. 3.2b, the largest inclusions should contain melt that experienced the greatest amount of crystal growth because of the greater amount of crystal needed to enclose larger inclusions. As such, larger MI should be more affected by boundary layer processes than smaller MI. If boundary layer processes had affected MI, the largest inclusions in allanite should contain the lowest concentrations of La, the largest inclusions in plagioclase should contain the lowest concentrations of Sr and the largest inclusions in zircon should contain the lowest concentrations of Yb. Similarly, the largest MI in zircon, plagioclase and quartz should have the highest La concentrations. None of these trends are observed when trace element concentrations are plotted as a function of inclusion size (Fig. 3.8). The largest MI investigated are not compositionally different from smaller inclusions.

Possible mechanisms that could cause the 'enriched compositions'

Compositions of MI discussed above do not vary as would be expected if they had been affected by boundary layer processes. A separate manuscript will address potential post-entrapment modifications experienced by this suite of MI. Here we briefly suggest that the MI contain the highest concentrations of the elements that are most compatible in the host crystal structure due to combined processes of:

(1) Trapping of melts that were not homogeneous in trace element compositions suggesting that the melt within the magma chamber may have been compositionally heterogeneous, with respect to the trace elements. The trace element compositions of MI trapped in the four different host crystals may reflect this heterogeneity.
(2) Dissolution and re-precipitation of the host crystal along the inclusion walls during attainment of its lowest interfacial free energy shape through "inclusion maturation" as discussed by Manley (Manley, 1996).
(3) Diffusive re-equilibration of the melt inclusion with the host crystal and/or external melt (Cottrell, 2002). The elements that may sustain the greatest extent of diffusive re-equilibration in MI are those elements that have high crystal/melt partition coefficients and those with high diffusivities in the crystal lattice of the host crystal (Cherniak, 1997; Dahl, 1997).

The first possibility indicates that the distinct trace element variations as a function of host crystal may be the result of compositional heterogeneity of the melt within the magma chamber. Even though the major element compositions appear to be fairly homogenous, trace element compositions may have been 'enriched' in the vicinity of growing crystals in which they were compatible. This interpretation suggests that the melt contained domains locally enriched in elements that were compatible in the host crystal. The 'enrichment' displayed by the MI is at the ppm scale and thus is not

apparent in the major element compositions. Specifically, the melts from which the host crystals precipitated may have contained high concentrations of highly compatible trace elements that are most similar in ionic radius and charge to the essential structural constituents required for host crystal growth, and the MI are samples of this 'enriched' melt. In the case of plagioclase, the compatible element Sr is most similar in ionic radius and charge to the essential structural constituent Ca compared to the other trace elements analyzed. In zircon, Yb is the most compatible element analyzed and it is closest in ionic radius and charge to the essential structural constituent Zr. Quartz does not incorporate any of the trace elements analyzed and the melts from which it precipitated contained the lowest concentrations of all the elements analyzed.

In support of "inclusion maturation" it is important to note that the MI in zircon with the lowest concentrations of Yb are hourglass shaped inclusions. This suggests that the attainment of the lowest interfacial free energy shape of the MI through solution and re-precipitation along the inclusion walls that occurs as the inclusion 'matures' may be an important process that affects the trace element compositions of MI. It is difficult to predict how complex trace element zoning of the host crystal could change MI compositions as the inclusion changes shape. We also suggest that as inclusions change shape during attainment of lower interfacial energy, that the rate at which compositions of MI are modified through diffusive re-equilibration may also change (enhanced?). Cottrell et al. (Cottrell, 2002) showed that the elements with the highest partition coefficients in the host crystal and high diffusivity in the host crystal were the elements that were most readily modified in the MI. Post-entrapment diffusive re-equilibration as described by Cottrell et al. (Cottrell, 2002) may certainly have affected the compositions of MI contained in plagioclase, quartz and possibly allanite. Diffusive exchange between a MI and its host crystal tends to reduce compositional variations amongst MI, especially for elements that are highly compatible in the host crystal. However, even though the zircon/melt partition coefficients are relatively high for the heavy REE in zircon, the low trace element diffusivities for trace elements in zircon (Cherniak, 1997; Dahl, 1997) precludes diffusive re-equilibration as a likely explanation for the observed higher concentrations of the most compatible elements in the zircon-hosted MI. Furthermore, the MI in zircon display the highest degree of compositional variation most likely because zircon is one of the best host containers due to its low ionic porosity (Dahl, 1997), especially for the heavy REE.

Conclusions

Geochemical evidence from MI contained in allanite, plagioclase, quartz and zircon indicates that boundary layer enrichment ($^{crystal/melt}K_M < 1$) or depletion ($^{crystal/melt}K_M > 1$) did not affect the 20 to 120 μm diameter MI studied here. In accordance with Lu et al. (Lu, 1995), we suggest that boundary layer development did not affect the MI investigated in this study, possibly because the rate of crystal growth was slow relative to diffusive transport of elements in the melt. As such, the concentrations of the major and trace elements in the inclusion-forming melt near the crystal surface were not significantly modified by growth of the host crystal. Based on these findings, we conclude that MI ≥20 μm represent melts from which the host crystals grew and were not

modified by boundary layer processes. This does not preclude that the compositions of MI smaller than 20 μm or larger than 120 μm may be affected by boundary layers. The finding that the MI contain the *highest* concentrations of the elements that are *most* compatible in the host crystal indicates that processes other than boundary layer development must have affected the melt inclusions investigated here.

References

Albarede, F., and Bottinga, Y. (1972) Kinetic disequilibrium in trace element partitioning between phenocrysts and host lava. Geochimica et Cosmochimica Acta, 36, 141-156.

Anderson, A.T., Jr. (1974) Evidence for a picritic, volatile-rich magma beneath Mt. Shasta, California. Journal of Petrology, 15, 243-267.

Anderson, A.T., Jr. (1991) Hourglass inclusions: Theory and application to the Bishop rhyolitic tuff. American Mineralogist, 76, 530-547.

Anderson, A.T., Jr. (2003) Melt (glass ± crystals) inclusions. In I. Samson, A. Anderson, and D. Marshall, Eds. Fluid Inclusions: Analysis and Interpretation, 32, p. 300. Mineralogical Association of Canada, Ottawa.

Anderson, A.T., Jr., Davis, A.M., and Lu, F. (2000) Evolution of the Bishop Tuff Rhyolite magma based on melt and magnetite inclusions and zoned phenocrysts. Journal of Petrology, 41, 449-473.

Anderson, A.T., Jr., and Wright, T.L. (1972) Phenocrysts and glass inclusions and their bearing on oxidation and mixing in basaltic magmas, Kilauea, Hawaii. American Mineralogist, 57, 188-216.

Aoki, Y., and Iyatomi, N. (1993) Concentration gradients in CaAl2Si2O8 melt near the crystals-melt interfac. Neues Jahrbuch fur Mineralogie: Monatshefte, 8, 374-384.

Bacon, C.R. (1989) Crystallization of accesory phases in magmas by local saturation adjacent to phenocrysts. Geochimica et Cosmochimica Acta, 53, 1055-1066.

Beddoe-Stephens, B., Aspden, J.A., and Shepherd, T.J. (1983) Glass inclusions and melt compositions of the Toba Tuffs, northern Sumatra. Contributions to Mineralogy and Petrology, 83, 278-287.

Brandeis, G., and Jaupert, C. (1987) The kinetics of nucleation and crystal growth and scaling laws for magmatic crystallization. Contributions to Mineralogy and Petrology, 96, 24-34.

Cashman, K.V. (1988) Crystallization of Mount St. Helens 1980-1986 dacite; a quantitative textural approach. Bulletin of Volcanology, 50, 194-209.

Charlier, B., and Zellmer, G. (2000) Some remarks on U-Th mineral ages from igneous rocks with prolonged crystallization histories. Earth and Planetary Science Letters, 183, 457-469.

Cherniak, D.J., Hanchar, J.M., and Watson, E.B. (1997) Rare-earth element diffusion in zircon. Chemical Geology, 134, 289-301.
Chesner, C.A. (1988) The Toba Tuffs and caldera complex, Sumatra, Indonesia: insights into magma bodies and eruptions. Geology, p. 428. Michigan Technological University, Houghton.

Chesner, C.A. (1998) Petrogenesis of the Toba Tuffs, Sumatra, Indonesia. Journal of Petrology, 39, 397-438.

Chesner, C.A., and Ettlinger, A.D. (1989) Composition of volcanic allanite from the Toba Tuffs, Sumatra, Indonesia. American Mineralogist, 74, 750-758.

Cottrell, E., Spiegelman, M., and Langmuir, C.H. (2002) Consequences of diffusive reequilibration for the interpretation of melt inclusions. Geochemistry, Geophysics, Geosystems, 5, 1-26.

Dahl, P.S. (1997) A crystal-chemical basis for Pb retention and fission-track annealing systematics in U-bearing minerals, with implications for geochronology. Earth and Planetary Science Letters, 150, 277-290.

Danushevsky, L.V., Della-Pasqua, F.N., and Sokolov, S. (2000) Re-equilibration of melt inclusions trapped by magnesian olivine phenocrysts from subduction-related magmas. Contributions to Mineralogy and Petrology, 138, 68-83.

Donaldson, D.H. (1975) Calculated diffusion coefficients and the growth rate of olivine in a basalt magma. Lithos, 8, 163-174.

Fedele, L., Bodnar, R.J., DeVivo, B., and Tracy, R. (2003) Melt inclusion geochemistry and computer modeling of trachyte petrogenesis at Ponza, Italy. Chemical Geology, 194, 81-104.

Gaetani, G.A., and Watson, E.B. (2000) Open system behavior of olivine-hosted melt inclusions. Earth and Planetary Science Letters, 183, 27-41.

Gaetani, G.A., and Watson, E.B. (2002) Modeling the major-element evolution of olivine-hosted melt inclusions. Chemical Geology, 183, 25-41.

Hervig, R.L., and Dunbar, N.W. (1992) Cause of chemical zoning in the Bishop (California) and Bandelier (New Mexico) magma chambers. Earth and Planetary Science Letters, 111, 97-108.

Kamenetsky, V.S., Crawford, A.J., Eggins, S., and Muhe, R. (1997) Phenocryst and melt inclusion geochemistry of near-axis seamounts, Valu Fa Ridge, Lau Basin: insight into mantle wedge melting and the addition of subduction components. Earth and Planetary Science Letters, 151, 205-223.

Koepke, J., and Behrens, H. (2001) Trace element diffusion in andesitic melts: an application of syncrotron X-ray fluorescence analysis. Geochimica et Cosmochimica Acta, 65, 1481-1498.

Lowenstern, J.B. (2003) Studies of melt inclusions prove critical to understanding the behavior of volatiles in volcanic systems. In B. DeVivo, and R.J. Bodnar, Eds. Melt Inclusions in Volcanic Systems: Method, Applications and Problems, 5, p. 1-21. Elsevier, Amsterdam.

Lu, F., Anderson, A.T., Jr., and Davis, A.M. (1995) Diffusional gradients at the crystal/melt interface and their effect on the compositions of melt inclusions. Journal of Geology, 103, 591-597.

Lu, F., Anderson, A.T., Jr., Davis, A.M., and Anonymous. (1992) New and larger sanidine/melt partition coefficients for Ba and Sr as determined by ion microprobe analyses of melt inclusions and their sanidine host crystals. Abstracts with Programs - Geological Society of America, 24, p. 44.

Manley, C.R. (1996) Morphology and maturation of melt inclusions in quartz phenocrysts from the Badlands rhyolite lava flow, southwestern Idaho. American Mineralogist, 81, 158-168.

Muncill, G.E., and Lasaga, A.C. (1987) Crystal growth kinetics of plagioclase in igneous systems: one atmosphere experiments and application of a simplified growth model. American Mineralogist, 72, 299-311.

Nagasawa, H. (1970) Rare earth concentrations in zircons and apatites and their host dacites and granites. Earth and Planetary Science Letters, 9, 359-364.

Nash, W.P., and Crecraft, H.R. (1985) Partition coefficients for trace elements in silicic magmas. Geochimica et Cosmochimica Acta, 49, 2309-2322.

Newman, S., and Chesner, C.A. (1989) Volatile compositions of glass inclusions from the 75Ka Toba Tuff, Sumatra. Abstracts with Programs - Geological Society of America, 21, p. 271.

Nielsen, T.F.D., Solovova, I.P., and Veksler, I.V. (1997) Parental melts of melilitolite and origin of alkaline carbonatite: evidence from crystallized melt inclusions, Gardiner Complex. Contributions to Mineralogy and Petrology, 126, 331-344.

Peterson, J.S., and Lofgren, G.E. (1986) Lamellar and patchy intergrowths in feldspar: experimental crystallization of eutectic systems. American Mineralogist, 71, 343-355.

Qin, Z., Lu, F., and Anderson, A.T., Jr. (1992) Diffusive reequilibration of melt and fluid inclusions. American Mineralogist, 77, 565-576.
Roedder, E. (1984) Fluid Inclusions. 644 p. Mineralogical Society of America, Washington D.C.

Roggensack, K. (2001) Sizing up crystals and their melt inclusions; a new approach to crystallization studies. Earth and Planetary Science Letters, 187, 221-237.

Sawka, W.N., Chappell, B.W., and Norrish, K. (1984) Light-rare-earth-element zoning in sphene and allanite during granitoid fractionation. Geology, 12, 131-134.

Skirius, C.M., Peterson, J.S., and Anderson, A.T., Jr. (1990) Homogenizing rhyolitic glass inclusions from the Bishop Tuff. American Mineralogist, 75, 1381-1398.

Smith, V.G., Tiller, W.A., and Rutter, J.W. (1955) A mathematical analysis of solute re-distribution during crystallization. Canadian Journal of Physics, 33, 723-744.

Sobolev, A.V., Migdisov, A.A., and Portnyagin, M.V. (1996) Incompatible element partitioning between clinopyroxene and basaltic liquid revealed by study of melt inclusions in minerals from Troodos Lavas, Cyprus. Petrology, 4, 307-317.

Sobolev, A.V., and Shimizu, N. (1993) Ultra-depleted primary melt included in an olivine from the Mid-Atlantic Ridge. Nature, 363, 151-154.

Sobolev, V.S., and Kostyuk, V.P. (1975) Magmatic crystallization based on a study of melt inclusions. Fluid Inclusion Research, 9, 182-253.

Swanson, S.E. (1977) Relation of nucleatin and crystal growth-rate to the development of granitic textures. American Mineralogist, 62, 966-978.

Thomas, J.B., and Bodnar, R.J. (2002) A technique for mounting and polishing melt inclusions in small (<1 mm) crystals. American Mineralogist, 87, 505-508.

Thomas, J.B., Bodnar, R.J., Shimizu, N., and Sinha, A.K. (2002) Determination of zircon/melt trace element partition coefficients from SIMS analysis of melt inclusions in zircon. Geochimica et Cosmochimica Acta, 66, 2887-2901.

Watson, E.B. (1996) Dissolution, growth and survival of zircons during crustal fusion: kinetic principles, geologic models and implications for isotopic inheritance. Transactions of the Royal Society of Edinburgh, Earth Sciences, 87, 43-56.

Watson, E.B., Sneeringer, M.A., and Ross, A. (1982) Diffusion of dissolved carbonate in magmas: experimental results and applications. Earth and Planetary Science Letters, 61, 346-358.

Webster, J.D., and Duffield, W.A. (1991) Volatiles and lithophile elements in Taylor Creek rhyolite: constraints from glass inclusion analysis. American Mineralogist, 76, 1628-1645.

Table 3.1. Melt inclusion analyses

Sample	T87												
Host Crystal	Allanite							Plagioclase					
MI #	A-31	A-77	A-78	A-80	A-83	A-85	A-86	P-13	P-15	P-69	P-70	P-72	P-75
P_2O_5 (wt.%)	n.d.	0.07	0.09	0.02	n.d.	n.d.	n.d.	0.14	0.24	n.d.	n.d.	n.d.	n.d.
SiO_2	76.17	75.29	73.38	75.49	72.10	74.80	74.77	77.24	74.84	77.80	77.87	77.42	75.83
ZrO_2	n.d.	n.d.	n.d.	n.d.	n.d.	n.d.	0.03	0.02	n.d.	n.d.	n.d.	n.d.	0.04
TiO_2	0.08	0.10	0.07	0.09	n.d.	0.05	0.1	0.07	0.1	0.14	0.03	0.12	0.02
Al_2O_3	12.13	11.53	10.87	11.67	11.80	11.41	11.78	12.55	10.77	12.35	12.19	12.35	12.1
MgO	n.d.	0.01	n.d.	0.04	0.01	n.d.	0.02	0.04	0.08	0.07	0.12	0.08	0.04
CaO	0.38	0.83	0.65	0.79	0.55	0.55	0.66	0.97	0.87	1.07	1.06	0.86	0.83
MnO	0.18	0.06	n.d.	n.d.	n.d.	n.d.	0.06	n.d.	n.d.	0.04	0.02	n.d.	0.08
FeO_t	0.2	0.4	0.22	0.86	0.26	0.35	0.86	1.11	0.46	1.08	1.05	1.06	1.14
Na_2O	3.16	2.45	2.43	2.64	2.72	2.49	2.43	2.97	3.01	2.92	2.69	2.68	2.36
K_2O	4.59	4.63	4.29	4.5	4.43	4.98	4.6	4.71	4.13	4.62	4.88	4.68	4.68
F	n.d.	0.02	0.16	0.03	0.13	0.04	n.d.	n.d.	n.d.	0.19	0.13	0.17	n.d.
Cl	0.13	0.23	0.14	0.13	0.08	0.09	0.06	0.11	0.14	0.09	0.13	0.14	0.13
Total	96.86	95.31	91.9	96.05	91.8	94.6	95.29	99.79	94.48	99.99	99.82	99.15	97.10
Sr (ppm)	21.03	26.66	20.41	30.88	20.61	10.65	27.64	48.8	62.42	56.66	53.47	51.64	41.45
La	42.57	46.95	50.23	19.02	45.41	65.82	29.26	26.46	24.99	31.47	27.23	22.28	16.54
Ce	98.59	80.53	104.92	38.06	100.6	131.61	55.54	48.65	44.85	57.29	29.7	41.55	31.96
Nd	20.43	17.63	24.92	8.76	23.62	25.58	11.95	11.18	9.21	13.18	10.99	8.96	9.29
Sm	4.09	2.55	4.61	1.86	4.28	2.91	2.38	2.24	1.76	2.2	1.59	1.21	1.97
Dy	5.08	2.41	5.59	1.66	5.36	1.36	2.0	1.81	1.05	1.76	1.65	1.42	2.55
Er	2.31	1.62	2.79	1.4	2.68	0.92	1.37	1.29	0.82	1.21	1.08	0.78	1.66
Yb	1.96	1.36	2.26	1.65	2.19	1.57	1.67	1.27	0.56	1.01	0.99	0.82	1.64
size (μm)	86	51	35	65	45	55	50	78	120	78	100	51	50

n.d. = element not detected
n.a. = element not analyzed
$FeO_t = FeO+Fe_2O_3$
h.g. = hourglass shaped melt inclusion

Table 3.1 (*Continued*).

Sample	T87												
Host Crystal	*Quartz												
MI #	Q-1	Q-8	Q-10	Q-16	Q-21	Q-22	Q-23	Q-24	Q-26	Q-28	Q-29	Q-30	Q-31
P_2O_5 (wt.%)	n.d.	0.12	n.d.	0.04	0.05	n.d.	n.d.	n.d.	0.04	0.07	n.d.	n.d.	0.09
SiO_2	75.03	75.47	76.23	75.23	76.03	76.77	76.27	77.93	75.24	75.1	76.34	76.08	75.66
ZrO_2	0.02	n.d.	0.03	n.d.	n.d.	0.03	0.04	n.d.	n.d.	0.05	0.01	0.02	0.02
TiO_2	0.07	0.06	n.d.	0.05	0.05	0.08	0.05	0.1	0.13	0.05	0.04	n.d.	0.1
Al_2O_3	11.79	11.28	11.01	11.74	11.43	11.84	10.34	11.43	11.59	12.53	11.84	12.3	11.07
MgO	0.04	0.06	n.d.	0.05	0.07	0.02	0.03	0.04	0.01	0.04	0.04	0.04	0.06
CaO	0.87	0.71	0.51	0.82	0.8	0.94	0.65	0.82	0.39	0.84	0.73	0.73	0.69
MnO	0.02	n.d.	0.1	0.03	n.d.	0.04	0.08	0.08	0.04	0.1	0.08	0.08	0.14
FeO_t	0.72	0.9	0.62	0.63	0.63	0.68	0.73	0.91	0.65	0.77	0.82	0.41	0.64
Na_2O	3.35	3.21	3.07	3.38	3.13	3.36	2.32	3.4	2.88	3.67	3.61	3.58	3.14
K_2O	4.18	4.45	4.26	4.36	4.16	4.05	3.65	4.52	4.67	4.44	4.36	4.47	4.22
F	n.d.	0.03	0.03	n.d.	0.05	0.17	0.14	n.d.	0.06	n.d.	0.03	n.d.	0.11
Cl	0.18	0.12	0.14	0.17	0.14	0.11	0.17	0.17	0.14	0.12	0.17	0.18	0.15
Total	96.05	96.22	95.79	96.28	96.3	97.7	94.06	99.19	95.58	97.64	97.83	97.65	95.74
Sr (ppm)	14.65	14.83	0.7	13.57	6.35	15.22	6.89	13.82	8.59	9.55	3.46	10.04	13.38
La	11.95	4.3	24.77	5.89	6.5	9.08	6.52	17.16	10.05	10.49	12.56	3.93	34.34
Ce	24.49	7.96	56.19	12.38	13.15	18.25	13.23	37.59	18.45	22.07	30.13	8.05	73.81
Nd	7.59	2.42	21.58	3.09	3.69	5.27	3.93	9.85	5.55	5.65	10.2	2.24	21.26
Sm	2.01	0.9	7.06	1.11	1.06	1.19	1.4	3.0	1.81	1.67	2.25	0.46	5.29
Dy	1.98	1.32	7.32	1.06	1.16	1.42	1.38	3.45	2.05	1.67	3.64	0.92	4.22
Er	1.28	1.02	3.56	0.9	0.91	0.87	1.04	2.39	1.18	1.15	2.18	0.61	1.87
Yb	1.36	0.78	4.02	0.98	1.0	1.0	1.11	2.75	1.99	1.40	2.87	0.99	1.92
size (μm)	35	48	45	27	35	23	27	30	37	24	29	23	31

*Quartz hosted MI have been corrected for 13% post-entrapment host crystallization (see text)

Table 3.1 (*Continued*).

Sample	T87								T89A2				
Host Crystal	Quartz		Zircon						Allanite		Plagioclase		
MI #	Q-33	Q-41	Z-16	Z-18	Z-23	Z-101	Z-104	Z-88hg	A-56	A-72	P-1	P-2	P-5
P_2O_5 (wt.%)	n.d.	n.d.	n.d.	0.05	0.24	0.11	0.1	n.d.	0.1	0.17	n.d.	n.d.	n.d.
SiO_2	75.91	74.4	78.75	77.11	77.7	75.56	77.89	74.94	74.69	75.52	77.48	76.39	75.75
ZrO_2	0.02	n.d.	n.d.	n.d.	n.d.	0.05	0.05	n.d.	0.03	0.09	0.04	n.d.	n.d.
TiO_2	n.d.	0.09	0.03	0.04	0.01	0.01	0.03	0.03	0.06	0.03	0.05	0.09	n.d.
Al_2O_3	11.22	11.03	11.42	10.19	11.74	11.6	11.87	11.48	12.07	12.25	11.98	12.0	12.61
MgO	0.04	0.04	0.05	0.03	0.1	0.03	0.05	n.d.	0.04	0.09	0.08	0.12	0.03
CaO	0.61	0.88	0.68	0.39	0.79	0.63	0.74	0.86	0.49	0.53	0.98	0.99	0.94
MnO	0.03	0.01	0.06	0.06	0.08	0.01	n.d.	0.04	n.d.	n.d.	n.d.	n.d.	0.14
FeO_t	0.62	0.93	0.62	0.02	0.64	0.2	0.76	0.29	1.16	1.46	1.07	0.94	0.95
Na_2O	4.06	3.24	2.81	3.02	2.87	1.33	2.75	2.43	2.91	2.9	2.84	2.92	2.92
K_2O	3.94	4.2	4.37	4.14	4.31	3.85	4.49	4.61	4.31	4.0	4.5	4.49	4.56
F	n.d.	0.04	0.03	0.02	0.23	n.d.	0.03	n.d.	0.23	0.03	n.d.	0.02	0.03
Cl	0.15	0.1	0.11	0.1	0.13	0.1	0.14	0.12	0.39	0.11	0.12	0.12	0.11
Total	96.43	94.78	98.75	95.02	98.35	93.35	98.69	94.66	95.68	97.01	98.98	97.91	97.86
Sr (ppm)	9.36	45.46	26.72	12.84	23.97	22.30	13.63	23.27	21.65	27.98	38.67	40.59	47.44
La	10.64	44.23	17.24	9.39	15.66	12.62	13.86	14.24	46.2	34.22	27.83	26.89	30.44
Ce	22.32	92.78	37.27	19.25	31.43	27.43	28.97	26.79	74.05	62.85	50.69	46.45	55.7
Nd	6.09	27.04	10.71	4.3	8.11	6.11	7.94	5.57	20.2	16.99	11.74	10.98	13.63
Sm	2.58	5.81	2.52	1.11	2.46	1.42	1.41	1.87	4.49	4.27	1.42	1.79	1.94
Dy	1.92	4.42	5.77	3.3	4.73	5.57	3.58	1.62	4.05	1.75	1.66	1.65	1.74
Er	1.55	2.42	8.37	5.43	7.53	11.4	6.95	1.16	2.51	1.42	0.89	1.19	1.35
Yb	1.76	2.64	12.7	13.16	16.31	20.08	14.02	2.27	3.03	0.99	1.12	1.37	1.76
size (μm)	34	33	35	46	29	31	55	55	70	50	50	33	51

Table 3.1 (*Continued*).

Sample	T89A2												
Host Crystal	Plagioclase						Zircon						
MI #	P-6	P-7	P-8	P-9	P-10	P-26	Z-12	Z-45	Z-47	Z-50	Z-52	Z-59	Z-39h.g.
P_2O_5 (wt.%)	0.45	0.24	0.18	0.08	0.15	0.07	n.d.	0.03	0.07	0.22	0.1	0.29	0.19
SiO_2	74.61	73.61	76.65	74.01	75.93	76.58	77.94	74.94	73.49	75.63	76.84	75.19	76.22
ZrO_2	n.d.	n.d.	n.d.	n.d.	n.d.	n.d.	n.d.	n.d.	0.02	n.d.	n.d.	0.04	0.09
TiO_2	0.66	0.31	0.21	0.06	0.05	0.1	0.07	0.08	0.1	0.1	0.11	0.07	0.09
Al_2O_3	12.47	12.71	12.35	12.76	12.24	11.8	12.59	11.9	11.69	11.88	12.66	11.56	12.3
MgO	0.1	0.1	0.09	0.05	0.08	0.01	0.06	0.02	0.08	0.03	0.02	0.04	0.16
CaO	1.15	1.06	1.01	1.16	0.93	0.9	0.97	0.1	1.36	1.03	0.26	0.34	0.87
MnO	n.d.	0.13	0.11	0.1	0.02	0.18	0.16	0.1	0.13	n.d.	n.d.	0.09	n.d.
FeO_t	0.96	1.11	1.05	0.92	1.0	1.07	1.07	0.44	0.88	0.71	0.27	0.47	0.67
Na_2O	2.63	2.55	3.04	2.77	2.51	1.87	2.62	3.7	2.75	2.83	4.77	1.4	3.02
K_2O	3.97	4.23	4.32	4.13	4.16	4.68	4.52	3.91	3.61	3.73	3.01	5.76	4.43
F	0.06	n.d.	0.12	n.d.	n.d.	n.d.	n.d.	0.03	n.d.	n.d.	0.07	0.05	n.d.
Cl	0.13	0.14	0.13	0.19	0.14	0.1	0.1	0.12	0.15	0.11	0.13	0.17	0.11
Total	96.94	96.0	98.92	96.0	97.04	97.23	99.98	95.18	94.14	96.12	97.99	95.18	98.0
Sr (ppm)	78.76	61.97	59.26	75.08	40.67	66.71	26.42	54.33	69.73	63.4	55.48	59.87	27.39
La	40.56	34.86	40.76	28.09	25.01	24.61	28.91	33.55	45.57	36.92	28.22	38.18	20.21
Ce	75.72	64.02	71.16	54.46	47.95	45.17	57.38	63.0	84.36	73.91	52.48	59.53	36.74
Nd	15.11	15.94	16.31	13.22	12.14	11.4	16.91	13.34	18.97	16.91	11.35	11.69	13.93
Sm	3.03	2.95	2.62	2.57	1.85	4.01	3.88	4.58	4.23	3.42	1.86	2.2	2.86
Dy	1.8	2.24	1.71	2.88	1.32	2.59	1.09	5.74	14.49	5.09	4.45	5.23	2.58
Er	0.91	1.49	1.19	1.72	0.95	1.54	10.3	7.32	21.19	5.51	7.78	5.44	1.63
Yb	1.56	1.48	1.43	2.35	1.25	1.93	15.73	9.85	42.81	7.43	17.38	9.17	1.62
size (μm)	20	55	81	38	29	30	50	58	20	20	29	25	41

Table 3.2. Analyses of matrix glass adhered to zircon crystals

Sample	T89A2		
	Z-36 m.g.	Z-38 m.g.	Z-42 m.g.
P_2O_5 (wt.%)	n.d.	n.d.	0.06
SiO_2	77.45	77.24	77.32
ZrO_2	0.09	0.13	n.d.
TiO_2	0.1	0.08	0.06
Al_2O_3	12.37	12.56	12.27
MgO	0.09	0.08	0.04
CaO	0.96	0.89	0.89
MnO	0.11	0.01	0.01
FeO_t	1.0	0.97	0.98
Na_2O	2.87	2.5	3.17
K_2O	3.99	4.54	4.23
F	n.a.	n.a.	n.a.
Cl	n.a.	n.a.	n.a.
Total	99.02	99.0	99.02
Sr (ppm)	62.11	64.69	63.4
La	37.28	41.72	39.89
Ce	65.65	80.48	69.96
Nd	16.53	18.5	15.29
Sm	3.67	6.69	2.79
Dy	3.07	3.62	1.8
Er	1.45	2.81	1.35
Yb	1.59	3.26	1.4

m.g. = matrix glass
Other abbreviations are the same as in Table 3.1.

Table 3.3. Partition coefficients (K_M) calculated from trace element concentrations of melt inclusions (Table 3.1) and host minerals

	Sample T87								
Host Crystal		K_{Sr}	K_{La}	K_{Ce}	K_{Nd}	K_{Sm}	K_{Dy}	K_{Er}	K_{Yb}
Allanite	A-31	7.631	3635	2295	2090	915.4	159.3	205.8	133.6
	A-77	3.979	2921	2562	2421	1700	394.1	285.7	240.7
	A-78	0.894	2512	2105	2291	1730	330.1	218.1	281.1
	A-80	3.476	6737	5317	4866	2464	629.0	325.2	203.3
	A-83	3.719	2984	2163	2088	1337	242.7	199.3	212.2
	A-85	2.020	1945	1652	2079	2378	1207.3	646.2	361.4
	A-86	5.812	4776	3736	3405	1640	430.5	342.8	164.9
Plagioclase	P-13	11.25	0.562	0.384	0.266	0.278	0.530	0.278	0.050
	P-15	7.964	0.445	0.292	0.234	1.609	0.187	0.548	0.196
	P-69	9.685	0.434	0.307	0.233	0.233	0.119	0.288	0.141
	P-70	10.26	0.430	0.464	0.170	0.363	0.126	0.357	0.189
	P-72	8.851	0.455	0.280	0.211	0.345	0.140	0.414	0.301
	P-75	9.287	0.689	0.449	0.336	0.278	0.089	0.209	0.035
Quartz	Q-10	0.172	0.003	0.004	0.007	0.015	0.011	0.007	0.015
Zircon	Z-16	0.168	0.112	0.789	0.256	1.626	15.60	22.76	27.91
	Z-18	0.221	0.205	0.674	0.411	4.291	11.78	20.28	16.51
	Z-23	0.174	0.037	0.563	0.104	0.987	14.28	20.24	17.70
	Z-101	0.442	0.426	1.345	0.764	5.263	41.79	38.21	32.13
	Z-104	0.360	0.031	0.826	0.122	2.517	29.49	33.56	39.92
	Z-88 h.g.	0.125	0.009	0.563	0.755	4.719	84.11	221.7	242.43

Abbreviations are the same as in Table 3.1.

Table 3.3 (*Continued*).

	Sample T89A2								
Host Crystal		K_{Sr}	K_{La}	K_{Ce}	K_{Nd}	K_{Sm}	K_{Dy}	K_{Er}	K_{Yb}
Allanite	A-56	3.745	3101	3070	2577	1326	356.7	237.2	174.1
	A-72	3.244	4202	3582	3063	1348	867.9	427.7	517.1
Plagioclase	P-1	13.315	0.539	0.355	0.238	0.090	0.043	0.274	0.083
	P-2	9.621	0.596	0.452	0.355	0.432	0.191	0.568	0.270
	P-5	10.81	0.496	0.340	0.271	0.323	0.000	0.823	0.011
	P-6	8.235	0.372	0.244	0.177	0.043	0.039	0.432	0.013
	P-7	9.085	0.381	0.259	0.174	0.142	0.124	0.279	0.036
	P-8	8.621	0.354	0.268	0.182	0.213	0.263	0.180	0.024
	P-9	7.084	0.576	0.439	0.268	0.189	0.075	0.256	0.018
	P-10	11.69	0.512	0.319	0.172	0.279	0.000	0.201	0.016
	P-26	6.594	0.351	0.238	0.315	0.548	0.099	0.393	0.115
Zircon	Z-12	0.108	0.035	0.286	0.240	1.321	90.48	19.27	29.74
	Z-45	0.048	0.001	0.547	0.659	3.812	49.47	63.85	86.27
	Z-47	0.042	0.001	0.544	0.182	1.262	8.815	11.75	12.90
	Z-50	0.060	0.001	0.422	0.098	1.517	22.03	45.78	85.82
	Z-52	0.140	0.018	0.902	0.091	2.608	23.41	29.65	37.44
	Z-59	0.240	0.251	0.506	0.465	1.277	14.49	27.58	36.77
	Z-39 h.g.	0.105	0.007	0.742	0.710	2.225	68.59	187.4	459.7

Table 3.4. Partition coefficients (K_M) calculated from trace element concentrations of matrix glass (Table 3.1) and adjacent zircon

	Sample T89A2								
Host Crystal		K_{Sr}	K_{La}	K_{Ce}	K_{Nd}	K_{Sm}	K_{Dy}	K_{Er}	K_{Yb}
Zircon	Z-36 m.g.	0.091	0.007	1.289	0.376	3.437	125.8	516.9	1303
	Z-38 m.g.	0.073	0.009	0.676	0.317	2.026	51.48	144.8	280.7
	Z-42 m.g.	0.050	0.007	0.468	0.735	7.581	202.4	410.7	700.7

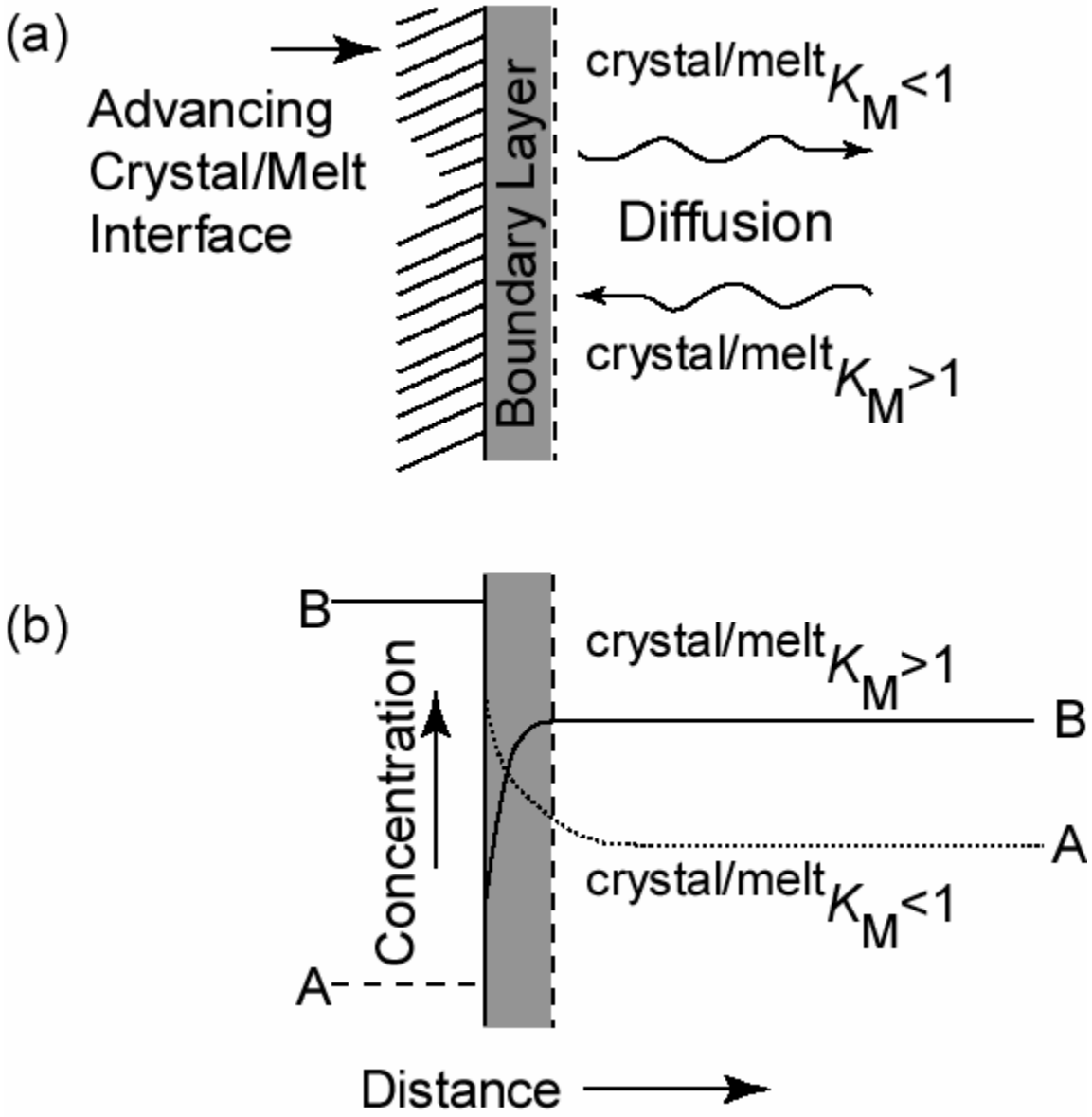

Figure 3.1. Schematic diagrams showing (a) diffusion of incompatible elements away from and compatible elements towards an advancing crystal/melt interface causing (b) development of a boundary layer as incompatible elements accumulate and compatible elements are depleted in the melt adjacent to a growing crystal.

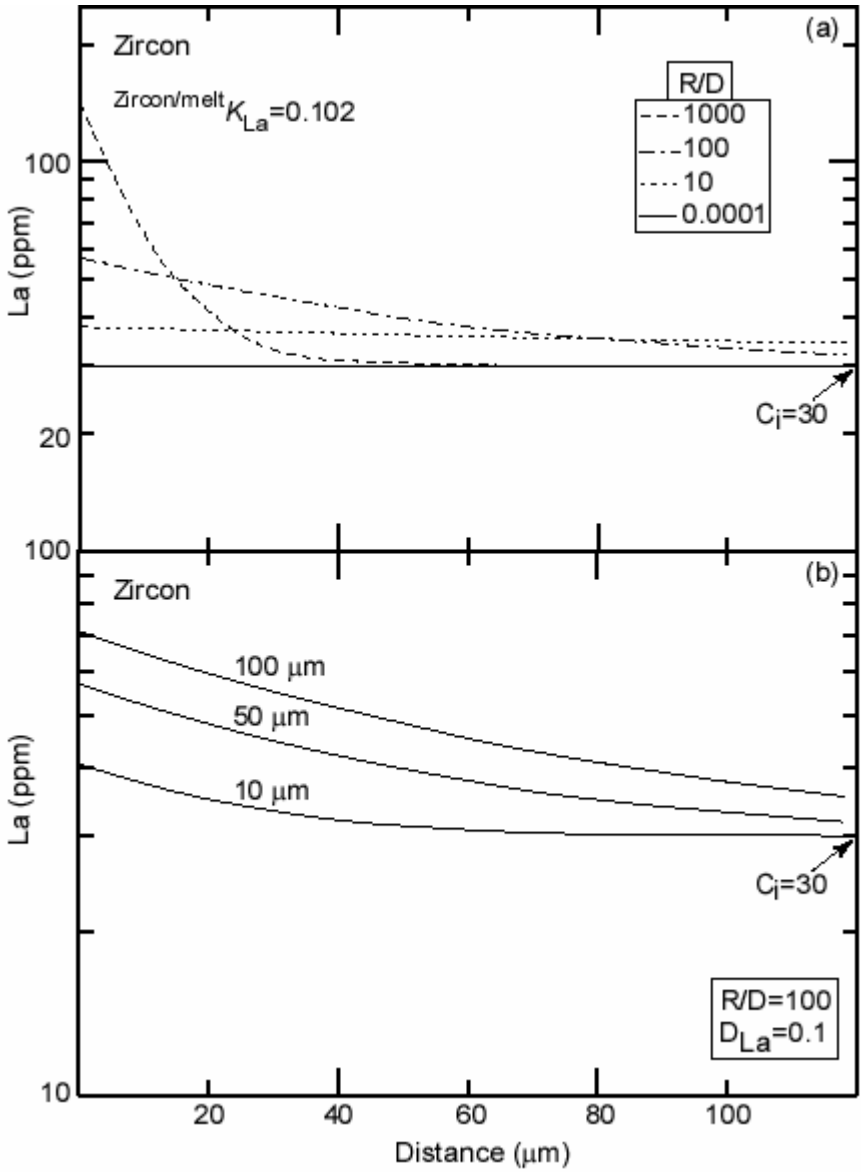

Figure 3.2. Boundary layer profiles obtained from one-dimensional modeling (using Equation 1) of La accumulation adjacent to a growing zircon crystal (a) for variable crystal growth rate to diffusion rate values (R/D) and (b) after 10, 50, and 100 μm of zircon growth necessary to enclose melt inclusions of these sizes using R/D=100. For example, a crystal must grow at least 100 μm to enclose a 100 μm melt inclusion.

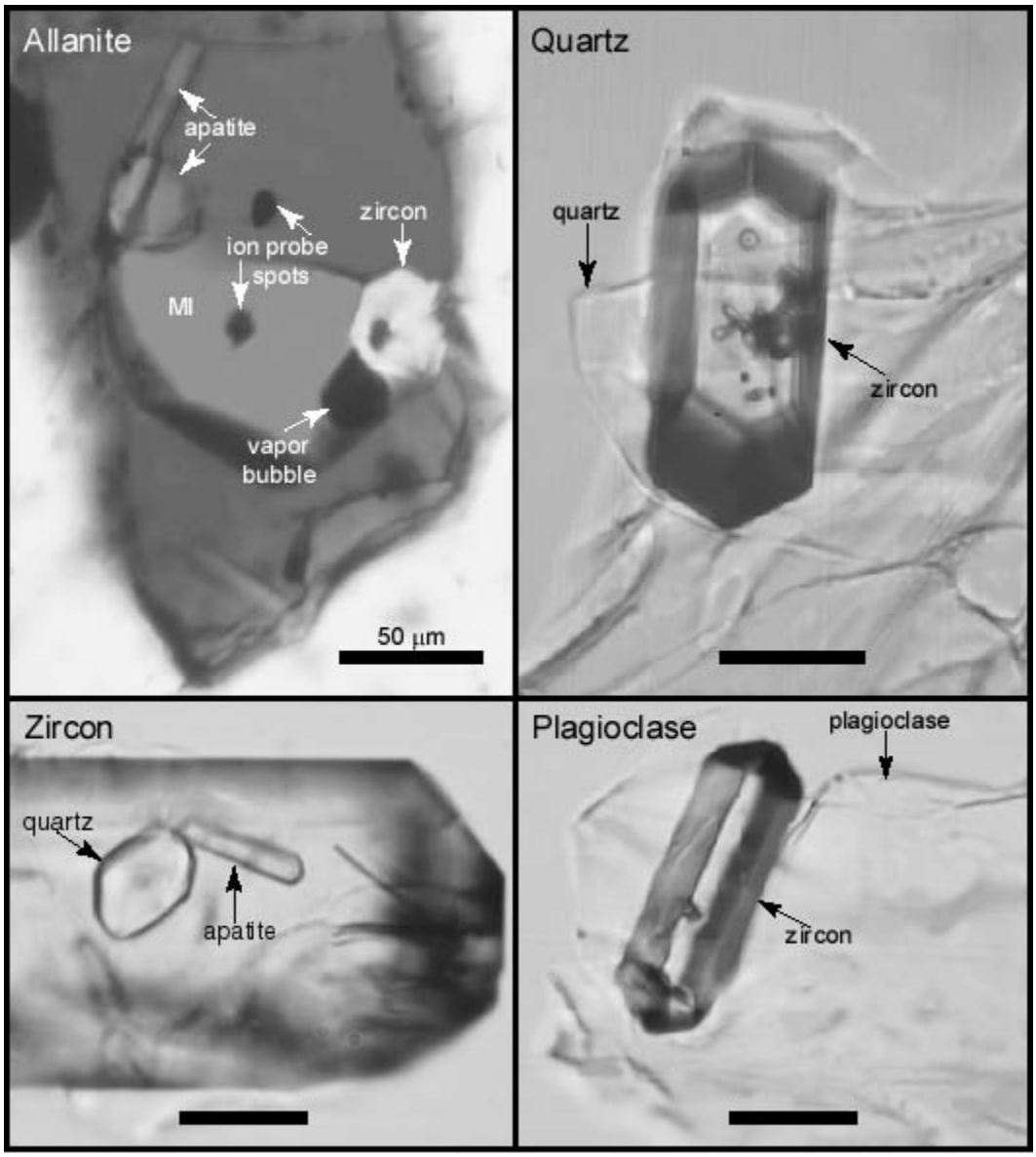

Figure 3.3. Transmitted light photographs showing solid inclusions of each of the host crystals contained in one another. All scale bars are 50 μm.

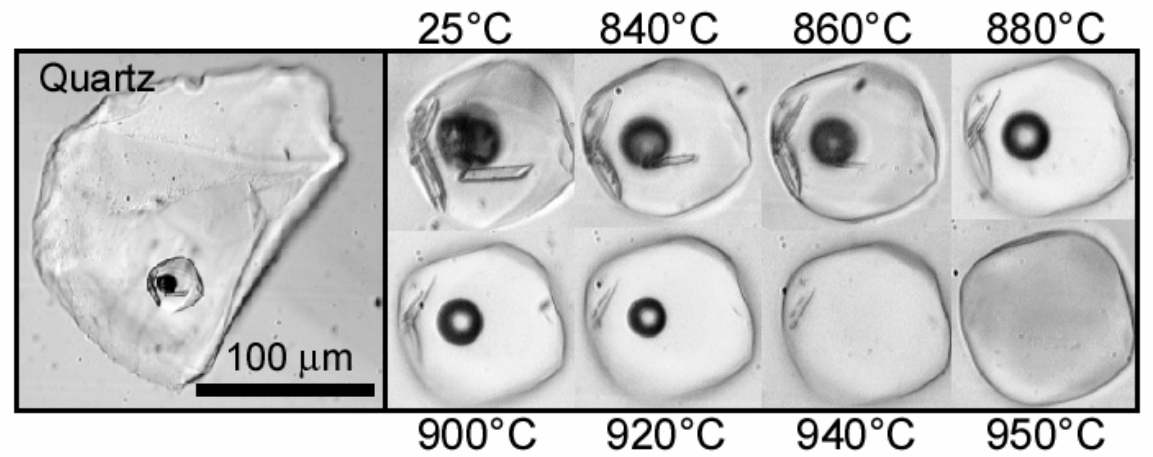

Figure 3.4. Transmitted light photographs of a quartz crystal containing a melt inclusion composed of glass, an augite daughter crystal and a vapor bubble. The series of photographs (right) show the same inclusion at higher magnification as the daughter crystals of augite and the vapor bubble continually decrease in size with each heating step until complete homogenization at 950˚C.

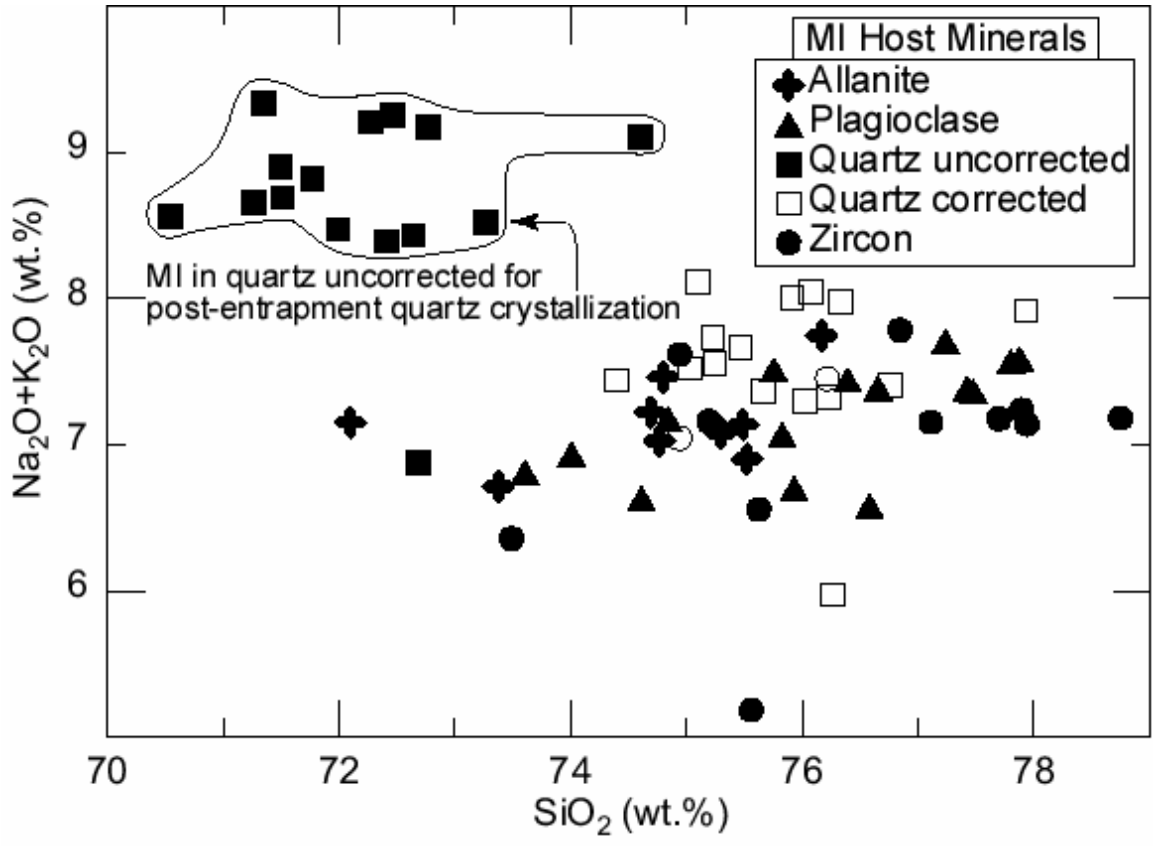

Figure 3.5. Variation diagram showing Na_2O+K_2O versus SiO_2 (wt.%) for melt inclusions. The quartz hosted melt inclusions were corrected for post-entrapment crystallization (13%) of quartz onto the inclusion walls. See text for details of correction. Two open circle symbols are for hourglass inclusions contained in zircon.

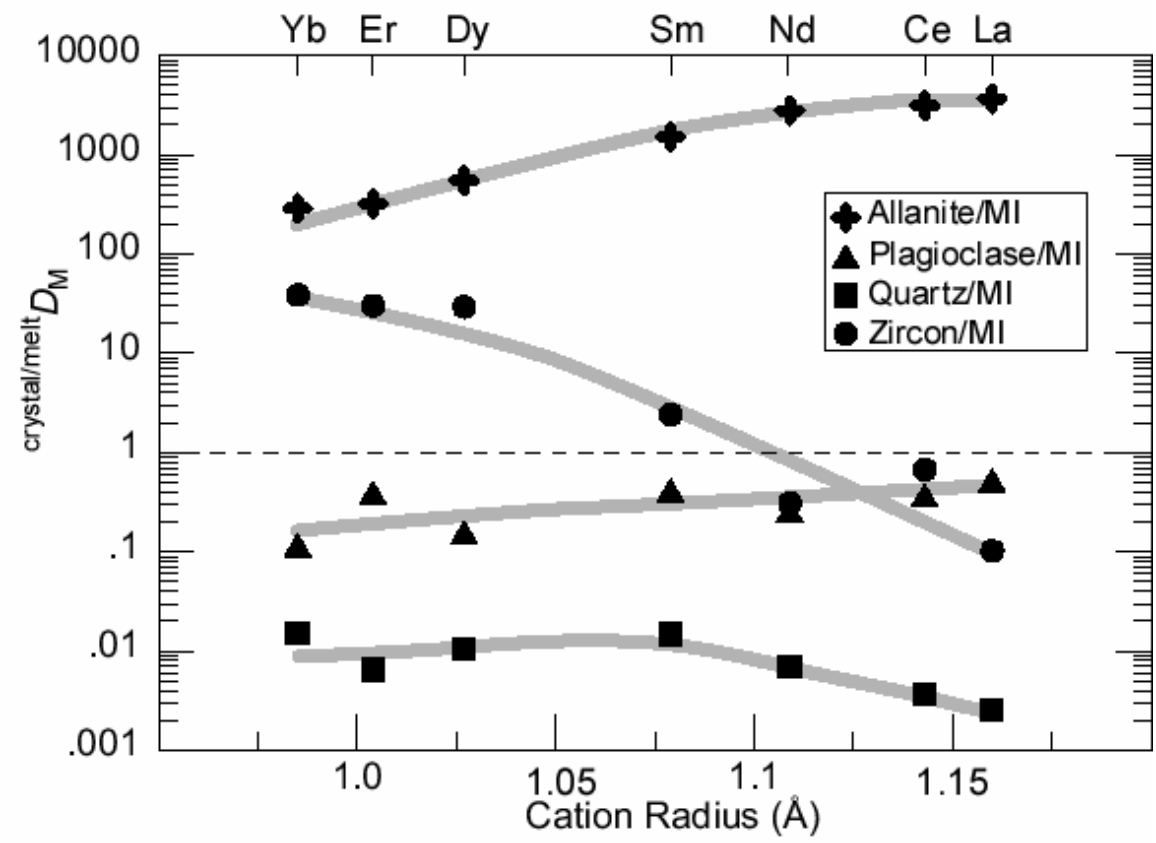

Figure 3.6. Crystal/melt partition coefficients ($^{crystal/melt}K_M$) calculated from analyses of host crystals and melt inclusion pairs. Data is listed in Table 3.1. The gray colored bands are diagrammatic and highlight partition coefficient trends for the different host crystals. Two open circle symbols are for hourglass inclusions contained in zircon.

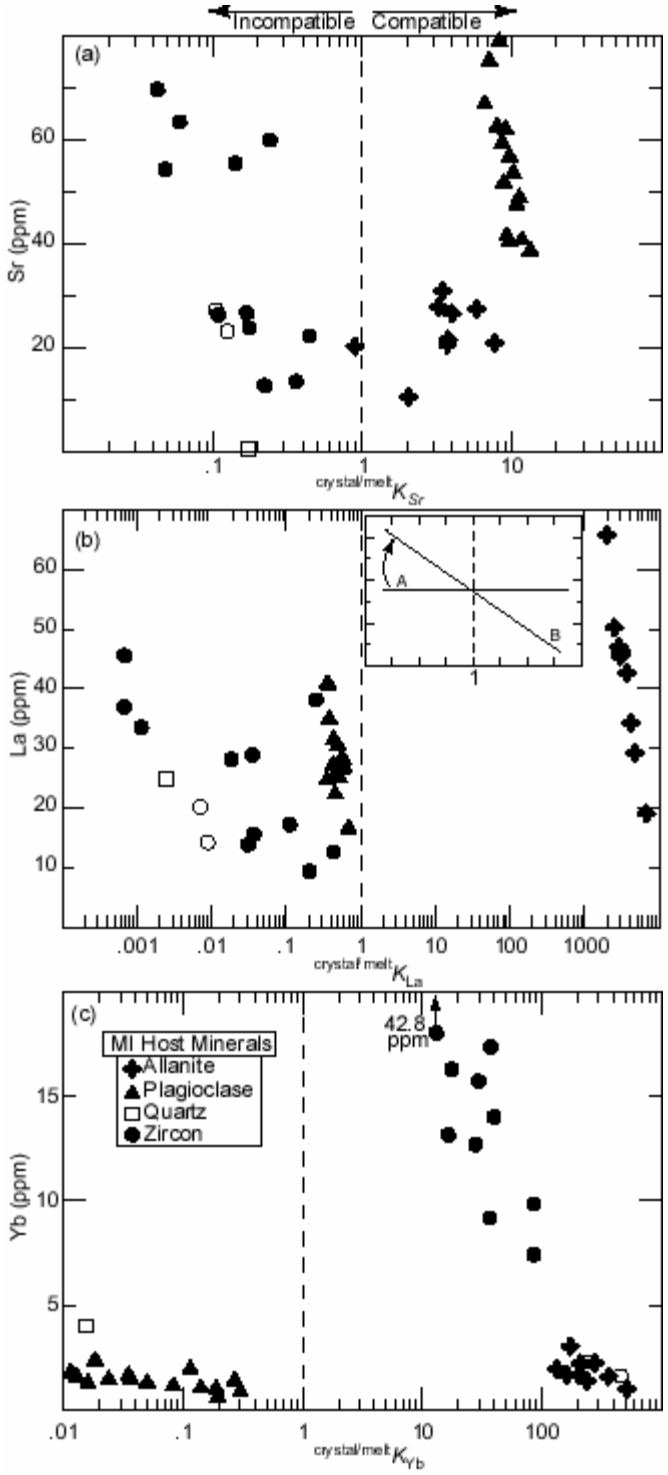

Figure 3.7. Crystal/melt partition coefficients for (a) Sr ($^{crystal/melt}K_{Sr}$) calculated from analyses of host crystal and melt inclusion pairs versus Sr content of melt inclusions, and (b) La ($^{crystal/melt}K_{La}$) versus La abundance in the melt inclusions. The inset shows the general trends that would occur if there is no boundary layer process (labeled A) and the trend that would result if boundary layer processes had affected the melt inclusion compositions (labeled B). Two open circle symbols are for hourglass inclusions contained in zircon.

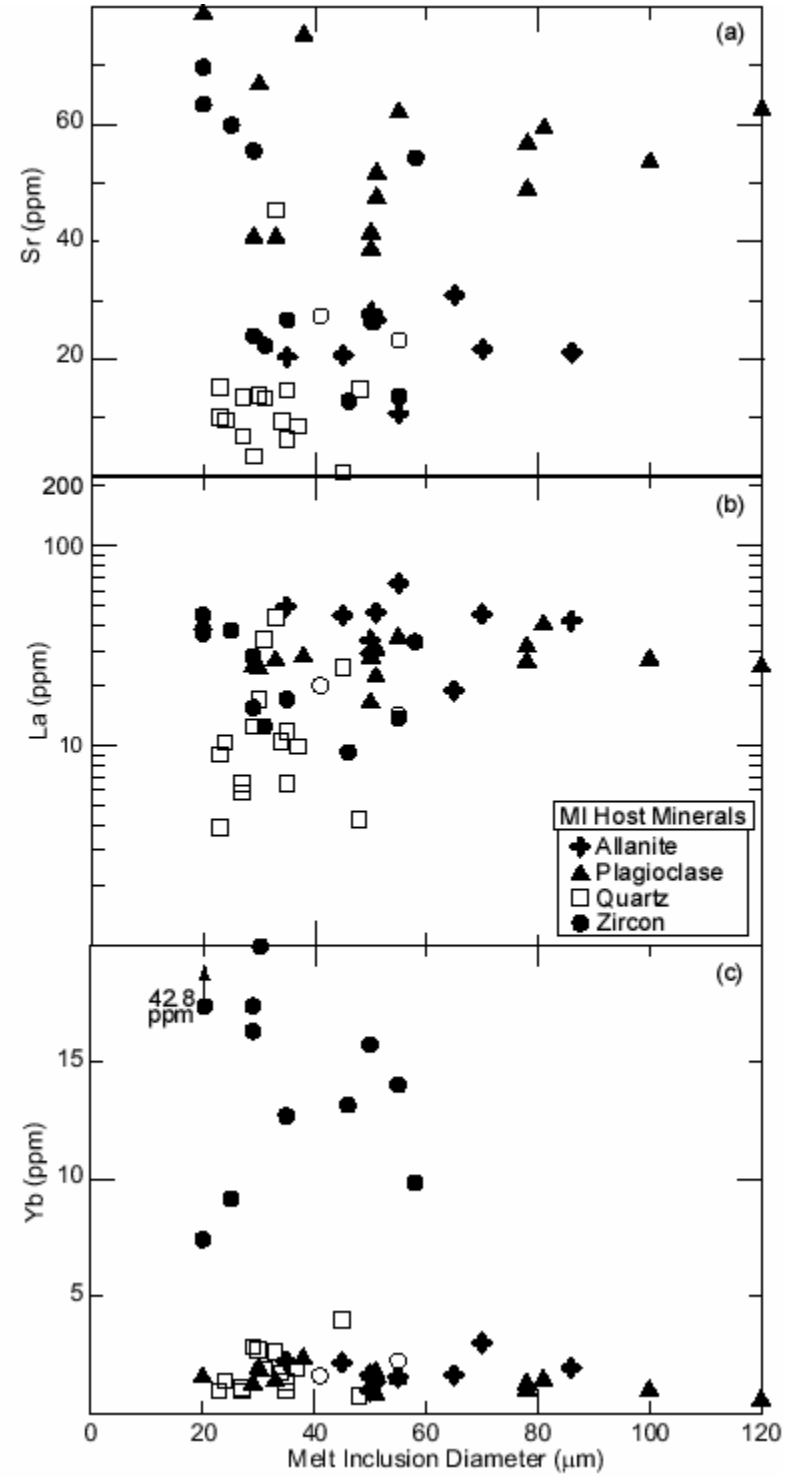

Figure 3.8. Trace element abundances of melt inclusions versus melt inclusion diameter for (a) Sr and (b) La. Two open circle symbols are for hourglass inclusions contained in zircon.

APPENDIX A: TOBA TUFF HOST CRYSTAL ANALYSES

Allanite analyses

Sample	T87							T89A2	
Host Crystal #	A-31	A-77	A-78	A-80	A-83	A-85	A-86	A-56	A-72
Sr (ppm)	160.49	106.08	18.25	107.34	76.65	21.51	160.62	81.05	90.76
La	154750.7	137129.5	126172.4	128140.1	135491.6	128028.1	139732.3	143245.8	143779.0
Ce	226272.3	206308.0	220869.0	202328.3	217538.0	217431.4	207498.5	227286.5	225128.7
Nd	42702.8	42690.7	57097.3	42613.9	49312.2	53178.5	40690.9	52051.4	52059.4
Sm	3745.2	4341.3	7972.5	4581.9	5720.5	6921.3	3907.4	5947.6	5750.2
Dy	808.71	949.01	1846.53	1041.53	1300.96	1639.44	862.61	1444.58	1518.78
Er	476.22	461.36	608.31	455.07	534.20	595.12	469.57	594.06	608.57
Yb	261.77	327.78	634.92	336.22	465.16	568.11	275.36	527.44	510.91

Plagioclase analyses

Sample	T87						T89A2								
Host Crystal #	P-13	P-15	P-69	P-70	P-72	P-75	P-1	P-2	P-5	P-6	P-7	P-8	P-9	P-10	P-26
SiO_2 (wt%)	61.31	60.29	61.02	58.53	60.41	60.03	59.48	57.40	58.51	61.86	59.60	58.97	54.75	59.60	61.90
Al_2O_3	25.40	25.67	25.08	25.58	25.55	25.43	26.70	26.93	24.94	23.94	25.45	25.78	28.77	26.20	24.71
CaO	7.83	8.43	7.66	7.68	8.06	8.00	8.78	9.62	7.79	7.17	7.65	7.75	10.97	8.22	7.30
FeO	0.26	0.28	0.21	0.22	0.20	0.25	0.28	0.35	0.18	0.16	0.09	0.22	0.29	0.20	0.05
Na_2O	6.31	6.35	6.79	6.27	6.29	6.07	6.33	5.48	6.51	6.10	6.63	6.40	4.65	6.52	6.80
K_2O	0.67	0.50	0.58	0.58	0.56	0.54	0.42	0.33	0.64	0.89	0.65	0.57	0.27	0.48	0.64
Total	101.77	101.51	101.33	98.85	101.07	100.32	101.99	100.15	98.57	100.12	100.07	99.69	99.69	101.24	101.40
Sr (ppm)	548.80	497.17	548.71	548.66	457.06	384.99	514.86	390.47	512.87	648.60	563.00	510.90	531.89	475.41	439.87
La	14.88	11.12	13.65	11.70	10.15	11.39	15.00	16.02	15.11	15.10	13.27	14.41	16.19	12.81	8.64
Ce	18.70	13.08	17.57	13.77	11.63	14.34	17.99	21.01	18.96	18.48	16.57	19.08	23.90	15.27	10.74
Nd	2.97	2.15	3.07	1.87	1.89	3.12	2.79	3.90	3.69	2.68	2.78	2.96	3.54	2.09	3.59
Sm	0.62	2.83	0.51	0.58	0.42	0.55	0.13	0.77	0.63	0.13	0.42	0.56	0.49	0.52	2.20
Dy	0.96	0.20	0.21	0.21	0.20	0.23	0.07	0.32	n.d.	0.07	0.28	0.45	0.21	n.d.	0.25
Er	0.36	0.45	0.35	0.38	0.32	0.35	0.24	0.68	1.11	0.39	0.41	0.21	0.44	0.19	0.61
Yb	0.06	0.11	0.14	0.19	0.25	0.06	0.09	0.37	0.02	0.02	0.05	0.03	0.04	0.02	0.22
[a]An%	39.08	41.10	37.12	38.95	40.09	40.73	42.34	48.25	38.31	37.24	37.47	38.73	55.66	39.91	35.83
[b]Ab%	56.97	56.02	59.52	57.55	56.59	55.98	55.24	49.76	57.93	57.28	58.75	57.88	42.70	57.33	60.42
[c]Or%	3.96	2.88	3.36	3.50	3.32	3.29	2.41	1.98	3.76	5.48	3.77	3.39	1.63	2.76	3.75

[a] An% = % anorthite

[b] Ab% = % albite

[c] Or% = % orthoclase

Other abbreviations are the same as in Table 3.1.

Zircon analyses.

Sample	T87						T89A2						
Host Crystal #	Z-16	Z-18	Z-23	Z-101	Z-104	Z-88*	Z-12	Z-45	Z-47	Z-50	Z-52	Z-59	Z-39*
P_2O_5 (wt%)	n.d.	n.d.	n.d.	n.d.	n.d.	n.d.	0.08	n.d.	0.02	n.d.	n.d.	n.d.	n.d.
SiO_2	31.31	30.92	32.01	31.44	31.04	32.06	32.80	32.56	32.81	33.05	33.08	32.96	33.39
ZrO_2	65.56	64.46	64.99	65.07	64.03	65.93	64.88	64.19	64.88	63.52	63.63	65.20	61.76
HfO_2	0.72	0.31	0.86	0.40	0.48	0.29	1.40	1.22	1.11	1.32	1.54	1.46	1.10
Total	97.58	95.68	97.86	96.91	95.54	98.29	99.16	97.98	98.81	97.88	98.25	99.62	96.24
Sr (ppm)	4.49	2.83	4.18	9.85	4.91	2.90	2.85	2.59	2.96	3.78	7.78	14.35	2.86
La	1.93	1.93	0.58	5.37	0.43	0.13	1.01	0.04	0.03	0.03	0.52	9.60	0.14
Ce	29.42	12.96	17.69	36.90	23.92	15.08	16.40	34.43	45.86	31.18	47.36	30.15	27.26
Nd	2.74	1.77	0.84	4.67	0.97	4.21	4.05	8.79	3.45	1.66	1.03	5.44	9.90
Sm	4.10	4.75	2.43	7.46	3.56	8.80	5.12	17.46	5.34	5.19	4.86	2.81	6.36
Dy	90.07	38.83	67.58	232.97	105.44	136.28	98.53	283.99	127.76	112.20	104.21	75.75	176.61
Er	190.44	110.17	152.34	435.63	233.25	256.14	198.46	467.12	249.09	252.09	230.80	149.90	305.51
Yb	354.34	217.28	288.72	645.08	559.73	550.92	467.80	850.03	552.09	637.92	650.66	337.19	745.70

Abbreviations are the same as in Table 3.1.

Analyses of zircon adjacent to matrix glass (see Table 3.2)

Sample	T89A2		
	Z-36	Z-38	Z-42
P_2O_5 (wt%)	n.d.	0.02	0.05
SiO_2	32.43	32.40	32.61
ZrO_2	64.18	61.81	65.17
HfO_2	1.69	1.55	1.17
Total	98.29	95.78	99.00
Sr (ppm)	5.64	4.71	3.17
La	0.26	0.38	0.30
Ce	84.61	54.43	32.77
Nd	6.21	5.87	11.24
Sm	12.61	13.55	21.15
Dy	386.07	186.37	364.28
Er	749.56	406.86	554.41
Yb	2071.26	915.13	980.99

Abbreviations are the same as in Table 3.1.

Quartz analysis

Sample	T87
Host Crystal #	Q-10
SiO_2 (wt%)	100.19
ZrO_2	0.05
TiO_2	0.04
Al_2O_3	0.06
MgO	0.01
CaO	n.d.
MnO	0.04
FeO	0.01
Na_2O	0.02
K_2O	0.01
Total	100.43
Sr	0.12
La	0.06
Ce	0.21
Nd	0.15
Sm	0.10
Dy	0.08
Er	0.02
Yb	0.06

VITA

Jay B. Thomas

I was born on October 1, 1970 in Roanoke, Virginia, USA

Education

Ph.D. (Sept. 2003) Department of Geological Sciences, Virginia Tech, Blacksburg, VA
Dissertation: Melt inclusion geochemistry: insights into melt evolution, mineral growth and processes operative at the crystal/melt interface.

M.S. (1998) Department of Geological Sciences, Virginia Tech, Blacksburg, VA
Thesis: Petrologic Significance of Multiple Magmas in the Quottoon Igneous Complex, NW British Columbia and SE Alaska.

B.A. (1995) Geology Department, Guilford College, Greensboro, NC
Senior thesis: Mapping, petrology and interpretation of volcanic and plutonic rocks of the Carolina Slate Belt, North Carolina.

Professional Experience

- May 2000-present, research assistant in the Fluids Research Laboratory at Virginia Tech. I am responsible for teaching students and visitors how to prepare samples for fluid-melt inclusion analyses. I also instruct instrument users in several of the Department's analytical facilities.
- Summer 1998, full time research assistant for David M. Wayne in the Chemistry and Metallurgy Research Division at Los Alamos National Laboratory, Los Alamos, New Mexico. Duties included maintenance of clean rooms, chromatographic separation of transuranium metals and operation of various mass spectrometers.
- Summer 1996, field assistant for M. L. Crawford in the wilds of southeastern Alaska and northwestern British Columbia where I assisted in field mapping and sample collection.
- 1992-1999, teaching assistant at Guilford College and Virginia Tech (see below for details)

Teaching Experience

Term	Course	Course Level
Fall 1992	Paleontology	2nd-4th year majors
Spring 1993	Historical Geology	1st-2nd year majors and non-majors
Fall 1993	Structural Geology	3rd-4th year majors
Spring 1994	Historical Geology	1st-2nd year majors and non-majors
Spring 1994	Historical Geology	1st-2nd year majors and non-majors
Fall 1996	Elements of Geology	1st-2nd year majors and non-majors
Spring 1997	Resources Geology	1st-2nd year majors and non-majors
Fall 1997	Meteorology	2nd-4th year majors and non-majors
Spring 1998	Meteorology	2nd-4th year majors and non-majors
Fall 1998	Meteorology	2nd-4th year majors and non-majors
Spring 1999	Meteorology	2nd-4th year majors and non-majors
Spring 2000	Meteorology	2nd-4th year majors and non-majors

Grants and Awards

May 2003- Virginia Tech Department of Geological Sciences Outstanding Service Recognition Award (selected by VT faculty) for exceptional leadership and guidance provided for peers

May 2000-I was the primary author of a proposal funded by the National Science Foundation (EAR-0001168) to Robert J. Bodnar and A. Krishna Sinha to investigate melt inclusions in accessory minerals for $240,059 USD

May 2000-I co-authored a proposal funded by the National Science Foundation (EAR-0001102) to A. Krishna Sinha, Maria L. Crawford and James S. Beard to investigate compositional variability of plutonic regimes along a crustal cross-section for $184,999 USD

May 1999-Virginia Tech Department of Geological Sciences Tillman Teaching Award (selected by VT students) for excellence in meteorology instruction

May 1997-David R. Wones Geoscience Scholarship Award (selected by professors) for innovative research achievements

Membership in Professional Societies

Mineralogical Society of America
The Geochemical Society
American Geophysical Union

Committee Involvement

2002 to 2003-Head of fundraising for the Geological Sciences Student Research Symposium at Virginia Tech (a professional-style forum for presentation of graduate and exceptional undergraduate research)

PUBLICATIONS

Refereed Publications (reprints, preprints or copies available upon request)

1. Thomas, J.B., Bodnar, R.J., Shimizu, N. and Chesner, C. (in press) Melt inclusions in zircon. Reviews in Mineralogy and Geochemistry, Mineralogical Society of America.

2. Thomas, J.B. and Bodnar, R.J. (2002) A technique for mounting and polishing melt inclusions in small (<1 mm) crystals. American Mineralogist, v. 87, 1505-1508.

3. Thomas, J.B., Bodnar, R.J., Shimizu, N. and Sinha, A.K. (2002) Determination of zircon/melt trace element partition coefficients from SIMS analysis of melt inclusions in zircon. Geochimica et Cosmochimica Acta, v. 66, 2887-2901.

4. Thomas, J.B. and Sinha, A.K. (1999) Field, petrographic, geochemical, and isotopic characterization of the Quottoon Igneous Complex, S. E. Alaska and N. W. British Columbia. Canadian Journal of Earth Sciences, v. 36, 819-831.

5. Thomas, J.B. (1994) Mangrove vegetation detection using remote sensing and image processing techniques. Proceedings of the Eighth National Conference on Undergraduate Research, v. 2, 699-703.

Abstracts

1. Thomas, J.B., Bodnar, R.J., Shimizu, N. and Chesner, C. (2002) The boundary layer problem and the reliability of melt inclusions as petrogenetic monitors: evidence from melt inclusions in zircon, allanite, plagioclase and quartz. Workshop-Short Course on Volcanic Systems, Geochemical and Geophysical Monitoring, Melt Inclusions: methods, applications and problems, 205-209.

2. Thomas, J.B., Bodnar, R.J., Shimizu, N. and Chesner, C. (2002) What boundary layer? Evidence from melt inclusions in plagioclase, quartz, allanite and zircon, from the Toba Tuffs, Sumatra, Indonesia. Eighth Biennial Pan-American Conference on Research on Fluid Inclusions Program with Abstracts, p. 103-104.

3. Thomas, J.B., Bodnar, R.J., Farley, C. (2002) A further test of the Raman technique for determining water contents of silicate glasses. Eighth Biennial Pan-American Conference on Research on Fluid Inclusions Program with Abstracts, p. 105.

4. Thomas, J.B., Bodnar, R.J., Shimizu, N. and Chesner, C. (2001) The role of boundary layers during entrapment of melt inclusions: evidence from the Toba Tuffs Sumatra, Indonesia. EOS Transactions AGU, 82 (47), Fall Meeting Suppl. Abstract V32D-1014.

5. Thomas, J.B., Bodnar, R.J., and Shimizu, N. (2001) Melt inclusions in zircon: microautoclaves for determination of trace element partition coefficients. Eleventh Annual Goldschmidt Conference, p. 3480.

6. Thomas, J.B., Shimizu, N., Bodnar, R J. and Sinha, A.K. (2000) Melt inclusions in zircon as recorders of melt evolution in crystallizing granitic plutons. Geologic Society of America Annual Meeting program with abstracts, v. 32, n. 7, A398.

7. Sinha, A.K. and Thomas, J.B. (1997) Terrane recognition in the Precambrian: examples from the Grenville orogen of the eastern United States. 13th International Conference on Basement Tectonics.

8. Thomas, J.B. and Sinha, A.K. (1997) The Quottoon Igneous Complex: A record of tectonic evolution along the Coast shear zone. Geological Society of America Annual Meeting program with abstracts, v. 29, n. 7, A83.

9. Sinha, A.K. and Thomas, J.B. (1997) Paleogene magmatism in NW British Columbia-SE Alaska: Evidence for change from transpression to extension. Geological Society of America Annual Meeting program with abstracts, v. 29, n. 7, A83.

10. Sinha, A.K. and Thomas, J.B., Crawford, M.L., and Beard, J.S. (1996) The nature of Paleogene magmatism along the ACCRETE corridor. American Geophysical Union fall meeting, v. 77, n. 46, F652.

11. Sinha, A.K. and Thomas, J.B. (1996) Lead isotope mapping of crustal reservoirs within the Grenville superterrane. Geological Society of America southeastern section program with abstracts, v. 29, n. 3, 69.

12. Thomas, J.B., Fisher, J.D., and Ahearn, D.S. (1995) Geologic mapping of the Bull Run drainage basin, Guilford County, North Carolina. Geological Society of America southeastern section program with abstracts, v. 27, n. 2, 92.

Unpublished Theses

1. M.S. thesis,

   Thomas, J.B. (1998) The Quottoon pluton: Petrogenesis of an igneous complex, northwestern British Columbia and southeastern Alaska. Master of Science thesis, Blacksburg, VA, Virginia Polytechnic Institute and State University, 134 p.

2. B.A. thesis,

   Thomas, J.B. (1995) Geologic mapping, petrography, and tectonic interpretation of Carolina Slate Belt schists and granitoids, senior thesis Greensboro, N. C., Guilford College, 67 p.

Ongoing Projects and Forthcoming Manuscripts

1. Thomas, J.B., Bodnar, R.J., Shimizu, N. and Chesner, C. (in preparation) Evaluation of boundary layer processes that develop adjacent to crystals growing from high silica rhyolite magmas and their effect on melt inclusions.

2. Thomas, J.B., Bodnar, R.J., Farley, C. (in progress) Determination of water contents in silicate glasses using laser Raman spectroscopy.

3. Spotila, J. and Thomas, J.B. (in progress) Deciphering complex zoning in apatite from plutons of the Blue Ridge Escarpment in southwestern Virginia.

LABORATORY SKILLS

- Development of a new technique for polishing small crystals (>30 μm) to expose melt inclusions in preparation for microbeam analysis of major-trace elements and isotopic compositions
- Microthermometry of fluid/melt inclusions using:
  Heating-cooling stages (up to 1500ºC, 1 atm)
  High temperature/pressure TZM vessels (up to 1000ºC, 3 kb)
  Internally heated pressure vessel (up to 900ºC, 10 kb)
  Vertical tube furnaces (up to 1500ºC, 1 atm)
- Scanning electron microscopy and cathodoluminescence imagery of melt inclusions and minerals
- All aspects of operating a Cameca® SX-50 electron microprobe for analysis of hydrous melt inclusions, silicate glass and minerals for major and trace elements
- Trace element analyses of melt inclusions and minerals using a Cameca® 3f Ion Mass Spectrometer
- Calibration and confirmation of a new technique that uses a Dilor XY laser Raman microprobe to determine the water content in melt inclusions and silicate glass
- All aspects of operation/maintenance of a VG Sector-54 thermal ionization mass spectrometer
- Development of techniques for processing microsamples for isotopic analyses containing <5 nanograms of total Pb utilizing synthetic isotope tracer solutions for isotope dilution analyses
- Development and calibration of various chromatography techniques
- Improvement and development of new laboratory techniques over a three month period to reduce total procedural blanks from ~200 picograms Pb to <10 picograms and reduction of U blanks from ~25 picograms to <1 picogram
- Calibration of isotope tracer solutions
- High-precision U-Pb age dating of minerals zircon and titanite
- U-Th-Pb analyses of zircon, allanite and monazite using a Cameca® 1270 Ion Mass Spectrometer